# NEW OBJECTIVE AND PSYCHOPHYSICAL TECHNIQUES TO STUDY THE PROCESSING OF VISUAL SIGNALS WITH EMPHASIS ON CHROMATIC AFTERIMAGES

Wei Bi

Doctor of Philosophy

City University

The Applied Vision Research Centre

Department of Optometry and Visual Science

September 2012

# TABLE OF CONTENTS

# LIST OF TABLES

# LIST OF FIGURES

Figure 6-4. Pupil response results from (a – d) a typical normal subject and (e – h) a subject with mild rod deficiency (e-h). The horizontal axis represents time in seconds and the vertical axis plots the pupil diameter. The black circled traces, the green rectangled traces and the blue triangled traces show the pupil responses to luminance, colour and rod/melanopsin modulation, respectively. Diagrams (a & e) in the top row show pupil responses on the original mm scale. The baselines in these traces show the corresponding steady-state pupil sizes and the absolute pupil constriction amplitude and latencies can be compared easily for each stimulus condition. The pupil constrictions in the bottom diagrams (b, c, d, f, g and h) have been normalized with respect to the individual subject's largest pupil response amplitude among all the 9 traces, so that each pupil trace would have a maximum pupil constriction of 1. Each trace illustrates a mean pupil response trace of 32 measurements for each stimulus condition (i.e., luminance, colour and rod/malanopsin stimulus modulation) at each light level. The 3 rows (b & f, c & g and d & h) in the bottom diagram section correspond to the pupil response measurements at the lowest light level (4.8cd/$m^2$), the mid light level (75cd/$m^2$) and the highest light level (456cd/$m^2$), respectively. Diagrams f, g and h show pupil responses for the mild rod deficient subject. The traces reveal much reduced pupil response amplitude to the rod/melanopsin stimulus when compared to his pupil response amplitudes to the luminance and colour stimuli, especially at the lowest light level. However, in the normal subject (b, c and d), the pupil response amplitude to the three stimuli are very similar.....168

Figure 6-5. Pupil response results from (a – d) a normal subject, (e – h) the Retinitis Pigmentosa subject who has no functioning rods and (i – l) the rod monochromat subject who only functioning rods in the eye. The results from the Retinitis

green and blue dot lines represent the colour confusion lines. The black dotted ellipse shows the colour thresholds for an average of 330 normal trichromats (Rodriguez-Carmona et al., 2005). The photoreceptor contrasts are calculated along this ellipse contour and are drawn in diagram (b) as a function of the chromatic displacement angle in degrees. The dots, crosses, squares and triangles show the contrasts generated in rods, L-cones, M-cones and S-cones, respectively. Point A has a chromatic angle of $118^{o}$ and B has angle of $298^{o}$ and both of them have 0 rod contrast for 0.1 chromatic displacement (CD) from the background chromaticity (0.298, 0.335) in the CIE – (x,y) chromaticity chart. (c) Pupil responses to the d-isoluminant stimulus in a normal subject. The red dotted curve shows the pupil response to the reddish stimulus (i.e., $\theta = 298^{o}$, CD = 0.1) and the green curve is for the greenish stimulus (i.e., $\theta = 118^{o}$, CD = 0.1). (d) Pupil responses to the d-isoluminant stimulus shown for the rod monochromat. Unlike the normal subject who shows good pupil responses to the d-isoluminant stimuli, there are no pupil responses for these stimuli in the rod monochromat. .....174

Figure 6-9. Pupil responses measured following stimuluation of the affected eye in the ON subject. The responses to the luminance and colour stimuli are almost absent. However, when light level is increased, the subject shows some pupil responses but only to rod/melanopsin stimulus.....179

Figure 6-10. Pupil responses measured in the ON subject. Tests were done monocularly in each eye. The dotted lines are responses from the affected eye and the solid lines are from the unaffected eye. The pupil responses are completely absent from the affected for all stimuli. (a) shows a comparison of pupil responses between the affected and unaffected eye. In (b), the pupil responses from the

# ACKNOWLEDGEMENTS

Firstly, I must express my sincere thanks to my supervisor Professor John Barbur. Over the years, he has provided many novel ideas, infinite advice, warm-hearted encouragement and great patience as I have struggled to keep up and grasp new concepts. His endless enthusiasm and diligent attitude in research deeply influenced and guided me in the correct direction. I really appreciate his help and I owe him a great deal.

Secondly, I would also like to thank our research collaborators: Professor Gordon Plant for providing me with valuable advice and for recruiting many participants for my studies. Professor Sei-ichi Tsujimura for providing useful advice and for making available novel equipment for my studies. Dr. Panitha Jindahra, Dr. Mithu Storoni and Dr. Anne-Caroline Bessero for recruiting and examining suitable projects and for becoming involved in some of the experiment work. I also wish to thank Alister Harlow and Arthur Collyer for providing technical support.

I am grateful to my participants, my friends and my colleagues who helped and advised me whilst studying at the Applied Vision Research Centre at City University. In particular, I want to thank Dr. Marisa Rodriguez-Carmona, Dr. Garry Bargary and Dr. Haogang Zhu for sharing lots of their research knowledge, and Evgenia Konstantakopoulou and Joseph Hickey for encouraging and helping me to complete my thesis.

Lastly, I must thank my parents for their support, encouragement and love at all times. You are and have always been the driving force in my life.

# DECLARATION

I grant powers of discretion to the University Librarian to allow this thesis to be copied in whole or in part without reference to me. This permission covers only single copies made for study purposes, subject to normal conditions of acknowledgement.

# ABSTRACT

The research work described in this thesis embodies a number of studies designed to investigate human vision with emphasis on aspects of the pupil response and chromatic mechanisms in relation to the perceived chromatic afterimages.

The aim of the first study was to establish the relationship between the perception of chromatic afterimages and the corresponding involuntary pupil responses. We started by designing and developing a new, computer-based, psychophysics program and employed it to measure the strength and duration of perceived chromatic afterimages in normal trichromats and in colour deficient observers. The dynamic luminance noise technique was used to isolate colour signals and to elicit pupil responses to coloured stimuli of known photoreceptor contrast. A model was developed to explain the afterimage results obtained in the normal trichromats and in colour deficient subjects. The model and the pupil colour responses provided an understanding of luminance and colour processing in dichromats that also helped to explain previously reported pupil colour responses. The model also predicts the colour confusion lines and the characteristics of pupil colour responses in dichromats at any given background chromaticity.

In the second study, we investigated and compared pupil responses to visual stimuli that isolate photopic luminance and colour in both the sighted and blind region of the visual fields on subjects with either acquired or congenital homonymous hemianopia. The measured pupil responses in the blind hemifield of patients with acquired cortical damage are either absent or of reduced amplitude when compared to those measured in the corresponding regions of the sighted field, whereas the patients with congenital loss of visual field show similar and even enhanced pupil responses when compared to their sighted hemifield. These results suggest that in the absence of normal functioning of the direct geniculostriate projection, other projections to midbrain nuclei or to extrastriate regions can be enhanced and these include the pupillary pathways. These findings suggest that early damage to the brain might be partly compensated for by reorganising the strength of neural projections to the remaining, non-compromised visual areas.

The purpose of the last study was to examine whether melanopsin contributes to the dynamic pupil light reflex responses in humans. A light source containing of four primary components was employed to generate pupillary stimuli that isolate luminance, colour or combined rod and melanopsin. Normal trichormats, rod deficient subjects, one subject with retinitis pigmentosa, one rod monochromat, three subjects with Leber's Hereditary Optic Neuropathy (LHON) and one subject with Optic Neuritis were investigated using this approach. The results from the LHON subjects suggest not all classes of ganglion cells are affected uniformly in LHON, and that the pupil light reflex responses mediated through rod photoreceptors were affected the least. The characteristics of the pupil responses to the rod/melanopsin stimulus from the rod monochromat and the retinis pigmentosa subjects suggest that melanopsin does not contribute to dynamic pupil light reflex response in humans.

# ABBREVIATIONS AND SYMBOLS

| | |
|---|---|
| L cones | Long wavelength sensitive cones |
| M cones | Medium wavelength sensitive cones |
| S cones | Short wavelength sensitive cones |
| ipRGCs | Intrinsically Photosensitive Retinal Ganglion Cells |
| IPL | Inner Plexiform Layer |
| OPL | Outer Plexiform Layer |
| M cells/pathway | Magnocellular cells/pathway |
| P cells/pathway | Parvocellular cells/pathway |
| dLGN | Dorsal Lateral Geniculate Nucleus |
| OPN | Olivary Pretectal Nucleus |
| EW | Edinger-Westphal nucleus |
| SCN | Suprachiasmatic Nucleus |
| SC | Superior Colliculus |
| fMRI | Functional Magnetic Resonance Imaging |
| LHON | Leber's Hereditary Optic Neuropathy |
| ON | Optic Neuritis |
| RP | Retinitis Pigmentosa |
| GUI | Graphics User Interface |
| SQL | Structure Query Language |
| CAD | Colour Assessment and Diagnosis |
| QAA | Quantitative Afterimage Assessment |
| CAA | Contrast Acuity Assessment |
| PLR | Pupil Light Reflex |

# 1 INTRODUCTION

This chapter describes the basic mechanisms of human vision with emphasis on the processing of colour signals and the control of the pupil response. It begins by describing the anatomy and physiology of the eye and the structures of the retina. This is followed by an examination of image formation in the eye and the neural processing of signals in the retina. The role of the pupil, the function of melanopsin and the processing of colour signals are discussed. A new afterimage measurement technique is then described in relation to some related studies on pupil response components. A brief summary of the contents of the experimental work is then given for each of the remaining chapters.

## 1.1 Anatomy and physiology of the eye

Vision is arguably the most important of all sensory inputs. A large amount of information about the surrounding environment is provided through sight. However, the visible spectrum is only a small portion of the electromagnetic spectrum (Figure 1-1). A typical human eye will respond to wavelength from about ~390nm to ~750nm and the rest will appear black. The process of visual perception starts with light entering the eye and forming a 2D representation of the object space on the retina. The information carried in the spatial modulation of intensity and spectral content is then processed and coded in the retina and then transferred to the Dorsal Lateral Geniculate Nucleus (dLGN) and from these to the primary visual cortex and to a number of midbrain nuclei.

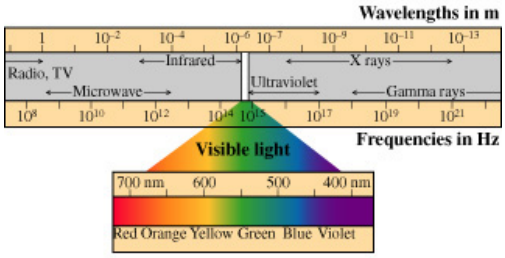


Figure 1-1. Visible spectrum. A typical human eye will respond to wavelength from about ~380nm to ~750nm.

### 1.1.1 The structure of the eye

A simple examination of the eye reveals dark pupil (as a disc aperture in the middle of the eye), the iris (a very colourful structure) and the sclera (the white of the eye) that extends into the orbit. The human eyeball is a slightly asymmetrical sphere of approximately one inch in diameter and a volume of about 6.5cc (I Arbus, 1967).

When light enters the eye, it passes though the cornea, the anterior chamber, the pupil, the lens and then the vitreous humour before finally reaching the retina.

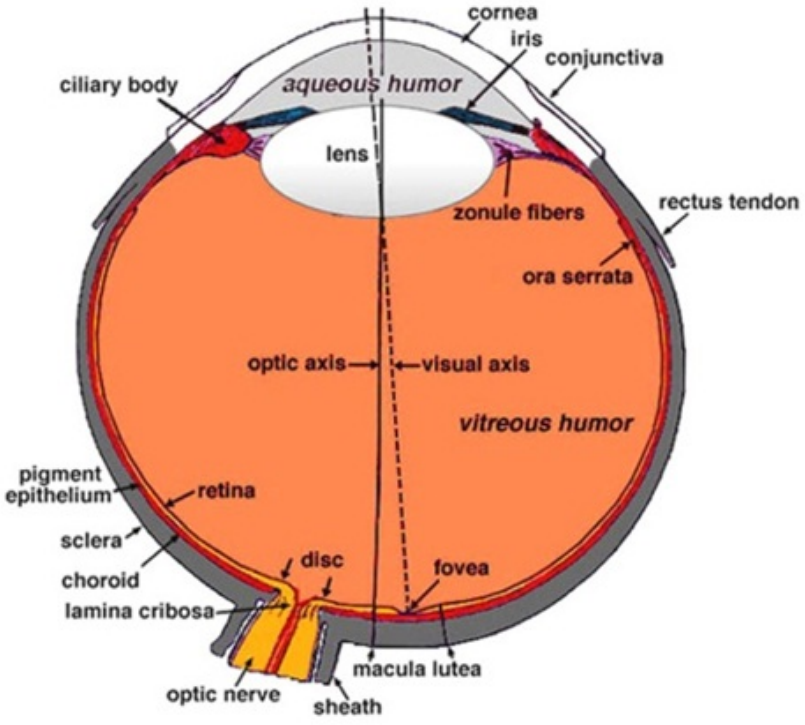


Figure 1-2. A Horizontal cross section of the human eye, reproduced from (Boynton 1979)

Figure 1-2 shows a horizontal cross section of the human eye (Boynton, 1979). From the outermost part of the eye to the inside, the eye can be considered to have 3 different layers: the external layer, which contains the cornea and sclera; the intermediate layer, which contains the iris, ciliary body and the choroid; and the internal layer, which is the retina of the eye.

There are 2 chambers in the eye that are filled with fluid. The Anterior chamber is located between the cornea and the lens. It is filled with aqueous humor. The posterior chamber or the Vitreous chamber is the area from the back of the lens to the retina and it contains vitreous humor.

#### *1.1.1.1 The cornea and sclera*

The cornea and sclera together form the tough, rigid, fibrous coating of the eye. The cornea is transparent and covers the iris and the pupil. It is the first refractive element of the eye and accounts approximately two thirds (~43 dioptres) of the human eye's total refractive power (Wald and Griffin, 1947). The human cornea has a radius of curvature of ~7.8mm and a thickness of ~0.5mm at the centre and ~1mm at the edge (Ehlers et al., 1975). The optical properties of the cornea do not change significantly with aging. The cornea transmits the light from 300nm to 2500nm, with the maximum transmittance between 500nm to 1300nm (Boettner and Wolter, 1962, Hart and Farrell, 1969).

The sclera is continuous with the cornea. In fact, the cornea and the sclera are made of the same tissue substance, but in the cornea, these fibers are arranged as parallel arrays and are oriented perpendicular to the surface normal of the eye, so that the light can pass through the cornea with minimum scatter (Laibson, 1971). However, the arrangement of fibres in the sclera is completely different. The net result is that the light passes through the cornea very easily but not through the sclera (Komai and Ushiki, 1991).

#### *1.1.1.2 Pupil*

When light passes though the cornea, it reaches the iris on its way to the retina. The pupil is the hole in the centre of the iris and it controls the light as it passes through the eye in a way that is similar to the aperture stop in a camera system. Usually depending on the properties of the light, the size of the pupil changes. As a result, the amount of light that lands on the retina will change accordingly. The size

of the pupil can also be affected by psychological effects or drugs. Pupil signals in response to specially designed stimuli can also reflect the processing of stimulus attributes in the visual cortex (Lucas et al., 2003, Barbur, 2003, Barbur et al., 1993, Barbur et al., 1980).

#### *1.1.1.3 Lens*

Behind the iris, the crystalline lens is suspended in place by the zonule fibers. It is a transparent, biconvex structure and surrounded by the lens capsule. Both the cornea and the lens refract light to the retina. When compared with the cornea, the refractive power of the lens only accounts for 1/3 of the total power (approximately 18 dioptres), but, it is able to change its shape / curvature. Depending on the distance of the object, the lens changes its focal length dynamically to form a clear image of the object on the retina. The process of the power change in the optics of the eye is known as accommodation (Schaeffel et al., 1988, Wolffsohn et al., 2011). The lens transmits light from short wavelength ultra-violet (360 to 380nm) to long wavelength infra-red (~2000nm). The transmittance of the lens is affected by aging, especially in the short wavelength range, which causes the lens to appear yellow (Boettner and Wolter, 1962, Pokorny et al., 1987).

### 1.1.2 The structure of the retina

The human retina is the innermost layer and lies at the back of the eye. After light passes through the pupil and the vitreous chamber, it ends up on the retina where the image is formed. The retina is the neural structure where the initial image processing occurs. The neuron signals from the retina are then transferred to the

brain via the optic nerve. The following figure shows the surface of the retina as seen through an ophthalmoscope.

Figure 1-3. A human retina seen through an ophthalmoscope

Figure 1-3 shows an example fundus photograph from a healthy right eye. The optic disk is located towards the nose and macular is in the centre of the image.

The optic disc is an approximately 1.5mm diameter oval to circular shaped area of high reflectance and lies about $16^{o}$ into the nasal hemiretina. The central retinal artery penetrates the globe through the optic disc and provides the blood supply to the retina. The blood vessels radiate across the retina, however they do not cover the macular area.

The macular lutea is approximately 5.5mm in diameter; its centre is about 3.5mm lateral to the edge of the optic disc and nearly 1mm inferior to the centre of the optic disc (Hubel, 1995). Due to the pigments in the macular area, the macular has a yellowish colour and hence it strongly absorbs short wavelengths (maximally blue light ~454nm) (Snodderly et al., 1984). In the centre of the macular area, it is the fovea - the centre of the visual field. Sharp images are formed in the fovea, a region

which provides high contrast acuity and colour sensitivity. From the fovea, a circular area of about 6mm diameter is considered the central retina and beyond 6mm, is considered to be the periphery (Kolb, 1991).

The cone photoreceptors have peak densities in the fovea region. The absorbance of the cornea, the lens and the macular pigment reduce preferentially short wavelength light. As a result, long wavelength light is more likely to reach the retina than light from the short wavelength region (Packer and Williams, 2003).

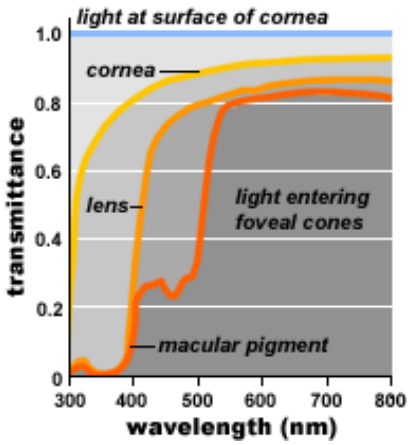


Figure 1-4. Prereceptoral filtering in an adult eye (adapted from Packer & Williams 2003).

In adult humans, the whole retina is approximately 72% of a sphere about 22mm in diameter (Polyak, 1941, Van Buren, 1963, Kolb, 1991). The retina is a complex neural structure containing more than 200 million nerve cells, but their positions are highly organised. Polyak (1941) showed that the retina comprises 10 distinct layers (Polyak, 1941). From the outer retina to inner retina, these layers are the Retina Pigment Epithelium layer (RPE), the outer segments layer (or photoreceptor layer), the outer limiting membrane layer (layer that separates the inner segment portions of the photoreceptors from their cell nucleus), the outer nuclear layer (cell bodies of

rod and cones), the outer plexiform layer (layer that rods and cones make synapses with dendrites of bipolar), the inner nuclear layer (bipolar cells, horizontal cells and amacrine cells), the inner plexiform layer, the ganglion cell layer, the nerve fibre layer (axons of the ganglion cell nuclei) and the inner limiting membrane layer (Muller cell footplates) (Figure 1-5).

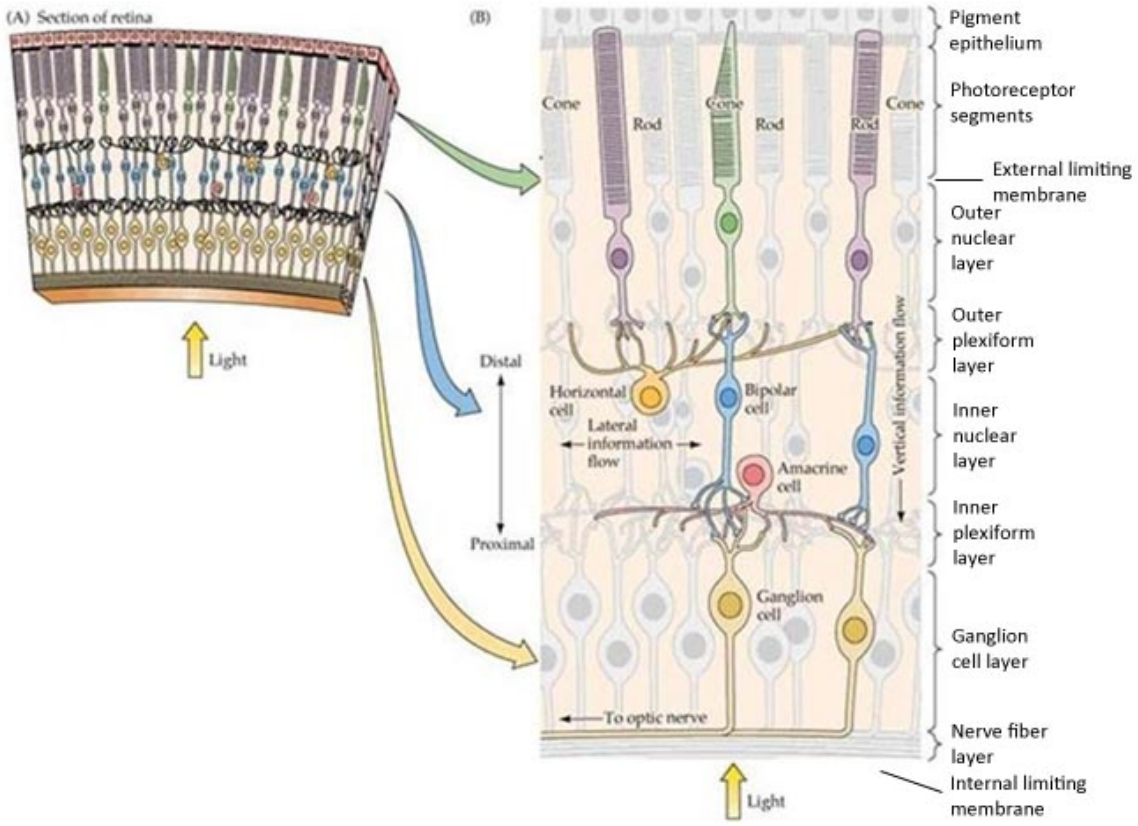


Figure 1-5. Schematic representation of the main layers of retina.
(Adapted from http://thebrain.mcgill.ca)

When the light reaches the retina, it passes through all the other retinal layers until it gets to the outer segment layer and the Retina Pigment Epithelium layer. The RPE's dark pigmentation absorbs light strongly and, as a result, it reduces the light scatter in the eye. The photosensitive photoreceptors in the outer segment layer absorb light and generate visual signals. These signals are then transferred to the

inner nuclei layer and are preliminarily processed by the horizontal cells, amacrine cells and bipolar cells. Then, they are sent to the ganglion layer where these visual signals are processed further and then transferred to the brain through the optic nerve via the Lateral Geniculate Nucleus (LGN).

### *1.1.2.1 Classical Photoreceptors - Rods and cones*

In the outer segment layer in human retina, there are two types of photoreceptors, rods and cones. These photoreceptors absorb some of the light that ends up in the retinal image and convert it into electrical visual signals, after which the signals are transmitted to the post-receptoral neurons. Figure 1-6 shows the different representations of the structure of rods and cones in the retina.

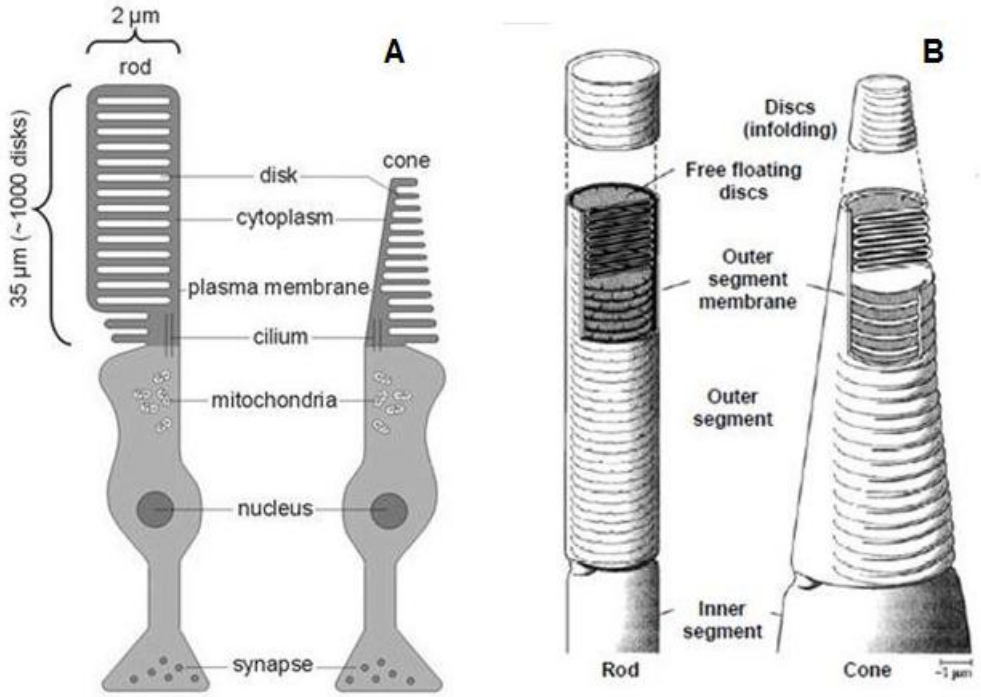


Figure 1-6. (A) The structures of the rods and cones and (B) their outer segments (Hubel et al., 1995).

Rods and cones have four distinct structures: the outer segment, the inner segment, the cell body and the synapse. The photopigment is located in the outer segment. The inner segment contains cellular metabolic machinery and the energy is used for phototransduction. The segments connect to the post-receptoral neurons through their base synapses. The shapes of the rods and cones are different: the rods are cylindrically shaped, whereas the cones have a pyramidal shape (Figure 1-6 (B)). In the outer segment of the rods, the membrane discs are free-floating, but are attached in the outer segment in cones.

The rods are not only significantly larger than cones, but are also much more sensitive to light. As a result, rod signals contribute more to visual perception than cone signals under low light conditions. The human visual system operates over an enormous range on the order of 10 log units light levels (Boynton, 1979). Rods operate under dim lighting conditions. The Rod-mediated vision, which is referred to as scotopic vision, manifests poor visual acuity (~6/60 vision) and is colour blind. Similarly, the cone-mediated vision shows excellent visual acuity (6/6) and colour vision and is often referred to as photopic vision. Figure 1-7 shows the illumination levels and the scotopic, mesopic and photopic regions. Some studies show that at high light level conditions, the rods become less sensitive and their contribution to visual response eventually diminishes (Aguilar and Stiles, 1954). The extent to which rod signals contribute to visual perception and drive the pupil response at high light level conditions is still under debate.

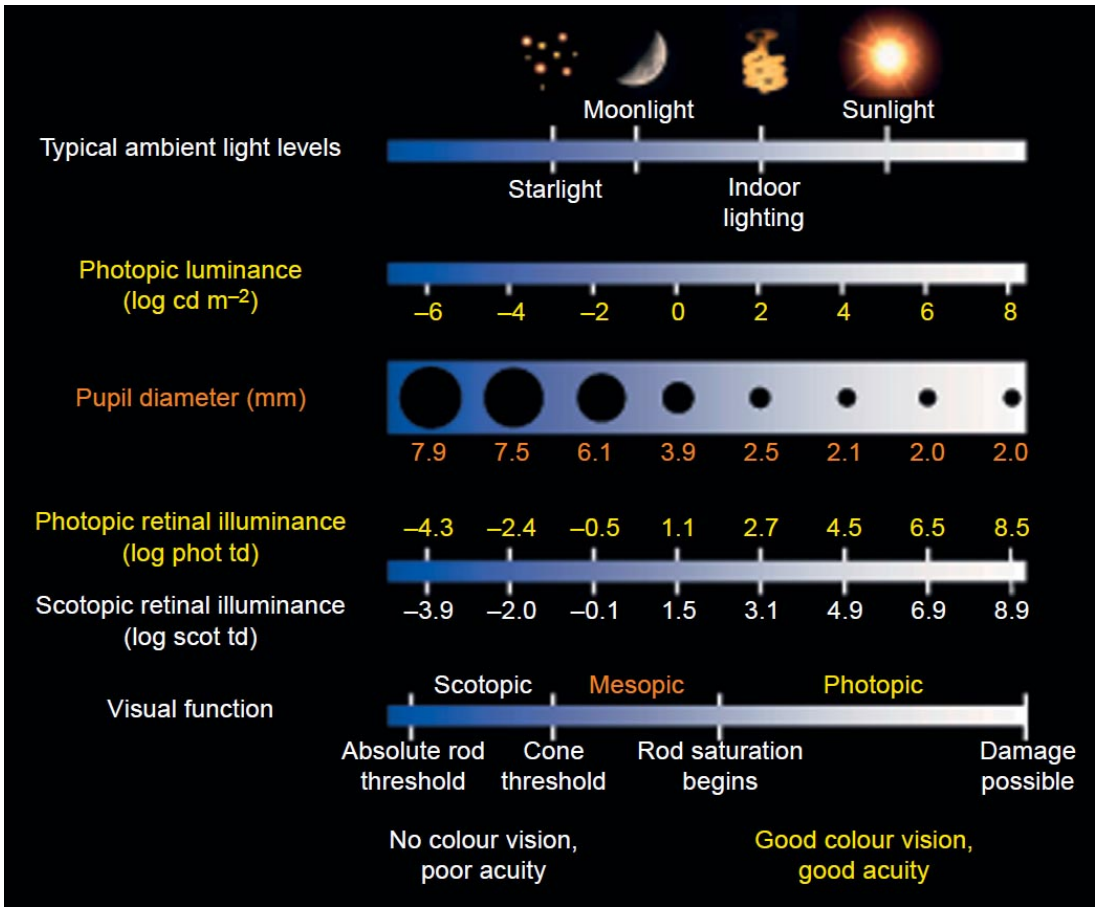


Figure 1-7. Illumination levels, mean pupil size and visual function, adapted from (Barbur and Stockman, 2010). The change in pupil size as indicated in the diagram is taken directly from the above paper. No reference to the original study is given, but similar results have been reported in other studies (Farrell and Booth, 1975).

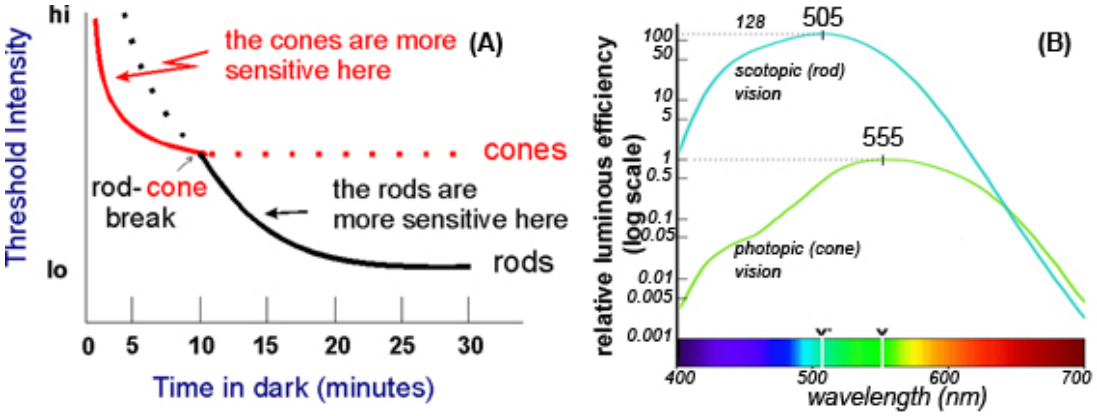

Figure 1-8. (A) Dark adaptation or recovery from light adaptation. The curve shows the increasing sensitivity for light detection with time in the dark and the initial phase reflects the recovery of cones and the second phase that of rods, redrawn from (Bouman and Ten Doesschate, 1962). (B) Spectral sensitivity of cones (green curve) and rods (cyan curve), redrawn from (Kaufman, 1974).

When the light level is high, rods start to saturate and the less sensitive cones become more dominant in mediating vision. Based on the different spectral absorbance, cones are classified into three classes: short-, middle- and long-wavelength sensitive cones or S, M and L cones. The peak absorptance for the L-, M-, S- cones and rods are 560nm, 530nm and 420nm and 495nm, respectively (Dartnall et al., 1983).

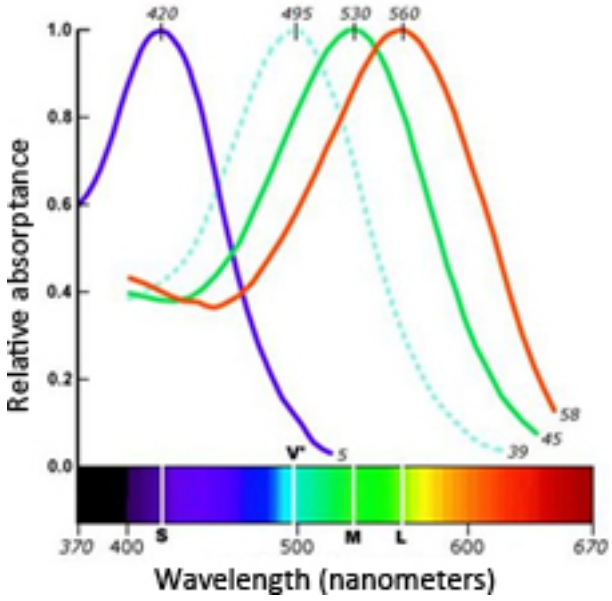


Figure 1-9. The photopigment absorption curves for rods and cones in the human eye. The red, green, blue and the dashed curves are the relative absorptance curves for the L-, M-, S-cones and the rods. The peak absorptances are 560nm, 530nm, 420nm and 495nm, respectively. The visible spectrum is labelled below the diagram as an indication of the perceived colours generated by the corresponding wavelength. Source data from (Dartnall and Bowmake, 1983).

The total number of rods in the eye is significantly larger than the total number of cones. There are approximately 90 to 120 million rods and 4.5 to 7 million cones in each retina (Stiles, 1939, Osterberg, 1935). The spatial distributions of the rods and cones are, however, different. The following figure shows the photoreceptor density for rods and cones as a function of location on the retina.

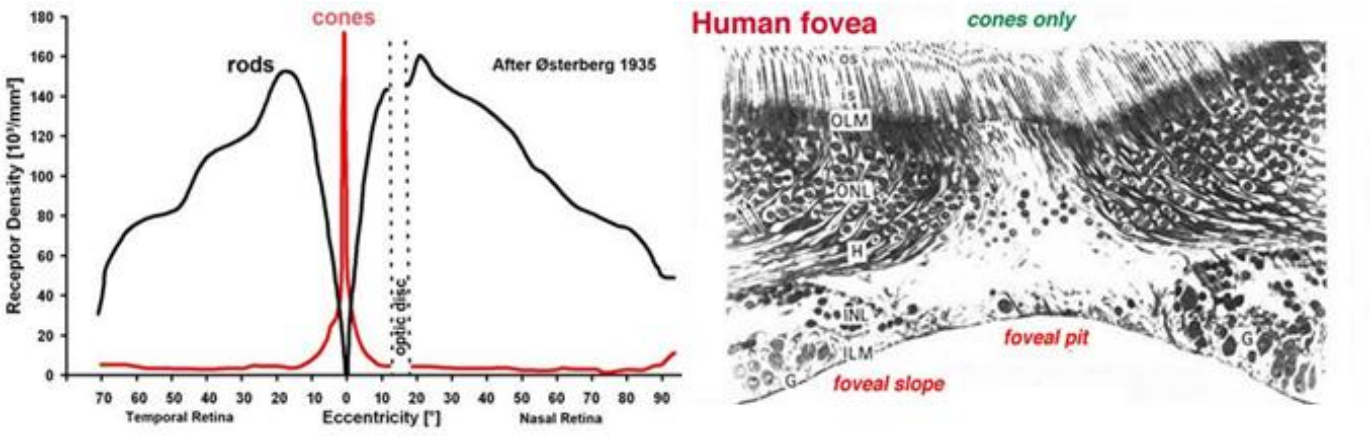


Figure 1-10. Rods and cones density as a function of eccentricity (Osterberg, 1935). The diagram on the right shows a cross section of the human fovea (1cm = 5µm).

In the periphery, the rods are dominant in number and the cones are fewer and are of larger diameter. The density of the rods increases as away from the fovea with a peak of 190,000 rods/mm$^2$ at 20$^o$ eccentricities and drops gradually further in the periphery (Osterberg, 1935). Within the central 20$^o$, the number of rods reduces significantly as the visual axis is approached. The cones are densely packed in the macular region, where spatial resolution is highest. In the foveal region (±2.5$^o$), where contrast acuity and chromatic sensitivity reaches the peak, the rods are largely absent, but the cones, on the other hand, become thinner and form the distinct cone mosaic. Figure 1-11 (a) shows that the L and M cones are densely packed and are dominant in the fovea, whereas the S-cones increase in number

away from the centre, peaking in density at approximately 2000 per $mm^2$ at around 0.1mm to 0.3mm eccentricity (Curcio et al., 1990). The L to M cone ratio can vary significantly amongst individuals with normal vision. Figure 1-11 (b) shows that the L to M cone ratios in 4 subjects can range from 1.1:1 to 16.5:1 (Robertson et al., 1991, Vimal et al., 1989).

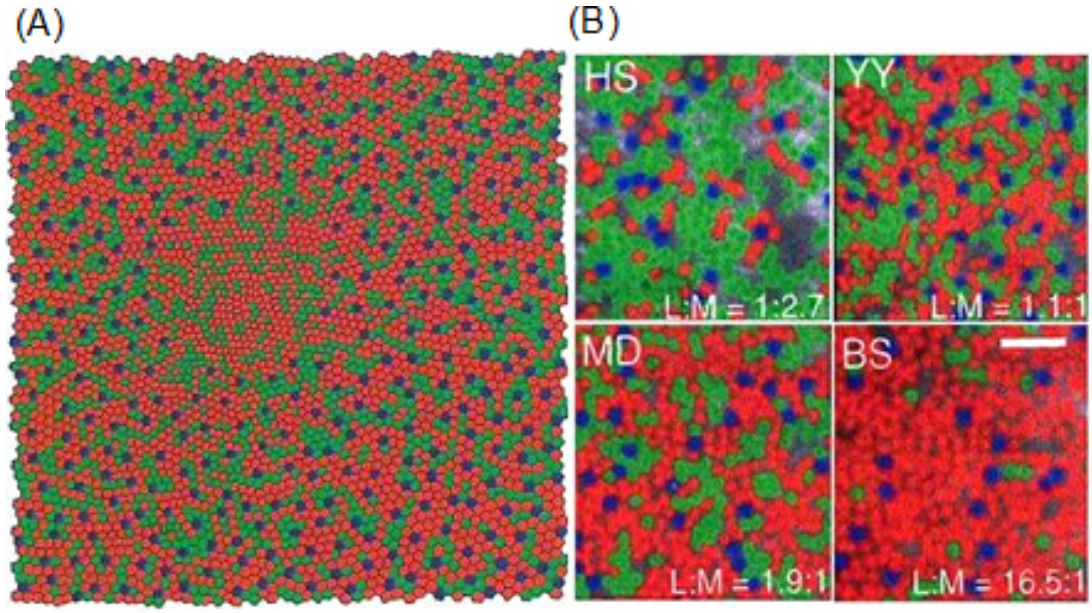


Figure 1-11: (a) Cone mosaic of the rod-free fovea region in a normal trichromatic subject. The S cones are absent in the central foveola (reproduced from Sharpe et al., 1999). (b) An adaptive optics view of the mosaic of L, M and S cones in four normal trichromats, adapted from (Williams and Coletta, 1987).

### 1.1.3 Post-receptoral and post-retinal processing

#### *1.1.3.1 Horizontal & bipolar cells*

In the outer plexiform layer, the photoreceptors synapse with the bipolar cells and horizontal cells. The horizontal cells are laterally interconnected with the photoreceptors. When the horizontal cells receive the visual signal, they become

hyperpolarized and provide a feedback signal back to the photoreceptors, which has an inhibitory effect and cause the photoreceptors depolarization.

The bipolar cells receive visual signals either from rods or cones, but not both. Hence, they are named rod bipolar or cone bipolar cells. The rod bipolar cells synapse with the amacrine cells, and not directly with ganglion cells (Figure 1-12). The cone bipolar cells however make direct synapses on to ganglion cells. These cells also accept synapses from the horizontal cells. After they receive the signals, they pass them vertically to the amacrine cells or to ganglion cells in the inner plexiform layer. Like the horizontal cells, the amacrine cells also introduce lateral inhibition, however, their roles are still not very well understood (Kaneko, 1970, Mills and Massey, 1995).

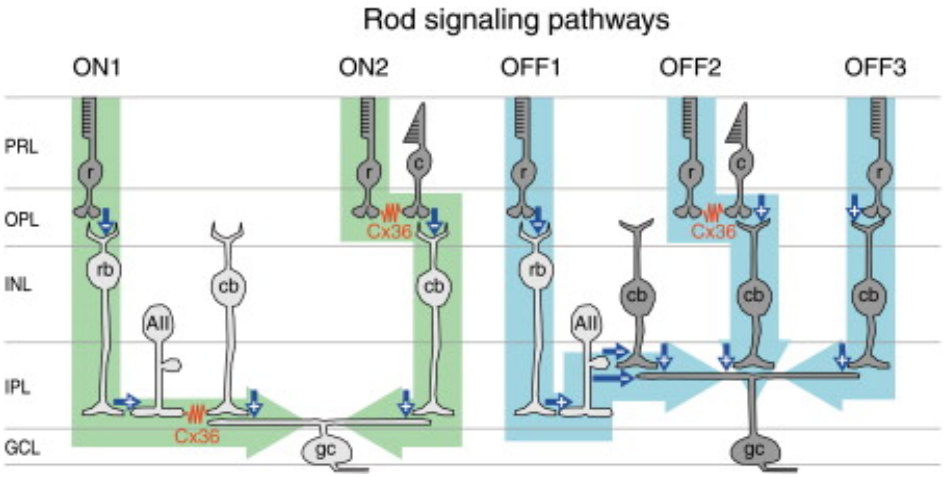


Figure 1-12. Five signaling pathways from rods to ganglion cells (adapted from (Demb and Pugh Jr, 2002)).

#### *1.1.3.2 Ganglion cells (Parasol, Midget ganglion cells and ipRGCs) and receptive field*

The primate retinal ganglion cells are categorized based on the cell body size and the shape of their dendrites. There are more than 20 different types of ganglion cells in the retina (Rodieck, 1998), but the majority of cells can be classed into two major groups – the Midget and Parasol ganglion cells. The Midget and Parasol ganglion cells form the largest distinct groups and project to the Parvocellular and Magnocellular layers of the dLGN, respectively. Unlike other retinal ganglion cells, a small subgroup of retinal ganglion cells are intrinsically photosensitive. These cells contain the photopigment melanopsin and are referred to as ipRGCs. IpRGCs have projections to the dLGN (Pickard, 1985), the Olivary Pretectal Nucleus (OPN) and the Suprachiasmatic Nucleus (SC) (Hendrickson et al., 1972, Pickard, 1985, Berson, 2007). Amongst these three ganglion types, the midget ganglion cells have the smallest cell bodies and least extensive dendrites whereas the ipRGCs exhibit the largest dendrites. The Midget and Parasol ganglion cells account for approximately 80% and 10% respectively of the total ganglion cell population, whereas the ipRGCs only comprise 0.2% (roughly 3000~4000 in number). The Midget cells have smaller sizes of dendritic trees and exhibit slow sustained response. They respond to stimuli that have colour changes but respond only weakly to contrast changes (Dacey and Petersen, 1992). The Parasol cells have larger dendritic sizes and they respond to the low contrast stimuli but not very sensitive to colour stimuli (Kaplan et al., 1990, Croner and Kaplan, 1995). The primary type of remaining 10% of ganglion cells are called Bistratified retinal ganglion cells and they have projections to the koniocellular layers in the dLGN. Compared to the midget and parasol ganglion cells, they are much smaller in size; they receive inputs from intermediate

number of rods and cones; they have moderate spatial resolution and respond to moderate contrast stimuli (Croner and Kaplan, 1995).

The ipRGCs contain a photosensitive pigment called melanopsin. These cells exhibit very slow temporal responses, integrate the ambient light irradiance over a long time course and their sustained depolarisation can be maintained for several seconds after the light offset (Dacey et al., 2005). The major function of the ipRGCs is to photoentrain the circadian rhythm. Some studies in both vivo and vitro have suggested that the ipRGCs play a role in the control of the pupil response, however the contribution melanopsin makes to the dynamic pupil response in human subjects remains controversial. In Chapter 6, we show that the melanopsin driven ganglions do not contribute to the human dynamic pupil light reflex response.

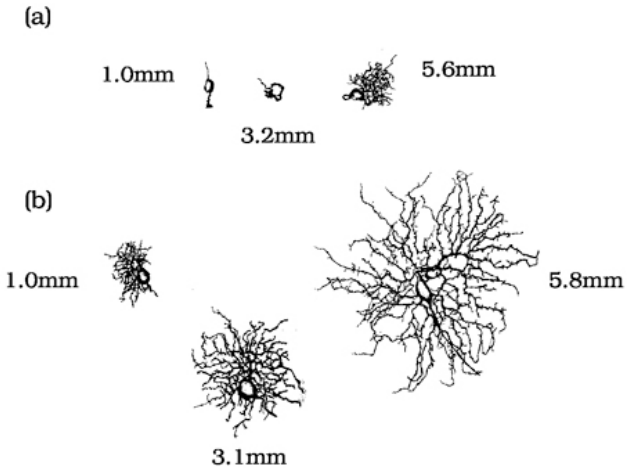


Figure 1-13. (a) Midget and (b) parasol retina ganglion cells from a series of positions within the retina. At the comparable positions, the dendrites of midget ganglion cells are smaller and denser than that of the parasol cells. However, the absolute size of the dendritic field are larger with eccentricity for both types of cells, source from (Watanabe and Rodieck, 1989).

There are about 1.2 to 1.5 million ganglion cells in the human retina, a total that is significantly outnumbered by that of the photoreceptors. So, rather than having a

one to one input from each photoreceptor, they receive visual signals that are integrated in specific areas in the retina, known as receptive fields.

In the periphery, a large receptive field with as many as 120 rods feeds signals to one ganglion cell. The number of the rods is reduced as the fovea is approached. In the fovea region, the cones have a one to one connection, i.e. only one cone is connected with one ganglion cell via one bipolar cell (Rodieck, 1998). As a result, this arrangement ensures that the fovea has the highest spatial resolution and best contrast acuity. The receptive field is roughly circular shaped and has a centre-surround organisation. The ON-centre ganglion cells are named so, because they are excited in the centre and inhibited in the surround, conversely, the OFF-centre ganglion cells exhibit the opposite, with the inhibition in the centre and excitation in the surround.

The centre-surround organisation of ganglion cells ensures that signals from a number of photoreceptors are processed and the output channelled into one ganglion cell and signals are processed (added or subtracted) to form the luminance and colour opponent channels (Hurvich and Jameson, 1957, Hering, 1964). The midget retinal ganglion cells have small sizes of dendritic trees and receive inputs from relatively small number of rods and cones. Most of these cells are connected to the midget bipolar cells and in turn are linked to one cone cell each. These single connections form simple center-surround receptive fields and hence they respond to the changes in high spatial frequencies and colour stimuli. The parasol cells have larger dendrite trees and cell bodies and therefore larger receptive fields which are also center-surround. Due to the large receptive fields, they receive inputs from many rods and cones, hence these cells exhibit large

spatial summation and respond to low contrast changes. More details of how luminance and colour signals are processed are described in section 1.2.

### *1.1.3.3 dLGN*

The ganglion cell axons form the optic nerve fibre layer and exit the retina via the optic disc. The nasal retinal nerve fibres leave the eye, cross over the optic chiasm to the other side, whereas the temporal nerve fibres remain uncrossed (Figure 1-14 (A)). The majority of visual information captured by the eye is transferred to the primary visual cortex in the brain through the dorsal Lateral Geniculate Nucleus (dLGN) via the optic radiations (Hubel, 1995).

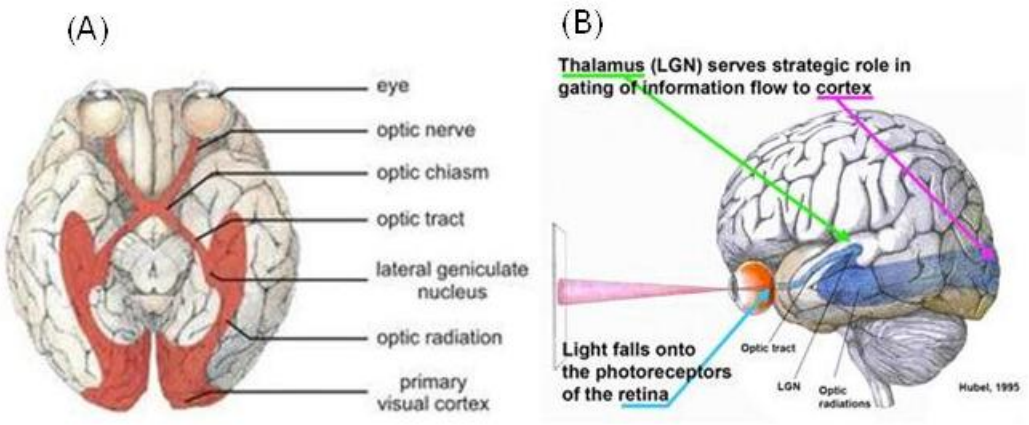


Figure 1-14. (A) The human visual pathway shown from below and (B) side view (adapted from Hubel 1995).

The dLGN acts like a relay and signal processing centre for the visual information before it reaches the visual cortex. The dLGN nuclei receive afferent signals directly from the retinal ganglion cells via the optic tract. The dLGN also receives feedback projections from the primary visual cortex. In mammals, there are two principle pathways linking the eye to the brain: the pathway containing projections to the

dLGN and a separate pathway which carries signals from the retina to Superior Colliculus and other midbrain nuclei (Goodale and Milner, 2005).

In humans, the dLGN is described as having 6 distinctive layers and several interlaminar regions (Kaas et al., 1978). The layers are labelled 1 to 6 from the bottom to top (Figure 1-15). The Magnocellular layers are located in the inner 2 layers and contain cells of large size. The outmost 4 layers are called Parvocellular layers. They have smaller cell bodies when compared with cells in the Magnocellular layers. There is also one additional interlaminar layer located in the ventral area to each of the magnocellular and parvocellular layers and these are often referred to as the koniocellular layers (Carlson, 2007). The koniocellular layers have the smallest cell size. Previous studies suggest that neurons in the koniocellular layers form a third pathway from the retina to the visual cortex (Casagrande, 1994, Casagrande, 1999). Projections to the interlaminar regions from a small number of bistratified ganglion cells that mainly carry the signals from the S-cones have been found in previous studies and these findings suggest that the koniocellular pathway may be linked to the yellow/blue colour processing channel (Dacey and Lee, 1994).

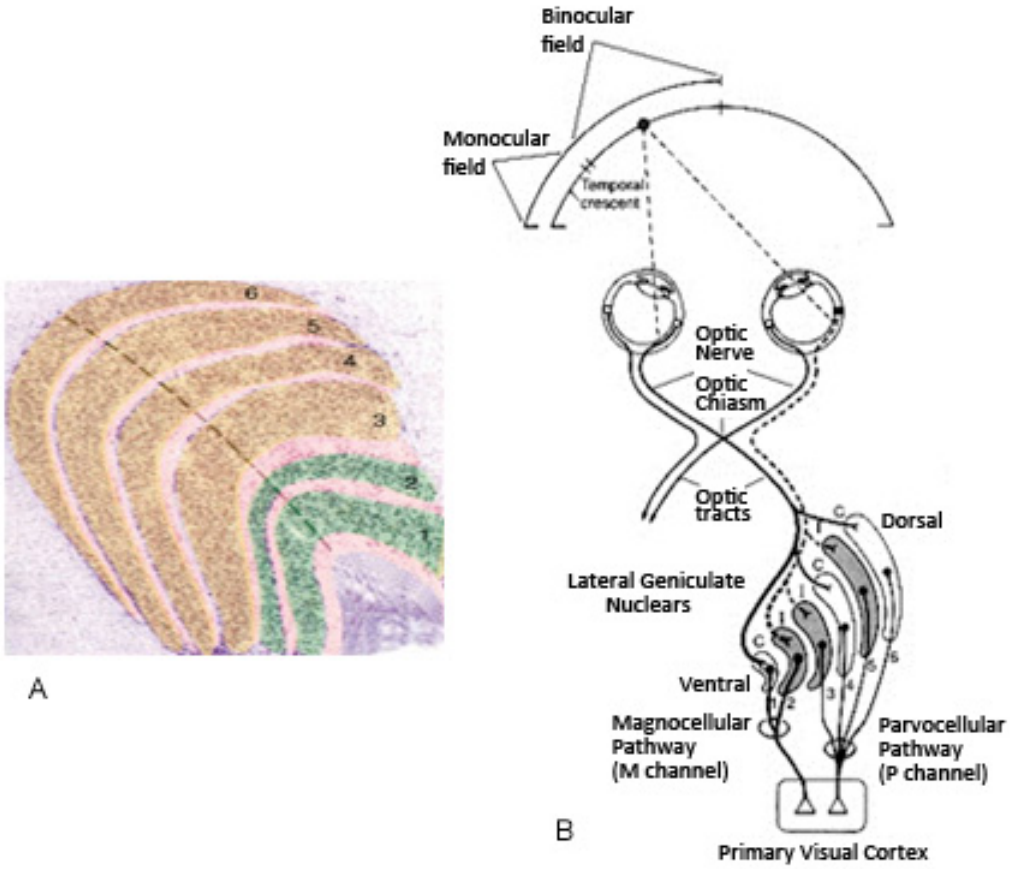


Figure 1-15. (A) The six layers in a cross section of a dLGN in the human thalamus: the Magnocellular layers are layer 1 and 2 (inner most layers and labelled in green on the figure); the Parvocellular layers are layer 3, 4, 5 and 6 and are labelled in yellow. Each layer receives monocular input. (B) Pathway of nerve signals from the retina to the striate cortex in the brain, (source from www.psych.ndsu.nodak.edu).

The parvo layers receive projections from the midget ganglion cells. Like the m-type ganglion cells, the parvo nucleus have small receptive fields and respond to fine spatial detail, colour and slow motion information. On the other hand, the p-type ganglion cells project to the magno layers (1 and 2). The receptive fields of cells in these layers are larger and are very sensitive to motion and dynamic luminance contrast changes.

Each layer of the dLGN receives segregate visual information from each eye. Neurone signals from the contralateral eye, mapping the nasal side visual field, project to layers 1, 4 and 6, whereas the temporal field fibres from the ipsilateral eye terminate in layer Layers 2, 3 and 5 after decussation at the optic chiasm (Kupfer et al., 1967). The visual information gathered from layers in dLGN is then transferred to the visual cortex. This segregation arrangement might be processed and integrated in a certain way in higher order brain areas, where the appropriate combination of the visual signals from different eyes allows for extraction of depth information.

#### *1.1.3.4 From dLGN to the brain*

After the dLGN, visual signals are transferred to the primary visual cortex (V1) in the occipital lobe via the optic radiations (Figure 1-14 (a)). There is a visual cortex in each hemisphere of the brain. The visual cortex in the left hemisphere receives visual information from the right visual field whereas the right visual cortex obtains inputs from the left visual field.

Figure 1-16 shows an unfolded striate cortex and its corresponding visual field mapping. The whole visual field is mapped very nonlinearly on the primary visual cortex, with the small central fovea region occurring a large region of V1, and this is known as cortical magnification. Conversely, the large periphery visual field is only mapped in a very small portion of V1.

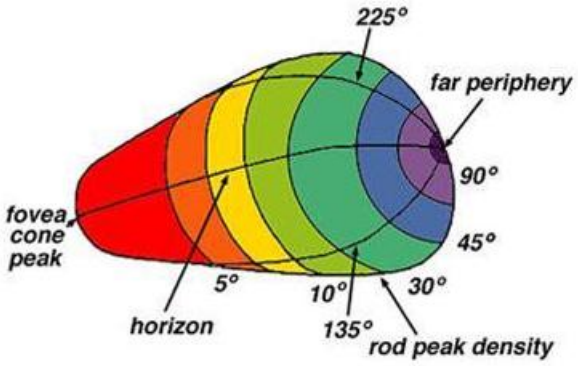


Figure 1-16. The unfolded striate cortex showing the projections from corresponding visual fields of the retina (Erwin et al., 1999).

In a typical adult human, there are approximately 140 million neurons in the primary visual cortex in each side (Leuba and Kraftsik, 1994). When the neurones in V1 are responsive to the same type of stimulus properties, e.g. luminance, orientation or colour, they are arranged together in parallel columns perpendicular to the surface of the brain and they are referred as columns (Figure 1-17). Smaller structures in the columns are known as blobs and the areas between them are called interblobs. Parallel to the surface of the brain, the primary visual cortex can be divided into six principal distinct layers, labelled from 1 to 6. The dLGN projects most visual signals to layer 4, which can be further divided into 4 functional layers, labelled as 4A, 4B, 4Cα and 4Cβ. The magnocellular and parvocellular layers of the dLGN project to the layer 4Cα and 4Cβ respectively (Schwartz, 2004).

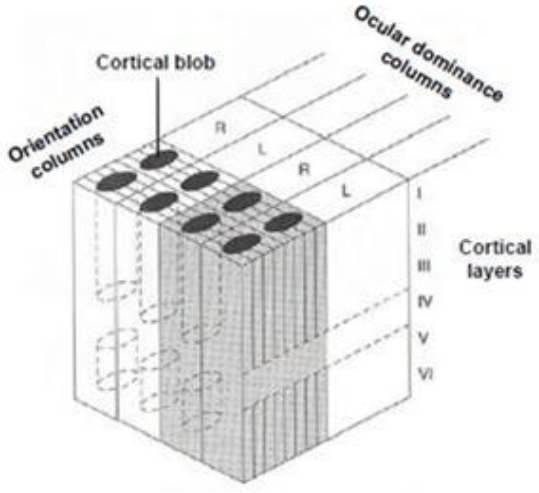


Figure 1-17: The structure of the striate cortex, showing blobs and orientation columns. R and L indicate the corresponding right and left eye (adapted from Schwartz 2004).

V1 processes the visual signals from dLGN and then distributes them to the extra striate cortical areas in the brain for further processing (Lennie, 1998). Based on the functions of extra striate cortical area, they are labelled as V2, V3, V4 and V5 (also known as MT– middle temporal cortex). Area V2 is also called prestriate cortex and it is located adjacent to V1. Results from electrophysiological recordings have shown that the cells in V2 exhibit direction and orientation selective properties (Shipp and Zeki, 1985). In addition, some cells in V2 do not show any responses in relation to monocular simulations, but are active to binocular simulations (Ts'o et al., 1986, Hubel and Livingstone, 1987). The clear role of V3 is still not very well understood, because cells in V3 lack distinctive visual characteristics and respond to a wide range of stimuli. Recordings from area V3 suggested that the majority cells were responsive to lines of specific orientation and they are also colour selective (Zeki, 1978, Felleman and Van Essen, 1987, Gattass et al., 1988). Area V4 receives some direct input from the pale and thin stripes in area V2 via the parvocellular and V1 pathway and cells in area V4 are primarily colour selective

(McAdams and Maunsell, 1999, Desimone and Schein, 1987). Other studies also suggested that patients with damage of lesions in V4 would show a loss of form and shape discrimination (Heywood and Cowey, 1987). Area V5 receives input from V1, V2, V3 and V4 and it is thought to play an important role in the perception of motion (Albright, 1984, Dubner and Zeki, 1971). Lesion studies have also supported the role of V5 in motion perception. Neuropsychological studies of patients with damage in the V5/MT area reported seeing no motion, but a series of static pictures (Hess et al., 1989, Baker Jr et al., 1991). However, other studies suggested that patients with primary visual fields loss could have motion discrimination spared in their blind visual fields.

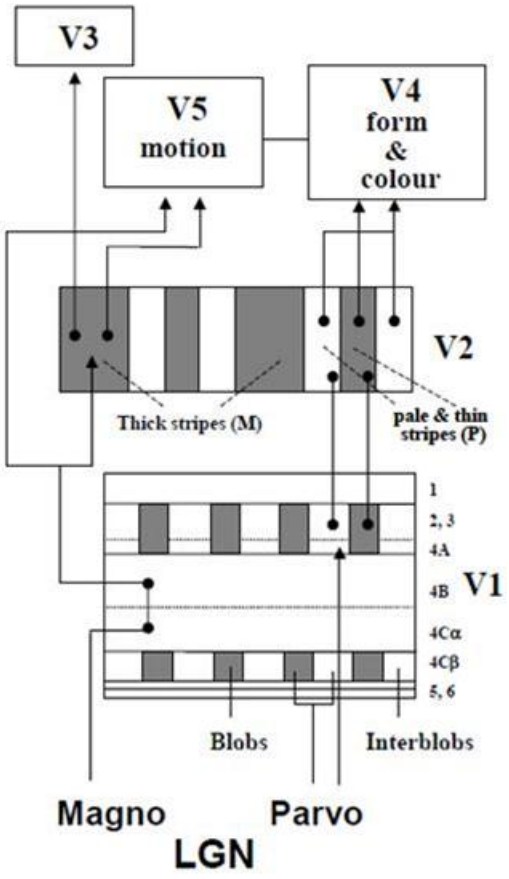

Figure 1-18. Laminar organisation in V1 and projections to other cortical visual areas, adapted from (Maunsell and Newsome, 1987).

Figure 1-18 shows a possible model of the functions for the different areas in the visual cortex. After the dLGN, visual signals are passed to the primary visual cortex (V1). Next, V2 receives a major input from V1 and then the signals are transferred further to higher areas, like V3, V4 and V5. Studies suggest that V2 might be related to the integration of signals from the two eyes that leads to binocular vision (Lennie, 1998, Leopold and Logothetis, 1996), V3 might be responsible for processing form and texture information (Zeki, 1978, Knierim and van Essen, 1992), V4 has been associated mostly with the processing of colour signals (Shipp and Zeki, 1995, Shipp and Zeki, 1985, Lueck et al., 1989) and V5 (MT) neurones respond preferentially to moving stimuli (Maunsell and Newsome, 1987, Allison et al., 1994, Barbur et al., 1993).

## 1.2 Colour vision

Colour vision codes change in the spectral reflectance of illuminated objects. The colours we perceive reflect largely the characteristics of light, i.e., wavelength or frequency. The perception of colour differences is however more complex, largely because of colour constancy which enables us to perceive largely invariant colours under changes of illuminant. The visible light wavelength for a human subject with normal colour vision ranges from 380 nm to 750 nm.

### 1.2.1 Normal trichromatic colour vision

In humans, normal colour vision is referred as trichromatic, because the colour signal processing starts with the three photoreceptors in the eye that respond optimally to different wavelengths.

As mentioned in the photoreceptor section (1.1.2.1), the 3 types of cones have different spectral responsivities. The spectral responsivities of cone photoreceptors are often based on measurements of spectral absorption of single cones. This is done using retinal densitometry, microspectroscopy and suction electrode recordings. Psychophysicists use psychophysical experiments, such as colour matching experiments, to measure spectral sensitivities. Figure 1-19 shows the normalized photoreceptor spectral sensitivity functions measured by Stockman and Sharpe (2000).

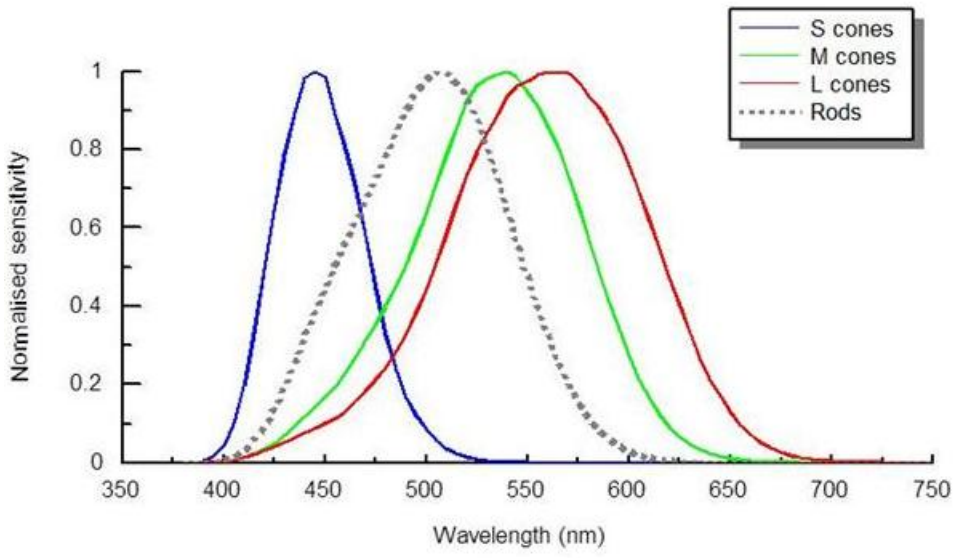


Figure 1-19. The normalized spectral sensitivity for L-, M- and S-cones and Rods (Stockman and Sharpe, 2000). In their data, the peak sensitivities for the L-, M-, S-cones and the rods are 565 nm, 540 nm, 445 nm and 507 nm. (The source data obtained from http://www.cvrl.org).

There are 2 colour processing channels and they are always referred to as the Red-Green and Yellow-Blue channels (or RG and YB). This approach is often linked to the colour opponent theory which is firstly proposed by Hering in 1892. The theory suggests that the colour signal is obtained by comparing the different signal strength from the different cone types. The subtraction of the L and M cone signals gives the Red-Green chromatic channel whereas the sum of the L and M cone signals and subtraction of the S cone signal strength gives the Yellow-Blue chromatic channel. Figure 1-20 shows a schematic diagram for the colour opponent theory. It also postulates a luminance signal which is derived by summing the L and M cone signals.

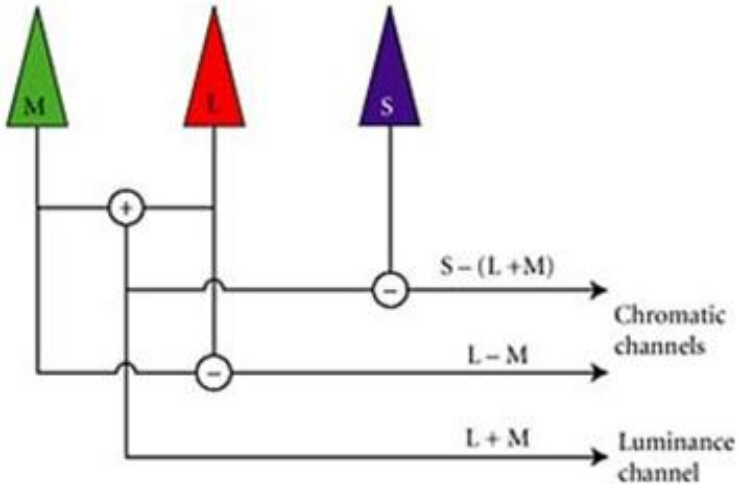


Figure 1-20. A schematic diagram shows the colour opponent model for a normal trichromat.

### 1.2.2 Anomalous trichromacies, dichromacies and monochromacies

There are about 0.4% of females and 8% of males that have colour deficiency in the population (Birch, 2001, Cassin et al., 1990). Compared to the normal trichromats, there are people who also have 3 different classes of cones in the eye, but they

perceive colours differently. Such subjects are usually referred to as anomalous trichromats. Amongst all the colour deficiencies, tritan deficiencies are the rarest.

| Type of deficiency | Males (%) | Females (%) |
|---|---|---|
| Protanopia (P) | ~1.01 | ~0.02 |
| Protanomalous trichromatism (PA) | ~1.08 | ~0.03 |
| Deuteranopia (D) | ~1.27 | ~0.01 |
| Deuteranomalous trichromatism (DA) | ~4.63 | ~0.36 |
| Tritan deficiencies | 0.2% to 0.01% | |
| Total | ~7.99% | ~0.42% |

Table 1-1. Congenital colour deficiencies in the population. The males are dominating the colour deficient group, with a total percentage as high as 8% in the population. On the other hand, there are only 1 in 200 females subjects that are colour deficient. (adapted from Wright, 1952, Went and Pronk, 1985, Sharpe et al., 1999, Birch, 2001). The results obtained for the Tritan deficiencies vary among studies.

The anomalous trichromacies are divided into three subgroups: protanomaly (PA), deuteranomaly (DA) and tritanomaly. Anomalous trichromats usually have one type of cone that carries abnormal (hybrid) pigment, which replaces the original cones. Protanomaly, deuteranomaly and tritanomaly refers to presence of abnormal L-, M- and S- cones. Because the abnormal cones have a different spectral sensitivity, the colour signals generated differ in strength when compared to a normal trichromat. This will eventually cause differences in chromatic sensitivity.

Protanomaly is also always referred as “red-weakness” (Taylor and Clemente, 2005). Any redness seen by a normal trichromat appears less so to a protanomalous subject, both in terms of its chromatic saturation and brightness. Similarly, deuteranomaly can be referred as “green-weakness” and deuteranomalous subjects are poor at discriminating chromatic difference in the green, yellow, orange and red region of the spectrum. However, deuteranomalous subjects do not exhibit the loss of brightness for long wavelength light. This is

because their luminosity curve is very similar as that of normal trichromats (Figure 1-22). Figure 1-21 shows a schematic diagram of a deuteranomalous subject's L-, M- and S- cone spectral sensitivity curve.

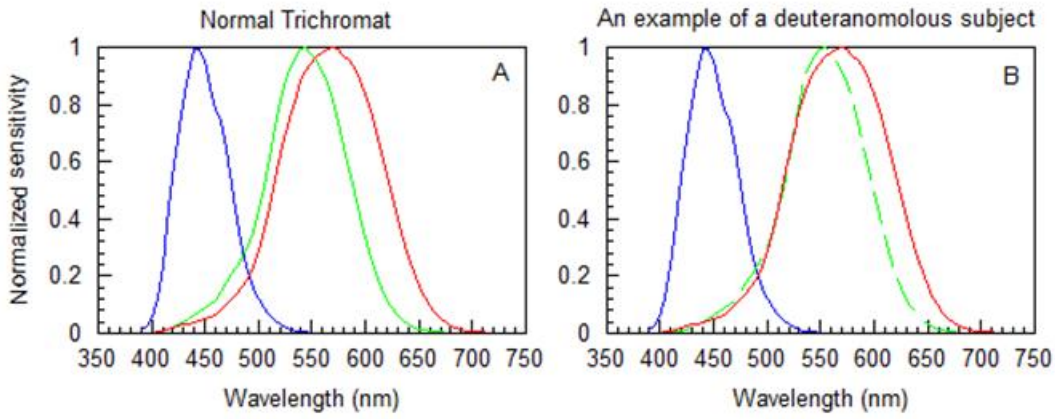


Figure 1-21. A schematic diagram shows the different spectral sensitivity function from a normal trichromat (A) and from a typical deuteranomolous subject (B). The deuteranomolous subject has abnormal M cones (L') which are shifted towards the L cones. The abnormal spectral sensitivity is drawn in dashed green line. The level of deuteranomaly depends on how far the spectral sensitivity of abnormal cones shifts.

### 1.2.3 Dichromacies & Monochromacies

People who lack one type of cone class completely are referred as dichromats. Protanopes have absent L cones, Deuteranopes lack M cones and Tritanopes have absent or non-functional S cones. People who only have one type of cone class are known as cone monochromats. There are also people who only have rods with cones being completely absent from the eye. These people are referred as rod monochromats.

Colour deficiency not only affects colour vision, but also causes changes in perceived brightness. Brightness is a very subjective attribute and cannot easily be

measured. Luminance, on the other hand, is the nearest measurable quantity to perceived brightness. Luminance depends on the signal strengths from the L and M cones, which is determined by the photopic luminosity function or V(λ). Because most colour deficient subjects have abnormal or absent L or M cones, the summed signals from L and M cones are different. Hence, their luminous functions are also different. Figure 1-22 shows the photopic luminosity function measured on a few normal and dichromatic subjects (Brown and Wald, 1964).

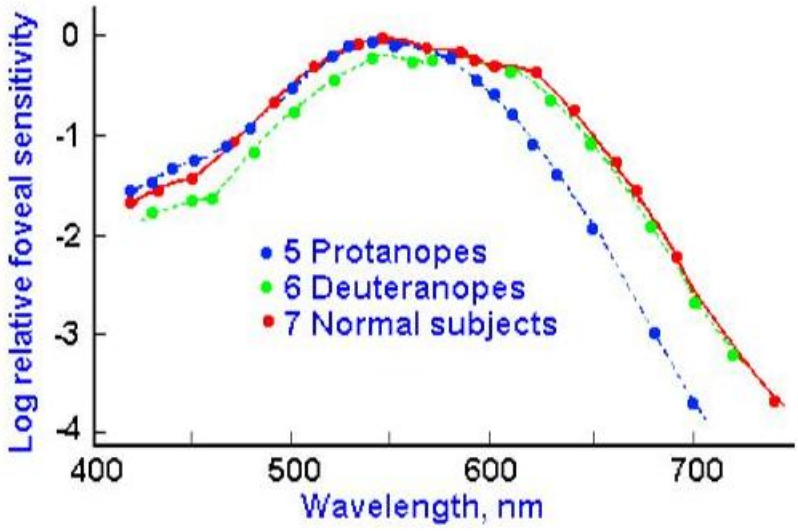


Figure 1-22. Luminosity curves of colour-blind and normal subjects. Downward in the graph represents loss of sensitivity, the log of the reciprocal of threshold energy (adapted from Brown and Wald 1964).

## 1.3 The function of pupil

The pupil of the eye acts like an aperture in a camera system. Its primary function is to adjust the amount of light entering the eye. The size of the pupil also affects the depth of field and the amount of spherical aberrations and coma in the eye. A relative larger pupil size allows more light to go into the eye, but provides less

image quality due to a shorter depth of field and more aberrations, whereas a smaller pupil size has a better image quality by having a larger depth of field and less aberrations (Oyster, 1999, Campbell and Gregory, 1960).

The mean pupil size in humans is affected by many factors and can range from 2mm to 8mm. The most significant factors are listed in Table 1-2. A single dilated pupil could indicate a brain injury, stroke or tumour. Pupil response disorders can reflect brain damage or diseases and have been labelled clinically as Anisocoria, Horner's syndrome, Parinaud's syndrome, etc.

| Factors affect pupil size | Note |
|---|---|
| Age | The mean pupil size reduces when one grows older (Birren et al., 1950). |
| Ambient light level | The ambient light level determines largely the steady-state pupil size which follows a non-linear function (Atchison and Smith, 2000). |
| Light flux | A rapid illumination change causes a transient pupil constriction which is referred as dynamic pupil light reflex response. The PLR is mediated primarily by dorsal areas in the mid-brain (Lowenstein et al., 1964) and may also involve the primary visual cortex (Barbur, 2004b). |
| Near reflex | The pupil size decreases when the fixation is shifted from far to near objects to increase depth of field, |
| Sleepiness and fatigue | Sleepiness and fatigue reduce the size of pupil and also cause oscillations of the pupil (Yoss et al., 1970). |
| Circadian rhythms | Loving (1996) and Wilhelm (2001) showed that the pupil size always peaks in a regular 24 hour cycle. |
| Drugs | Some drugs can cause the pupil to either dilate or constrict, such as Epinephrine, Tropicamide, Pilocarpine, Guanethidine, etc. More extensive studies on the drug effects to the pupil are given elsewhere (Alexandridis et al., 1985, Thompson, 1992, Oyster, 1999). |
| Psychological factors | Many psychological factors affect the size of the pupil, such as attention, alertness, mental workload, pleasantness and other emotions (Van Orden et al., 2001, Wilhelm et al., 1996) |

Table 1-2. Some significant factors that affect the pupil size.

### 1.3.1 Anatomy of the iris – sphincter and dilator muscles

The size of the pupil is constantly regulated by two types of antagonistic muscles – the sphincter muscle and the dilator muscle.

The sphincter muscle is innervated by the parasympathetic system and it encircles the border of the pupil. Its contraction causes the pupil to constrict. On the other

hand, the dilator lies radially from the sphincter and is innervated by the sympathetic fibres. The action of the dilator muscle causes the pupil to dilate (Loewenfeld and Lowenstein, 1993).

### 1.3.2 Pupillary pathways

By differentiating the directions of the signals, the pupil pathways can be categorized as the ‘Afferent pupillary pathway’ and the ‘Efferent pupillary pathway’. The afferent pathway carries the visual information flowing from the eye to the brain, whereas in the efferent pathway the brain receives and processes the afferent signal and then sends a response signal back to the pupil.

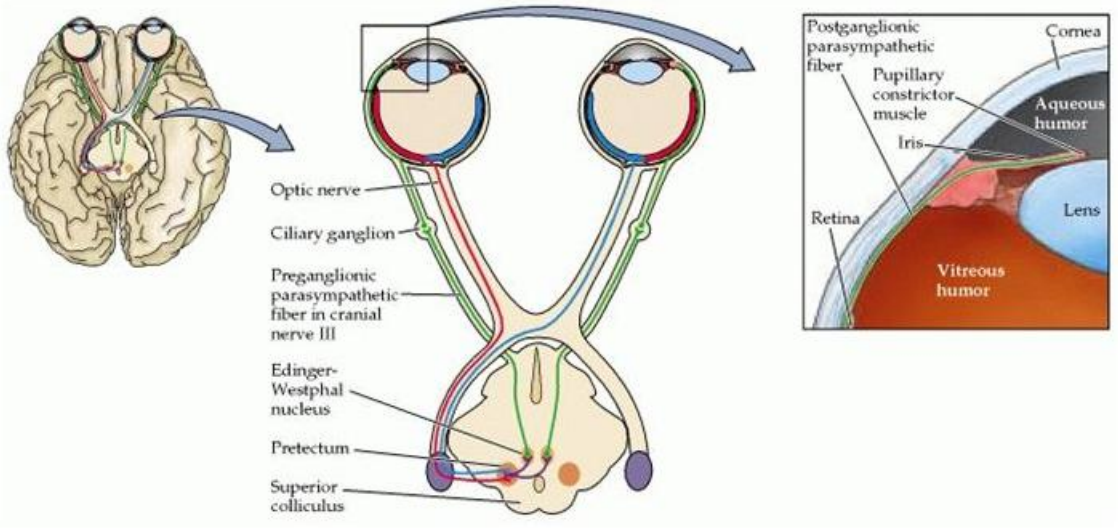


Figure 1-23. The parasympathetic pupil response pathway. The afferent pathway is drawn in blue and red lines and efferent pathway is shown by the green line, redrawn from (Loewenfeld and Lowenstein, 1993)

The classical pupillary pathway to the midbrain is shown in Figure 1-23. When the light is captured by photoreceptors in the eye, the visual signals are processed and transported through ganglion cells along the optic nerve and, after crossing over at

the optic chiasm and before reaching the LGN, part of the visual signal diverts via pupillary fibres to innervate the Olivary Pretectal Nuclei (OPN) in the midbrain via the brachium of the superior colliculus. The OPN then sends these signals to the Edinger-Westphal (EW) nuclei, from where the efferent signals are sent to iris sphincter muscle after synapsing with the ciliary ganglion (CG) (Alexandridis et al., 1985).

Evidence shows that only the light flux signals that project to the midbrain contribute to the pupil responses. Wilhelm (2002) reported that patients with Parinaud's syndrome (dorsal midbrain damage) had absent pupil light reflex responses, however pupil responses to colour, motion and gratings were preserved (Wilhelm et al., 2002).

Barbur (2004) proposed a more extensive pupil response mechanism based on various experiments and observations and he concluded that, besides the classical pupil pathway to the midbrain, the cerebral cortex, V1, V2, V3, V4 and MT all contributed to pupil responses (Barbur, 2004b). Based on his model (redrawn in Figure 1-24), many results can be explained. Those with Parinaud's syndrome have a damaged OPN in the midbrain, and therefore the pupil responses to light flux responses are absent whereas signals from the extra-striate regions (V2, V3, V4 and V5/MT) project to the EW and bypass the OPN. Therefore, pupil responses to stimuli that isolate colour and spatial structures (such as gratings) are preserved. Hemianopia patients with half side of primary visual cortex damage have absent PLR responses in the blind hemifield when the stimuli are of low contrast (< 20%) and small sizes. The dynamic light reflex response to briefly presented stimuli requires normal afferent signals to the OPN and the striate cortex. The absence or

abnormal functioning of either one or the other of these pathways causes a loss of the dynamic light reflex response. On the other hand, when visual stimuli cause large changes in light flux, the signals go to the midbrain are large and the pupil yields similar response amplitudes when compared to that of the sighted hemifield.

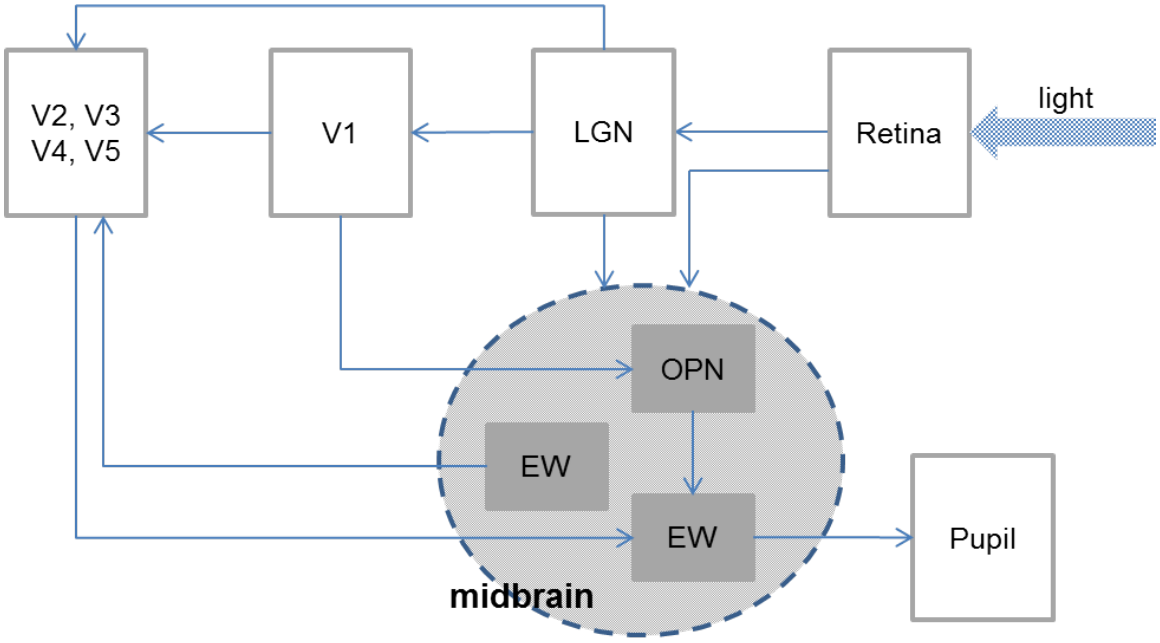


Figure 1-24. Schematic diagram of known pupil pathways. In addition to the main geniculostriate projection, signals from the retina can reach extra striate areas of the cortex, such as V2, V3, V4 and V5, either through small direct projections that bypass V1 (Stoerig and Cowey, 1997) or through indirect projections from midbrain nuclei (such as the superior colliculus (Gross, 1991)), that receive either direct retinal inputs or inputs from the LGN. In addition to the retinal input, the OPN may also receive inputs from the cortex (possibly V1, (Barbur, 2003)). The EW nucleus receives inputs from the OPN and also from extrastriate areas of the visual cortex. The latter may be responsible for the generation of stimulus specific, transient pupil constrictions such as those measured in response to colour, gratings and movement, even when such stimuli cause a net reduction in light flux level on the retina (Barbur, 2004b).

# 2 EQUIPMENT AND METHODS

## 2.1 Introduction

The studies described in this thesis use a number of different experimental techniques that have been implemented on bespoke equipment designed for vision research studies. This chapter describes briefly the various experimental techniques, measurement methods and apparatus developed for such studies. In the following chapters, only the stimuli of interest are described.

## 2.2 Pupillometry

The pupil measurements were performed using the P-SCAN system, which allows the simultaneous, binocular measurement of pupil size and the corresponding 2-D movements of the eye. The statistical methods employed in extracting the parameters of interest are equivalent to fitting the best circle to the pupil, and then the pupil diameter was extracted by calculating the diameter of the circle. The results yield a resolution for the measurement of pupil diameter and eye-movements better than 0.01 mm and 4 min arc brespectively (Barbur et al., 1987, Alexandridis et al., 1991, Barbur et al., 1992).

The P-SCAN system employs bespoke hardware for the processing of the video image and the extraction of pupil size is a computer based system (Figure 2-1). It uses a number of infra-red LEDs to illuminate the eye and captures the pupil image

using an infra-red sensitive CCD camera. The latter has a temporal resolution at 50Hz. The algorithm that is employed to extract the pupil diameter is based on calculating the spatial coordinates of its centre, from intersection points between the circumference of the pupil and a specified pattern of lines.

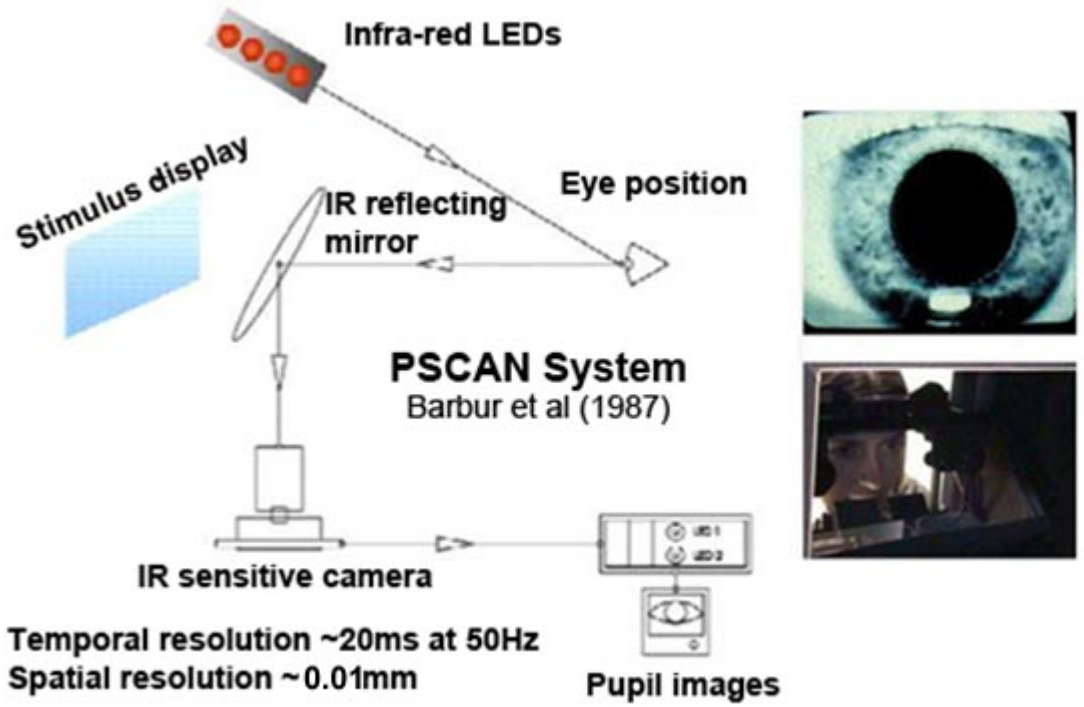


Figure 2-1. A schematic diagram illustrates the structure of the P_SCAN system which is employed to generate various stimulus conditions and measure pupil responses (Adapted from Barbur 1987).

Varies types of visual stimuli can be generated using the P_SCAN system. For example, stimuli with different spatial structures, like sinusoidal/square gratings; achromatic stimuli with different luminance contrasts and isoluminant chromatic stimuli with different chromatic displacement and angles (example stimuli are shown in Figure 2-2). All the stimuli can be modulated with sin/square envelopes with different durations. A spatial and temporal luminance contrast modulation can also be added to any stimulus. Figure 2-3 shows a typical pupil response trace to a

480ms light flash stimulus. The duration of the tests depend on the stimuli employed and the number of tests needed. For the example tests shown in Figure 2-3 with one stimulus and 32 pupil measurements, the test takes about 5 minutes to finish.

Figure 2-2. Two double-isoluminant stimuli that are employed in various studies are shown on the left and in the middle. Both of them are photopically and scotopically isoluminant when presented against the display background. An achromatic sinusoidal grating is shown on the right.

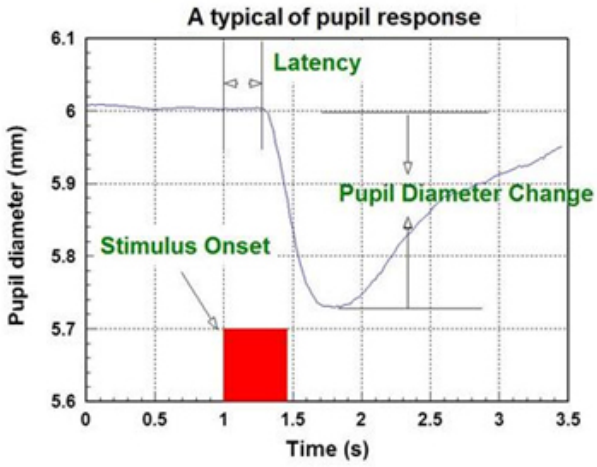


Figure 2-3. A typical pupil response trace to a 480ms light flux increment.

## 2.3 Assessment of Visual Acuity

Figure 2-4 shows the typical Landolt ring stimulus employed in the contrast acuity assessment (CAA) test. The CAA test measures and quantifies the subject's visual

acuity with or without crowding. The test can measure both contrast sensitivity, where the stimulus has a fixed size, but varies in contrast, and visual acuity when the stimulus has high contrast and vary in sizes. The contrast sensitivity is then obtained by calculating the inverse of the contrast threshold for gap orientation discrimination as measured with the CAA test.

The stimulus is presented at the centre of the screen and the stimulus size for correct gap orientation discrimination (i.e., top-left, top-right, bottom-left, bottom-right) is measured using a four-alternative, forced-choice staircase procedure. The subject's task is to press one of the four buttons to indicate the position of the gap in the ring after each presentation (Barbur et al., 2001). Two correct successive presentation responses for the same stimulus eccentricity are needed before the measurement variable (i.e., target size / contrast) is changed. This approach results in a chance probability of 1 in 16.

The properties of the background and the stimulus can be adjusted according to the study. The stimulus shown in Figure 2-4 is generated on a 19" CRT display (LaCie Ltd, London, UK) which subtends $20^o$ x $16^o$ and is presented on a uniform background of a luminance of 26 cd/$m^2$ and chromaticity of 0.2868, 0.3309, as measured in the CIE1931 chromaticity diagram. For a typical visual acuity measurement with one stimulus presented, the test usually takes around 3 to 4 minutes.

Figure 2-4. An example of the contrast acuity stimulus. The stimulus has a fixed contrast of close to -100% for background luminance of 26cd/$m^2$.

## 2.4 Colour Sensitivity Assessment

A broad range of colour vision tests has been developed by vision scientists to examine different properties of colour vision in the past decades. Clinical colour vision assessment tends to rely on the use of a battery of tests, but unfortunately the results are difficult to interpret and are often inconclusive (Squire et al., 2005).

The Colour Assessment and Diagnosis (CAD) test is a novel computer based test which is optimised to detect minimum colour deficiencies and to quantify the severity of colour vision loss by evaluating both red-green (RG) and yellow-blue (YB) thresholds in an internationally recognised colour system. It has been validated and compared with the most commonly used colour vision tests. The results from CAD test are expressed in standard normal units based on mean data obtained in 330 normal trichromats (Rodriguez-Carmona et al., 2005).

Because the luminous efficiency function of the eye varies amongst individuals, the subjects can often detect luminance content signals in coloured stimuli that are isoluminant for the standard CIE observer. To isolate the use of only colour signals,

the CAD test employs dynamic spatiotemporal luminance contrast masking techniques to mask any residual luminance contrast signals that may contribute to the detection of test stimuli (Barbur, 2004a, Barbur et al., 1994b, Birch et al., 1992). The design of the spatial random luminance contrast masking technique (RLMs) is similar to the original pseudoisochromatic plates, where the stimulus is buried into an array of achromatic checks. Although these achromatic checks vary in luminance, the overall luminance generated in the whole stimulus patch is constant and equal to the background luminance. The stimulus condition is often called 'static luminance contrast (LC) noise'. When the temporal random luminance contrast masking technique (RLMt) is used together with the RLMs, the condition is referred to as 'dynamic LC contrast noise'. In the presence of the dynamic noise, the threshold of the first order motion is proportional to amplitude of the dynamic noise employed (Barbur, 2003). If the target has features (such as colour) which are significant from the background noise, the detection of coherent motion becomes independent of the background noise. Therefore, in the CAD test, the CIE isoluminant colour defined stimulus was buried in the dynamic LC noise to mask the detection of any luminance contrast component and to ensure the measured threshold is only from the colour component.

The most commonly used recipe in the CAD test measures chromatic detection thresholds along sixteen hue directions in the CIE1931 chromaticity chart, using randomly interleaved staircases with variable step sizes and a four-alternative forced-choice procedure. Subjects are instructed to view the display from a distance of 2.5 meters and the tests are carried out binocularly at 26 cd/m$^2$. The chromaticity of the background is (0.305, 0.298). The stimulus is generated in the centre of a uniform background field which subtends $28^o$ x $23^o$ and consists of a 15 x 15 square

array of achromatic checks which subtends a horizontal visual angle approximately $3.3^{o}$. These achromatic checks vary randomly in luminance above and below the background every 40 to 80ms, but the overall mean luminance provided is the same as the background. The colour-defined, moving target consists the outline of a square made up of 5x5 checks and subtending approximately $0.8^{o}$ at the eye and moves diagonally through a visual angle of approximately $2.9^{o}$ at a speed of approximately $4^{o}\,s^{-1}$. Spatiotemporal luminance noise is employed in the CAD test to mask the detection of any residual luminance signals so as to ensure that the subject can only make use of colour signals to detect the moving stimulus. The subject's task is to report the direction of motion of the colour-defined stimulus by pressing one of the four buttons located at the corners of a square. When unable to see the stimulus, the subject's instruction was to press any of the four buttons. The colour thresholds were measured using a number of interleaved staircases and the direction of the motion had to be reported correctly twice in a row for the same stimulus before the colour signal was decreased. The probability of randomly guessing a correct response is therefore one in sixteen. The measured thresholds along the RG and YB axes are then averaged to produce mean RG and YB thresholds. The visual stimuli are generated on a LaCie electronblue 19" CRT display (LaCie Ltd, London, UK) with a central fixation point (Barbur et al., 2010). An example stimulus and results for a normal trichromat, deuteranope and protanope from the CAD test are shown in Figure 2-5 & Figure 2-6. The test usually takes about 12 minutes to finish with the most commonly used recipe.

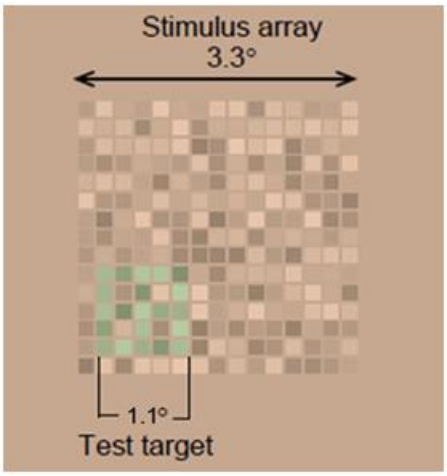


Figure 2-5. An example stimulus from the CAD test.

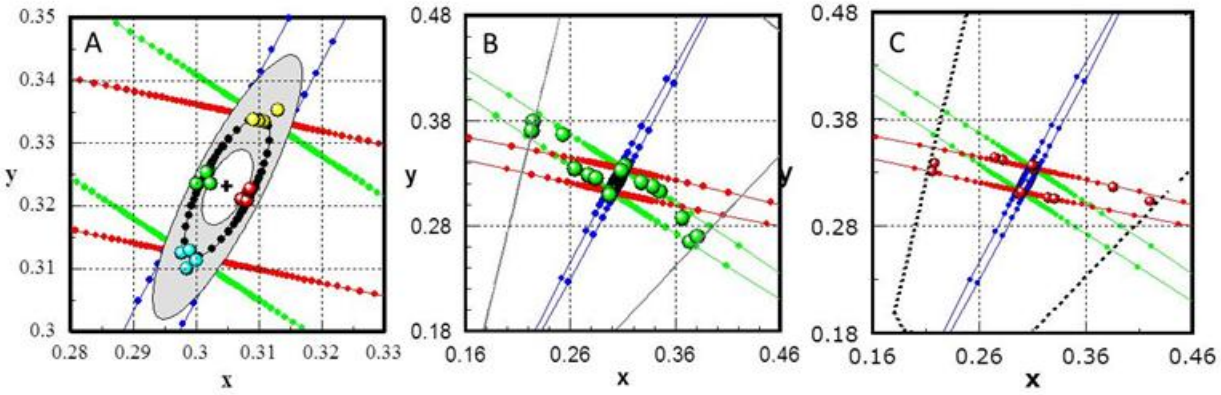


Figure 2-6. CAD test results for a normal trichromat (A), a deuteranope (B) and a protanope (C). The dotted red, green and blue lines indicate the protan-, deutan- and tritan- colour confusion lines. The gray region indicates the normal threshold range and is based on the statistical distribution of RG and YB thresholds measured in 330 normal trichromat (Rodriguez-Carmona et al., 2005). The dotted ellipse shows the medium threshold.

## 2.5 Coherent Motion test

The coherent motion test stimuli are generated using the same program that measures colour sensitivity. Instead of generating the isoluminant stimulus and measuring the CD needed to detect the direction of the stimulus motion, the moving

stimulus can be defined by luminance contrast and so the measured thresholds are the luminance contrasts needed to detect first order motion.

The stimuli can be buried in either static or dynamic luminance contrast noise. Motion detection is primarily mediated by the magnocelluar pathway, which exhibit band-pass temporal properties unlike the P-pathways which exhibit low pass temporal properties. As a result, first order motion thresholds are not affected by static spatial noise. When dynamic noise is used, motion threshold increases monotonically with noise amplitude (Barbur 2008). This is simply because the spatial noise affects the sensitivity of the M-pathway and the subject needs to rely more on the P-pathway to detect the moving stimulus. A typical motion test with one stimulus usually takes 2 to 3 minutes to finish.

## 2.6 Melanopsin apparatus – isolation of melanopsin response

A four-primary illumination system designed by Tsujimura (Figure 2-7) (Tsujimura et al., 2010) was employed to generate visual stimulus that stimulate selectively either cones or rods and melanopsin. The system uses the silent-substitution technique (Pokorny et al., 2004) to selectively stimulate the cones or rods and melanopsin.

The illumination system consists of an optical diffuser illuminated by light from an integrating sphere and subtending a visual angle of $17^{o}$. Four different kinds of light-emitting diodes (LEDs, OptoSupply Ltd, Hong Kong) were employed as internal light sources in the integrating sphere and their light output was controlled by a microcomputer using pulse width modulation (PWM) techniques. The peak output

wavelengths of the four LEDs were 615 nm, 525 nm, 500 nm and 470 nm respectively, with half-height bandwidths of 20-36 nm. An integrated microprocessor was used to control the PWM. The PWM unit is connected with the P_SCAN system. This arrangement allowed simultaneous measurements of the pupil response to the various photoreceptor specific stimuli.

In CIE1931 cone-excitation space, three fundamentals correspond to the excitation of three types of cones and they are specially designed, so that the sum of excitation from the L and M cones is equivalent to the photopic luminous efficiency function V(λ) (Shapiro et al., 1996). In the illumination system, Tsujimura assumes that the S cones, rods and melanopsin do not contribute significantly to the photopic luminosity function. The system uses Stockman & Sharp's 10 degree cone fundamentals (Stockman and Sharpe, 2000) to calculate the excitations of cones and the melanopsin spectral sensitivity from a pigment template nomogram (Dartnall, 1953) with a peak wavelength of 482nm (Govardovskii et al., 2000). The lens and macular pigment density spectra employed are the average function reported by Stockman (Stockman et al., 1999).

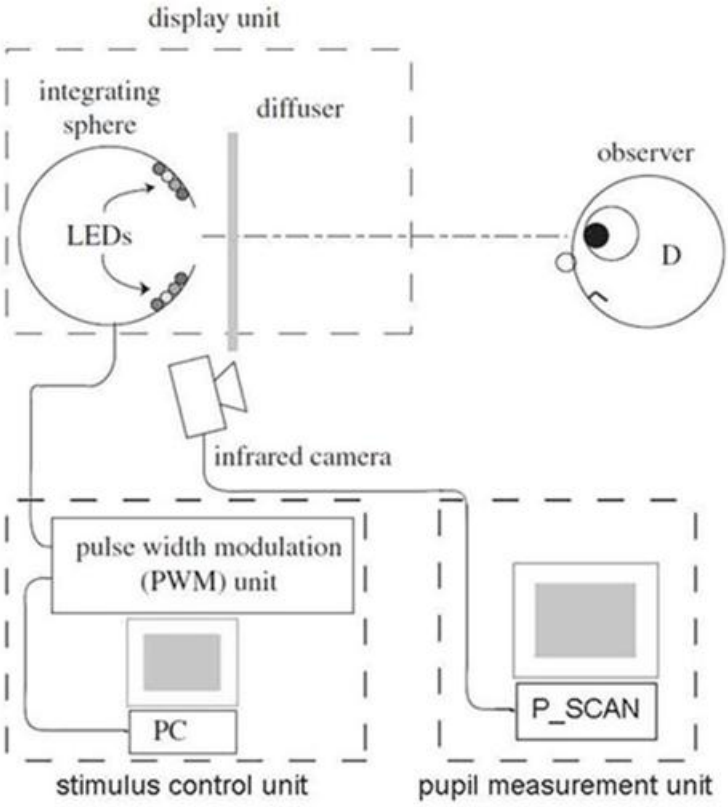


Figure 2-7. A four primary illumination system from Tsujimura (Tsujimura et al., 2010) is employed to isolate photoreceptor responses. The stimulus consists of an optical diffuser, illuminated by an integrating sphere, microcomputer and a PC. The illumination system connects to the P_SCAN system (Barbur et al., 1987) which is used to measure the pupil responses simultaneously (adapted and reproduced with permission from S. Tsujimura).

## 2.7 Quantitative Afterimage Assessment

Patients with palinopsia experience longer persistence of visual images when compared with normal subjects (Bender et al., 1968, Meadows and Munro, 1977). Palinopsia often appears with other visual disturbances such as visual snow and can be attributed to a number of conditions affecting the brain including tumors, visual pathway lesions, medications, etc. However, many patients with palinopsia

and/or visual snow syndrome (VS) have completely normal vision and show no clinical abnormalities. Existing clinical tests fail to detect any signs that could be considered abnormal on these patients. It is of great interest to discover the extent to which the perceived afterimage contributes to visual perception and affects image quality. The first step was to develop a new technique to quantify the strength and duration of perceived afterimages.

The Quantitative Afterimage Assessment test (QAA) is a new computer based vision test that measures the strength and duration of perceived chromatic afterimages. It employs novel psychophysical techniques and was designed to obtain results in a relatively short time.

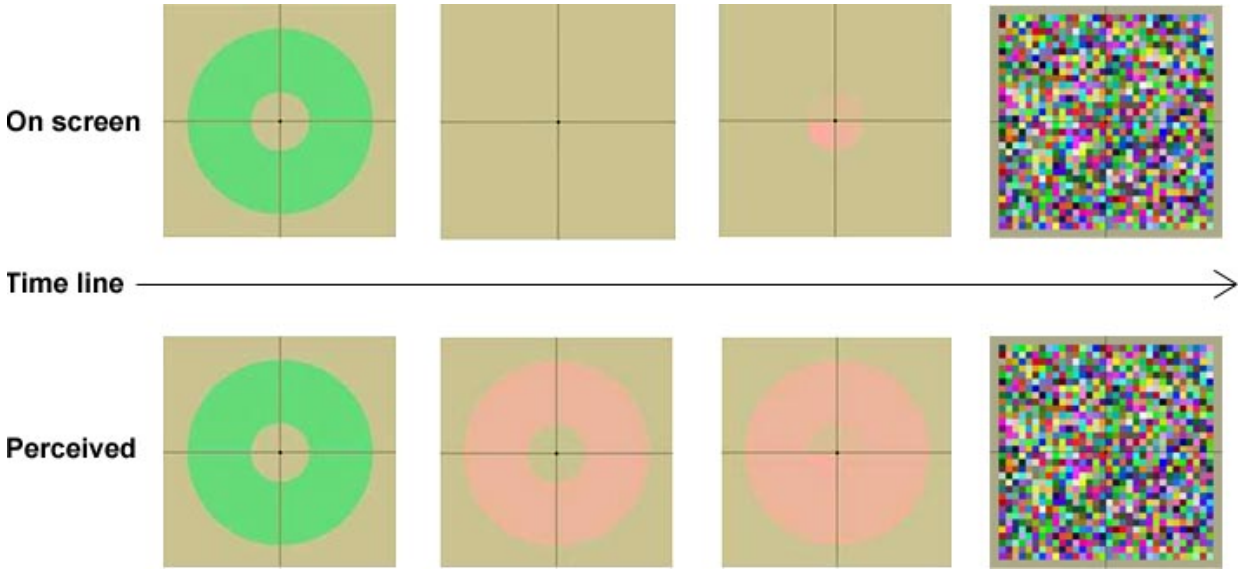


Figure 2-8 A schematic diagram that illustrates the four-alternative forced choice QAA test. The upper show shows the stimulus presentation sequence that is presented on the screen. In a typical QAA test, the reference (adaptation) stimulus is presented for 5s, followed by a blank screen for certain durations according to the gap time. Then the test stimulus is presented. At last, a square patch with random luminance and coloured noise is presented. The bottom row shows an example of perceived images from a trichromat. The trichromat sees the reference stimulus when it is presented on the screen. However, when the reference stimulus is turned off and the blank screen is presented, the subject perceives

a coloured afterimage of the reference stimulus which has an opposite colour of the reference stimulus. At the time when the test stimulus is displayed, the subject perceives the coloured afterimage as well as the test stimulus and the subject's task is to choose which quadrant of the test stimulus matches the most closely to the coloured afterimage. Finally, the random noise is used to minimize or eliminate any perceived afterimages before the next trial.

Figure 2-8 illustrates an example of the displayed real images and the corresponding perceived scene for a normal trichromat. The top row shows the time sequence of the stimuli (reference stimulus, blank screen and the test stimulus) that are displayed on the screen while the bottom row shows the perceived stimuli sequence (bottom row) for a normal trichromat subject. The normal subject firstly perceives the reference stimulus (top left picture), but when the reference stimulus is gone, the subject perceives the negative afterimage of the reference stimulus (middle picture in the bottom row). As soon as the test stimulus (top right picture) is displayed, the subject presses one of the four buttons that corresponds to the quadrant that matches closely the strength of the afterimage the most.

A typical QAA experiment involves two tests: a four-alternative-forced-choice test and a staircase test. Figure 2-8 shows a schematic diagram for the four-alternative-forced-choice afterimage test.

In the four-alternative forced choice test, an approximate threshold is obtained usually within 1 minute. The subject is instructed to look at the fixation located in the centre of the background at all times. When the subject hears the first beep, the reference stimulus is displayed (see top left picture of Figure 2-8). After a period of time, such as 5 seconds, the reference stimulus disappears and the subject perceives the afterimage of the stimulus. Next, the test stimulus will be display followed by a second beep. When the test stimulus is displayed, the smaller test

stimulus and the bigger afterimage form a whole disc. Because the strength (chromatic displacement) of four quadrants in the test stimulus is always different, subjects are asked to select one quadrant in the test stimulus that matches most closely the appearance of the surrounding afterimage.

The algorithm allocates the Chromatic displacement (CD) for the four quadrants that differ significantly from each other and cause as large as ten times the normal colour detection threshold. The four quadrants change their CD values according to subjects' response until the subject select the same answers twice in succession, when the test terminates.

In the typical staircase algorithm, when the approximate threshold is unknown, a large number of reversals are needed (usually > 11). In the QAA staircase test, the start increment value was based on an approximate threshold obtained using the rapid four-alternative-forced-choice test. This procedure reduced the number of reversals needed in the main staircase. 7 reversals were used and the threshold was estimated by averaging the last four reversals. The standard error associated with the last four reversals rarely exceeded 11% of the mean.

The QAA program was developed to investigate the strength of afterimages in subjects with congenital red/green deficiency and also for the use in another related study that involved patients with visual snow and palinopsia syndrome.

# 3 THE DESIGN OF THE QAA TEST

## 3.1 Introduction

The psychophysics part of the QAA application has been described in section 2.7. In this chapter, the implementation of the Quantitative Afterimage test is described. Details of the application are discussed together with the procedure for monitor calibration and the use of the program. Appendix A provides a practical guide to the QAA application project.

In terms of software engineering, the QAA project follows a typical waterfall software engineering development life cycle – requirement analysis, design, implementation, maintenance and testing. The QAA is designed to be highly extendable and reusable. As a standalone psychophysics application, not only does the QAA contain a psychophysics module that measures the duration and the strength of chromatic afterimages, but it provides a fully functional graphical user interface module (GUI) in the front side which allows users to adjust various common stimulus parameters. In addition, it comprises a database module which stores the experiment data and results in the server side and a website portal module which displays selected results based on the user groups. If a new psychophysics program (module) is implemented, such as visual acuity test, it can be integrated into the whole application smoothly with very little changes of the other modules.

## 3.2 Requirements

“The hardest single part of building a software system is deciding precisely what to build. No other part of the conceptual work is as difficult as establishing the detailed technical requirements...No other part of the work so cripples the resulting system if done wrong. No other part is as difficult to rectify later.” (Brooks, 1987)

In software engineering, a typical software development includes a few stages. Laplante once said “Software engineering is a profession dedicated to designing, implementing, and modifying software so that is of high quality, affordable, maintainable, and fast to build. It is a “systematic approach to the analysis, design, assessment, implementation, test, maintenance and reengineering of software, that is, the application of engineering to software (Laplante, 2007).” To be concise, software development usually contains 5 stages: “requirement analysis”, “design”, “implementation”, “testing” and “maintenance”. The first stage of building a computer program is to do the requirement analysis and estimate feasibility. Figure 3-1 shows a typical software development life cycle.

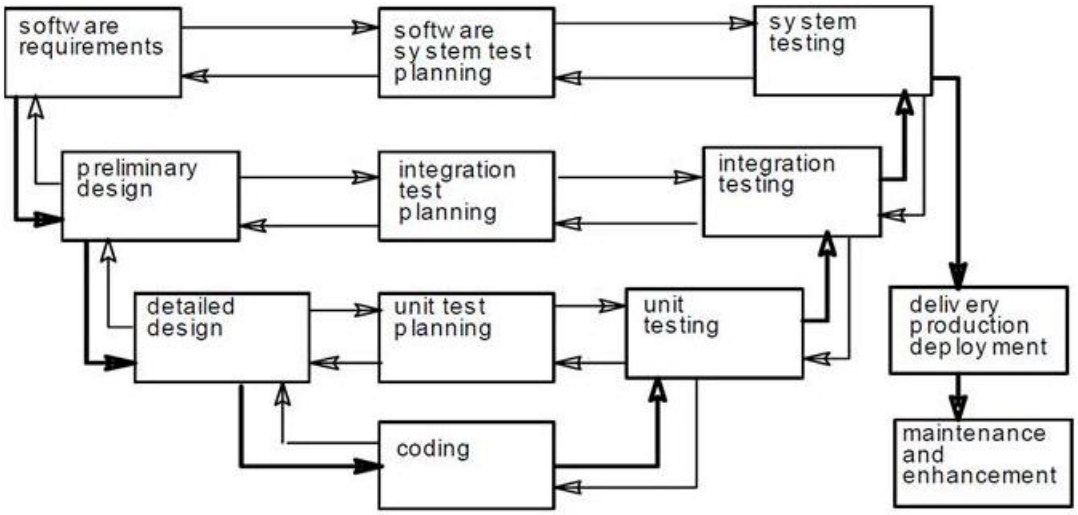


Figure 3-1. Software development cycle. The darker arrows specify the main software development process, adapted from (Faulk, 1995).

The task was to develop a new computer application to measure the duration and the strength of chromatic afterimages. The functional and non-functional requirements are shown below:

### 3.2.1 Functional requirements

The desired application should fulfil the following functions:

1. The application should be able to measure the duration and strength of the afterimages using appropriate psychophysics algorithms. (This section can divided into subsections)
    a. The application should be a computer program which is able to display the stimuli of interest. To the computer, these stimuli are basically shapes and colours drawn on a calibrated screen.

b. The application should be able to respond to users input, i.e., mouse, keyboard or joystick events.
c. Based on the user responses, the application should be able to adjust the presented stimulus at runtime using psychophysics procedures and algorithms.

2. The application should provide an interface for experimenters to set up the desired experiment parameters. E.g., background luminance, stimulus chromaticity, location, duration, shapes, etc.
3. The application must be able to present the desired stimulus in a way that is suitable for psychophysical measurement.
4. The application should provide appropriate views for experimenters, subjects and researchers to read the details of the test results.
5. Different users from different groups should be able to search for a specific subject's results with different views. i.e., the experimenters should be able to view all parts of the result whereas the subjects' views of results are limited. E.g. they might be only able to see if they pass or fail the test or if they have prolonged afterimages.

### 3.2.2 Non-functional requirements

1. When a desired stimulus is specified by an experimenter, any hardware limitations, such as a monitor phosphor's limits, must be taken into account. Monitor calibration has to be done before creating the application.
2. The application should be divided into modules to achieve maximum software reusability.

3. Other modules should be independent of the psychophysics module, so that once a new psychophysics module (such a new contrast acuity test) is implemented, the new module can be integrated into the system with no or very little changes made in other modules.
4. The application should be well designed, so that it can be extended easily.
5. As a vision research experiment that is used to test people and perhaps have the potential to be used clinically, the application should be reliable.
6. The application should have high performance. The adopted algorithm in the application should be optimised to ensure that it is efficient and fast enough to render the desired stimulus on the screen without jitters and lags.
7. The application should be easy to use. E.g., it should have an easy to use GUI, a help menu or a guide.
8. This research project is time constrained and should be finished and preliminary tests carried out in 4 months. Further development should be done according to the preliminary results.

Based on these requirements, the application is feasible within the given time scale. A use case diagram containing the essential requirements is derived and illustrated in Figure 3-2.

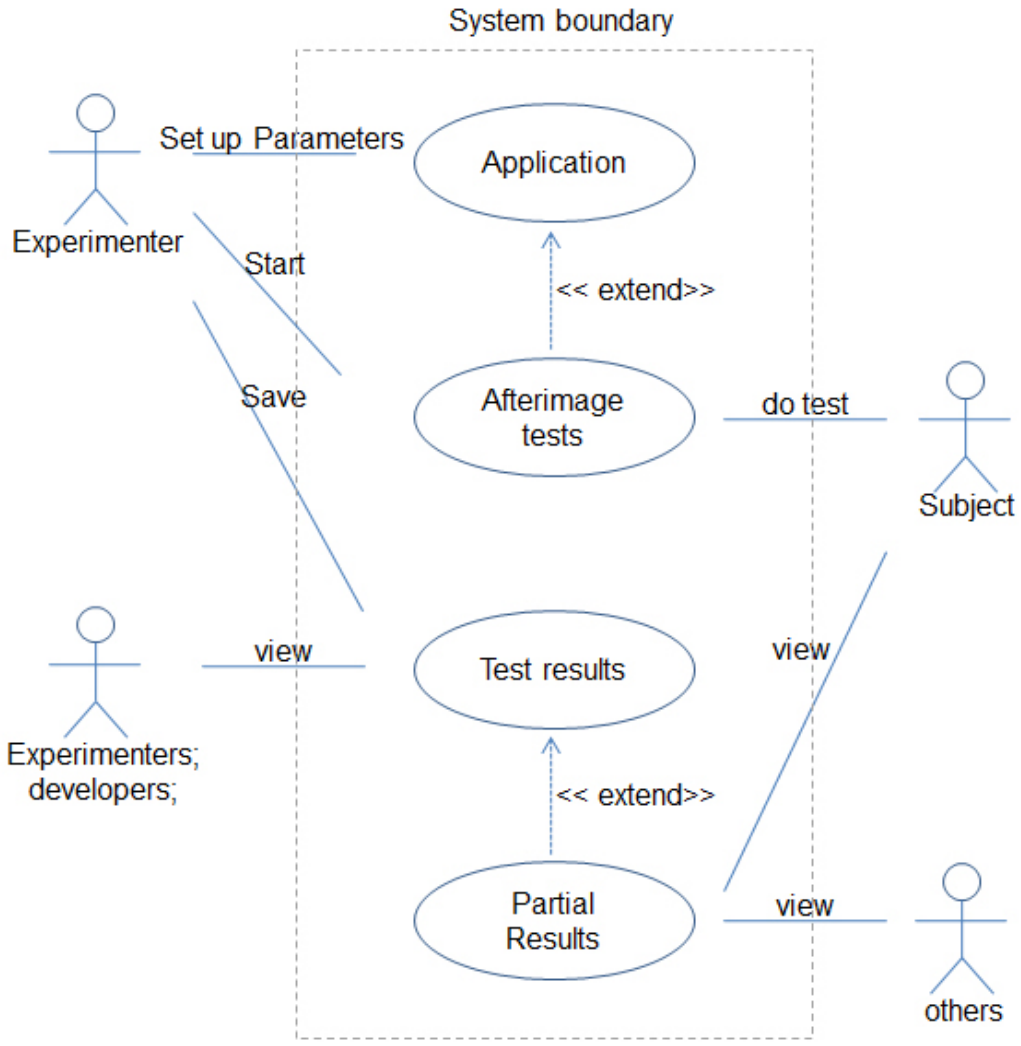


Figure 3-2. The QAA system use case diagram. The diagram describes the essential interactions of the application. Experimenters setup parameters in the application, run it and instruct participants how to do the tests. When tests are finished, experimenters save results. The application also needs to provide different privileges for different subjects.

## 3.3 System design

The design stage in the software development life cycle is usually considered as the most important stage, which always takes longest amount of time. A good design in software development takes advantage of the requirement analysis, makes the

implementation stage easy and ensures the overall quality of the software (Shaw and Garlan, 1996).

### 3.3.1 The modules of the QAA test

From the essential interactions in the use case diagram, 4 modules can be separated and derived based on the functions: a Front End Graphics User Interface (GUI) module, a psychophysics vision test module, a Backend server module and a Results Website module.

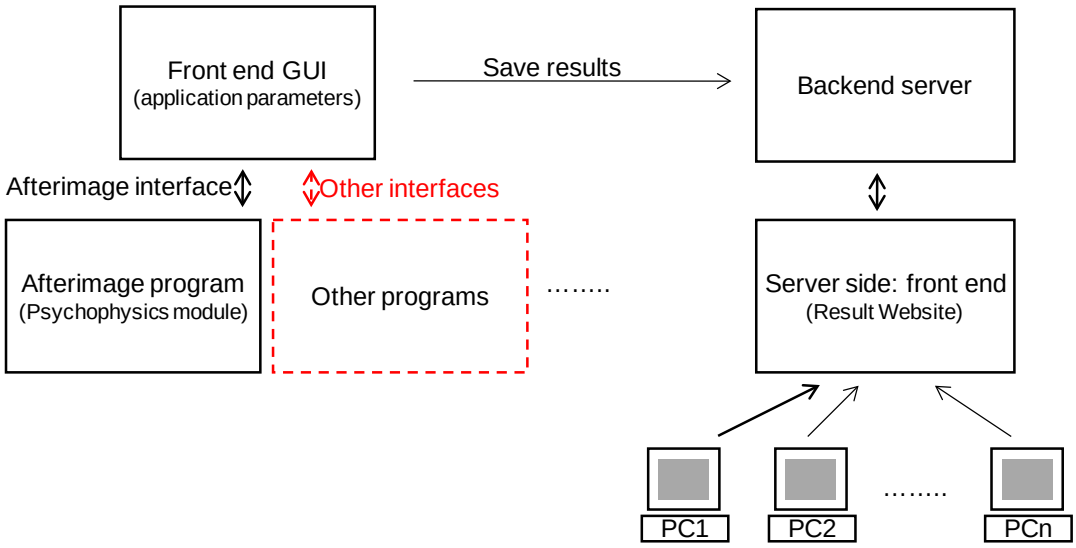


Figure 3-3. The QAA application module structure. The application contains 4 main modules: (1) Front-end GUI module, where the application parameters can be set; (2) Experiment module (psychophysics vision test module), the core psychophysics program is in this module; (3) Backend server module, which stores all the results and corresponding tests' information; and (4) the website module, which queries the results from the server database and presents the partial results according to groups that users belong to. The application is designed to be very flexible to extend. When a new Experiment module is designed, it can be easily inserted in the application with an added interface. The front GUI just needs to add a button to run the new corresponding application.

Figure 3-3 shows the modules of the QAA application. The red dotted box shows a new pseudo psychophysics module (e.g. a colour vision test or an acuity test), which can be easily inserted in the application without changing other modules. These psychophysics modules only have communication with the front end GUI. The front GUI validates the input parameters, runs the psychophysics application, and connects to the server. In the server side, the website module is designed to display the information in the database of the server.

This separation of the modules makes the application easy to be extended. Each module is designed to be a standalone program and can be integrated with other sections seamlessly. Each module talks (sends or receives data) to the other modules through interfaces. Interfaces are highly abstracted and save the most fundamental parameters. When a new psychophysics program is designed, it can be simply inserted in the whole application with one more added interface and perhaps an added ‘Launch’ button on the GUI that corresponds to the new psychophysics program. The GUI, server and website can remain unchanged.

The Front end GUI is where experimenters set up the experimental parameters and read results, i.e., background luminance, stimulus chromaticity, etc. Once a test is done, the results are displayed on the GUI and can be sent to the database. It should contain a few sections, which are organized into taps. Each tap includes several parameters that come from the same group. Once the parameters are set, experimenters can start the Psychophysics tests by pressing the corresponding button on the GUI. It also provides validation of the parameters. E.g. if a luminance of the screen background is set higher than the screen phosphor’s limits, the GUI

pops up an error window with the error information and requires experimenters to reset the luminance value.

The Psychophysics vision test module is the core module. It reads the parameters from the front end GUI through its interface and renders the desired stimulus on a background based on psychophysics algorithm (a staircase procedure). It can only be started through the GUI after the parameters are set. Once the staircase procedure is finished, the results are written back to the front end GUI though its interface, this module terminates itself and the current “focus” returns to the GUI.

The server module contains a secured database which can be written only by the Front end GUI when it has a validated result. Otherwise, it is only readable to the website module. A database is a structured collection of raw data and, in the QAA test, it stores the experiment details such as the stimulus conditions, subjects’ details and results etc..

The website module is designed to display the results that are saved in the database of the server. The website works as a content management system, which is also extremely robust and extendable. It makes the QAA results to be ‘accessible’ from anywhere in the world. The website portal not only provides a display of the results, but it also classifies the results into different groups according to the user privileges or user groups. For example, a patient can only see his/her own results, but an experimenter can see all the results.

The integration of these modules in the QAA test makes it possible for a future clinical application. For instance, with very few modifications, the GUI module can be designed for people who have specific clinical skills; the database can store thousands of experiment data and test results and this information can be retrieved

and analysed for other studies at any time; the website portal can be used to generate special views for the results, such as formal clinical reports for patients.

### 3.3.2 The psychophysics module

The psychophysics module is the main program of the application. It is invoked and started by the GUI after all testing parameters are set. According to the parameter, it runs the psychophysics algorithm (four alternative forced choice and staircase procedure) until the program is terminated.

The psychophysics module is a standalone program itself. It runs on top of the operating system and its architecture is shown in Figure 3-4.

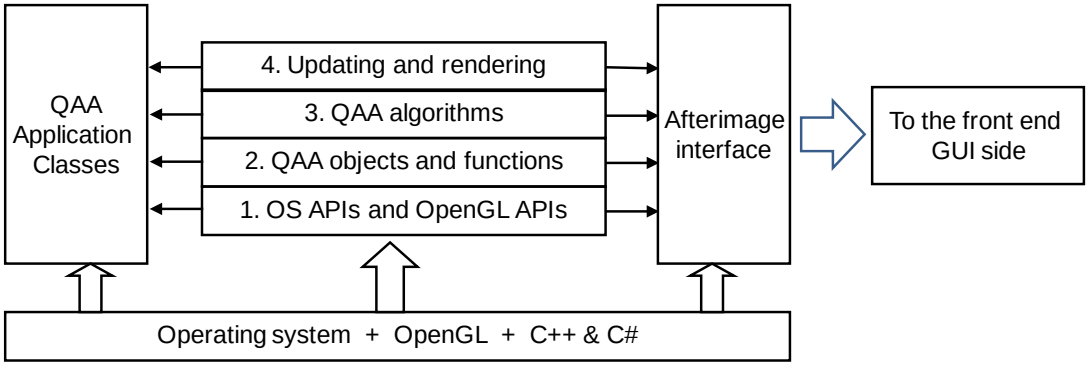


Figure 3-4. The architecture of the psychophysics module. The QAA experiment module has a hierarchy structure. The QAA objects and functions invoke the C++ language Application Programming Interfaces (APIs), OS APIs and OpenGL APIs, and then appropriate algorithms are used to process data before the rendering on the screen. The results are then transferred back to the front end GUI for further actions.

The psychophysics vision test module is constructed by classes using the Object Oriented Design technique. All the algorithms and functions are contained in the QAA classes. It only communicates with the front end GUI through the Afterimage

interface. In the module, it uses the message-driven programming paradigm (or event-driven). Figure 3-5 shows the message flow of the psychophysics vision test module.

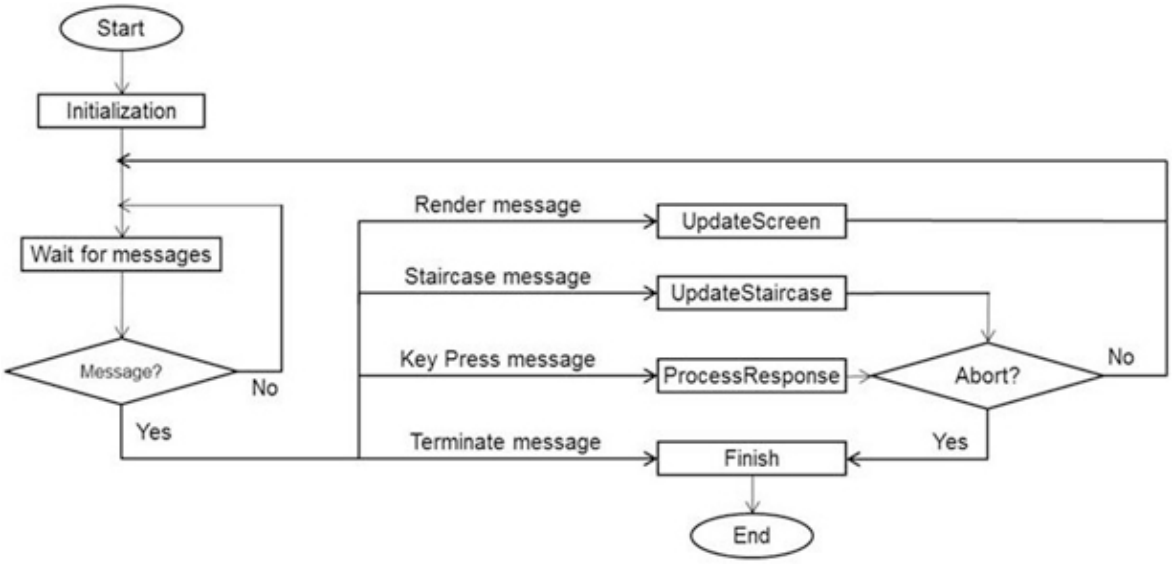


Figure 3-5. The message flow chart of psychophysics vision test module. The module uses the message driven programming paradigm.

## 3.4 Implementation

Software implementation is the part of the process where the actual coding work is done following the software design. Based on the QAA module diagram in section 3.3, the application should be implemented as separate independent modules with connections only through public interfaces. This design provides a lot of flexibility and maximizes effectiveness and robustness in the implementation, because details of individual module's implementation can be totally different as long as they provide the right functionalities and talk to other modules correctly through the interfaces. A list of implementation details such as programming languages and

development tools is shown in Table 3-1. The implementation of the psychophysics module is discussed in the next section, but the implementation of the remaining modules is skipped since these are less relevant to the work described in this thesis.

| QAA modules | Implementation languages or tools |
|---|---|
| Afterimage program (Psychophysics module) | C++ and OpenGL with Visual Studio |
| User interface | C# with Visual Studio |
| Database | SQL with MySQL database |
| Result website portal | PHP |
| Server | Apache |

Table 3-1. The programming languages and tools used in the QAA development.

### 3.4.1 Implementation of the psychophysics module

C++ and OpenGL are used together to create the psychophysics module. The C++ programming language is undoubtedly one of the most efficient and popular programming languages with many available libraries. OpenGL is the most widely adopted graphics standard and provides high performance and control of image performance. The model (actual psychophysics algorithm, logic and data) and graphics parts are also maximally abstractly and separately to achieve high data abstraction based on the commonly used Model-view-controller (MVC) design pattern (Krasner and Pope, 1988). For instance, the staircase algorithm employed only modifies the data and the graphics objects are loaded separately in the main

program. Only when a presentation is needed, the graphics objects read data from the model and present or update themselves on the screen.

An Object Oriented Design and Programming approach is employed in the programming stage (Rumbaugh et al., 1991, Booch et al., 2007). For instance, the background, reference stimulus and the test stimulus are designed to be subject classes of an abstract Stimulus class, in which only the most abstract members and methods are defined as shown in Figure 3-6.

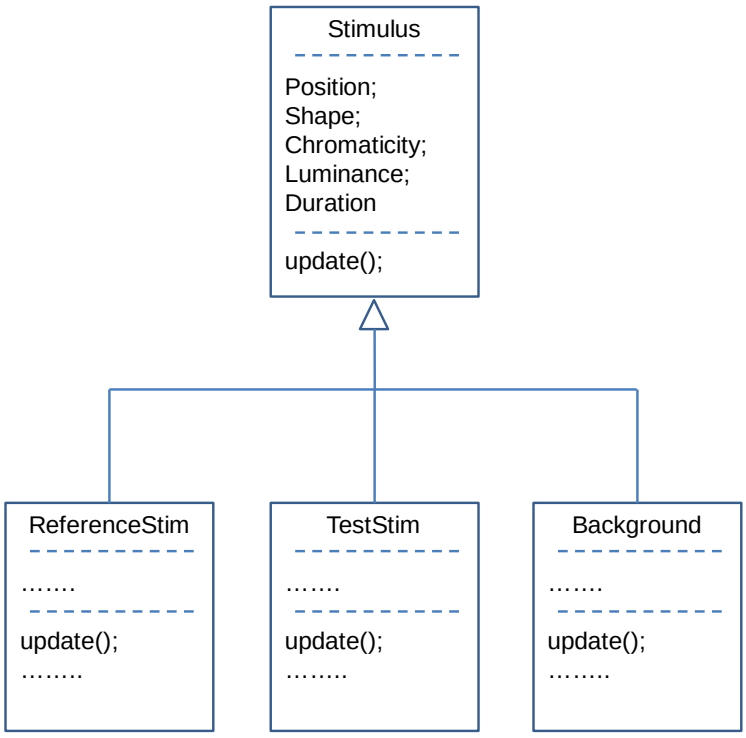


Figure 3-6. The class hierarchy of the Psychophysics module. The update() method is defined as a pure virtual method in the base class.

The class hierarchy design makes use of polymorphism. e.g., a simple loop of the base class' update() method in an OOP program updates the subclass objects. In the real afterimage program, the updates are always started from background

object. This is because both the reference and the test stimulus draw on top of the background.

```
for (eachStimulus needs to be update() )
{
    Stimulus[i].update();
}
```

The psychophysics module main program is implemented based on the message flow that is shown in Figure 3-5. The message boxes in the figure are implemented as procedures (or functions) following the same sequence in the flow chart. After a user response (a key press message), a staircase message is sent out to invoke the staircase procedure followed by an 'Abort' check to see if the program is finished based on the result from the staircase. If not, a rendering message is sent to render the next presentation on the screen.

The staircase algorithm is implemented as a template function in the psychophysics module, so that it can be invoked in any other psychophysics programs with any data types. It has 3 parameters – the start increment (start), the end increment (end) and the number of reversals (r). The most commonly used staircase follows either a linear or a log algorithm to change its increments and in the afterimage psychophysics module, we use the log algorithm to calculate the current increment:

$$\frac{start}{end} = e^{k(r-1)}$$

The parameter k can be solved in the above equation, and then the current increment can be computed with the following equation:

$$current\ increment = start \cdot e^{-k \cdot current\ no.of\ reversal}$$

Figure 3-7 shows an example calculation of the 'Current Increment' values in the staircase algorithm with a 'start increment' of 0.012, 'end increment' of 0.001 and a 'number of reversals' of 7 (A). An example staircase obtained in the test using example staircase values.

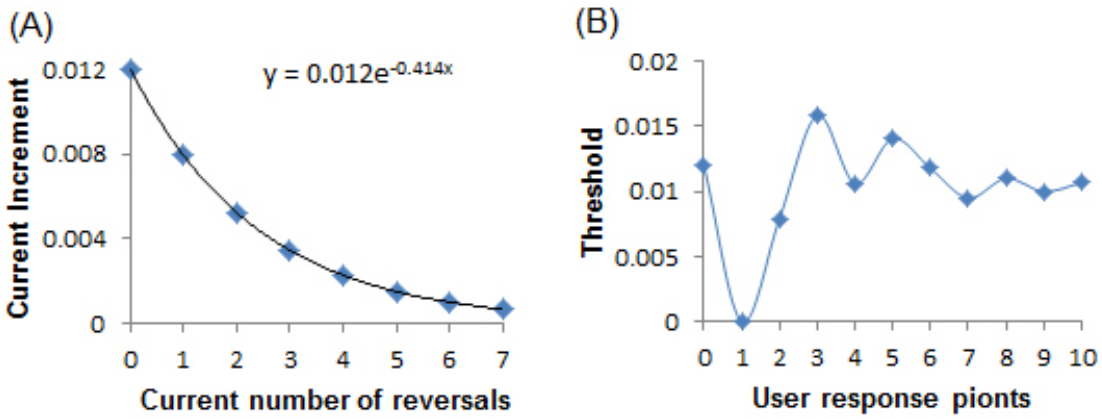


Figure 3-7. Examples of calculation of the 'Current Increment' values and thresholds values obtained in a test using example staircase values.

The refresh rate of the psychophysics module is fixed at 85Hz at a resolution of 1280x1024 under fullscreen mode on a calibrated 20" CRT monitor (Sony Trinitron, model GDM-400PST). The program runs on a Toshiba laptop (Toshiba Tecra M10) under Windows XP SP3 with an integrated Mobile Intel GMA 4500MHD graphics card. This ensures that each frame of the stimulus presentation of the psychophysics module takes approximately ~12ms on a visual field of $29^{o}$ x $22^{o}$.

### 3.4.2 The implementation of interfaces between modules

Figure 3-3 shows the modules of the QAA application. Each module communicates with the other necessary modules through interfaces. The afterimage

psychophysics module only communicates with Front end GUI module in which a ‘save result’ communication to the database is also found.

The QAA application starts from the GUI interface. When the GUI is initialized, it checks if the computer has a valid internet connection and tries to connect to the server. Once a connection is established, users can setup all the desired parameters. After the experiment finishes, the results are saved on both the experiment computer and server side. Otherwise, the program runs in a non-server mode and results are saved only on the experiment computer.

When the desired parameters are set, the GUI creates a new file and stores these parameters in a local drive, after experimenters click buttons to the run Psychophysics module. The stored file will be read only by the psychophysics program, after which the psychophysics test starts. When the psychophysics program finishes, it creates another file and stores all the details of the experiment including the results in it. In the detailed implementation, both of these files are called ‘machine-readable-files’ which have an optimized format for these programs.

Then, if there is a valid connection with the server, the Front end GUI creates relevant SQL scripts, opens the database and saves these results. Otherwise, the GUI saves a ‘human-readable-result-file’ which is an Excel file that contains all necessary information for the last test on the experiment computer.

## 3.5 Monitor calibration for the QAA

A proper and reliable display calibration is required and is very important for a vision experiment. Based on the calibration results, the application is able to generate

stimuli accurately, given that it is within the phosphor' limits of the monitor. This section describes the procedure of monitor calibration that was employed in the QAA application.

### 3.5.1 The QAA calibration procedure

The display used in the system is a 20" CRT monitor (Sony Trinitron, model GDM-400PST). The control program runs on a Toshiba laptop (Toshiba Tecra M10) under Windows XP SP3. Instruments that are used in the Monitor calibration process mainly include a telespectralradiometer (Minolta, CS2000 telespectralradiometer), an LMT photometer (LMT L1003, made in West Germany) and a ruler. The telespectralradiometer is used to measure the spectral radiance, the LMT photometer is used to measure the luminance (in $cd/m^2$) and the ruler is used to measure the pixel distance on the screen.

The first steps in the procedure for screen calibration are to mount the screen in place, adjust the screen menu options to set the screen properties to the desired values, like the shape, colour and viewing size. Normally, the shape of the viewing area needs to be adjusted to be a rectangle and get rid of any distortion, and also try to make the viewing size to be as large as possible. One of the purposes of the preliminary screen adjustments is to make the screen reproduce the desired luminance levels with stable operation. This can be achieved by repeatedly adjusting the values of the "contrast" and "brightness" on the screen and using the luminance meter to measure values at each end until the proper value is achieved.

Next, the spectral radiance scan and luminance calibration is measured. The spectral radiance scan and luminance calibrations are done on each gun independently. For the luminance calibration, the luminance of the test patch for each gun is measured in steps. In the QAA program, the drive signal is considered as an 8 bits integer. Therefore, the luminance needs to be measured at 256 steps for each gun, i.e., from 0 to 255. So, for the red-gun luminance calibration, for example, the drive signal of the red-gun is increased but the other guns are kept to be 0. I.e., from (0,0,0), (1,0,0) to (255,0,0). At each step, several readings from the luminance meter were taken and the averages were computed. In the spectral radiance scan, the purpose is to obtain the spectral radiance curve of each gun. The absolute amplitude of the curve (the shape at each gun signal step) is proportional to the calibrated luminance values in the luminance calibration. So, in the spectral radiance scan, the scan is only needed to be measured for 3 times - (255,0,0) for the red gun, (0,255,0) for the green gun and (0,0,255) for the blue gun.

### 3.5.2 The QAA calibration results

Figure 3-8 shows the spectral radiance scans for the red, green and blue guns. Each gun is measured separately at the maximum drive signal. E.g. for the red gun, it is measured when the drive signal is set at (255, 0, 0) in the calibration program.

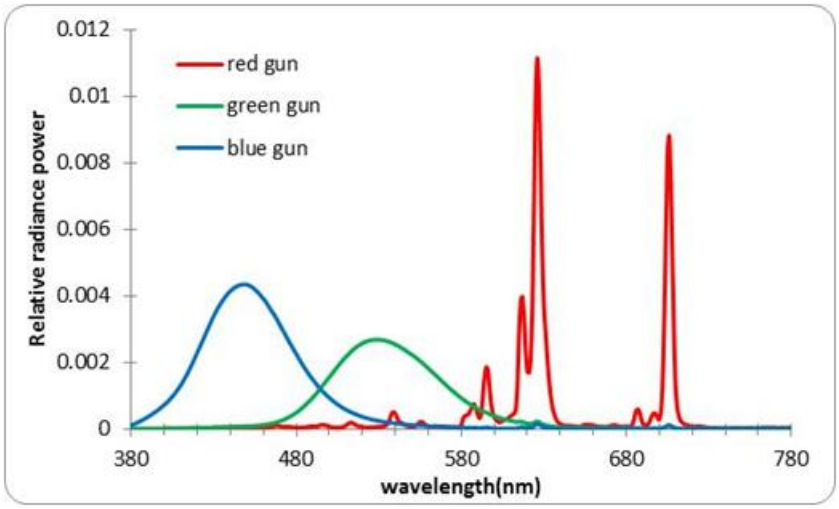


Figure 3-8. The QAA spectral radiance scan results.

Figure 3-9 shows the luminance calibration results for the red, green, blue guns and the “white” channel. Apart from the white, each gun is measured individually as the drive signal increases. The white channel is measured when the 3 guns increase with the same intervals and this measured result is used to compare the total luminance of the three individual guns. The luminance values are measured with luminance meter (LMT L1003, made in West Germany).

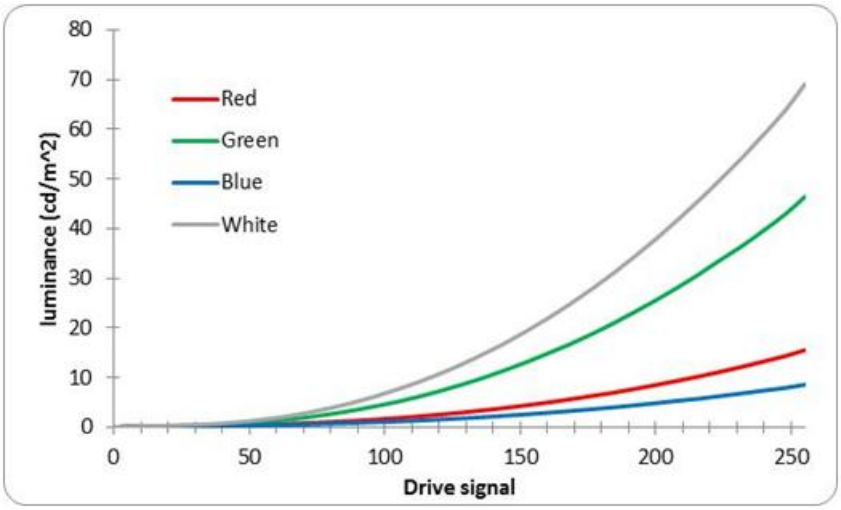


Figure 3-9. luminance calibration for each phorsphor gun. Driven signal from 0 to 255. The real calibration process employed a interval step of 4 to save time, and the values in between were then interpolated.

### 3.5.3 The usage of calibration in the QAA application

#### 1. Generate correct tristimulus values in colour space

Generally speaking, one of the most important requirements in a psychophysics program is the production of stimulus colours and luminance correctly in an acceptable and reproducible way. In the case of the CIE1931 XYZ colour space, the stimulus is specified using tristimulus values and chromaticity coordinates. The tristimulus value also represents the luminance of the stimulus.

In the QAA program, the conversion is specified in the following formula. Note that, in the following formula, the (R, G, B) are not tristimulus values from the CIE RGB space; they are the real drive signals that are needed for the program to produce the (X, Y, Z) tristimulus values.

$$(X, Y, Z) \xrightarrow[map]{} \text{(R, G, B)} \qquad (▲)$$

If the given stimulus is specified using (x, y, L), they can always be easily transferred to XYZ using the following formula (these formula are the properties of CIE 1931 XYZ chromaticity diagram):

$$X = \frac{Y}{y}x$$

$$Y = L$$

$$Z = \frac{Y}{y}(1 - x - y)$$

In the QAA application, all the tristimulus values are specified in the CIE 1931 xy colour space which was created by the International Commission on Illumination in 1931 (Judd et al., 1964). It is a mathematical transformation from CIE RGB colour space which was studied by W. Wright and John Guild in the 1920s using their colour matching experiment (Guild, 1932, Wright, 1929). The results from the colour matching experiments are refered as colour matching functions. The CIE 1931 XYZ colour space has a few advantages over the CIE RGB and other colour spaces in terms of colour matching functions. The most significant advantages of the CIE 1931 colour space are:

1. The colour matching functions are always positive.
2. The $\overline{y}(\lambda)$ colour matching function is equal to V(λ) – photopic luminous efficiency function.

For given tristimulus values (X, Y, Z) in CIE 1931 colour space, the tristimulus values are converted to the gun driven signals (R, G, B) in the following steps:

1. For Y, it is luminance of the desired stimulus. Its value is the sum of Yr, Yg and Yb. In other words, the total luminance of the stimulus is contributed from the sum of all the three guns' luminance. This is also true for the X and Z. Therefore, for X, Y and Z, 3 equations are derived.

$$X = X_r + X_g + X_b; \textbf{ (1)}$$

$$Y = Y_r + Y_g + Y_b; \textbf{ (2)}$$

$$Z = Z_r + Z_g + Z_b; \textbf{ (3)}$$

2. The Xr, Yr, Zr, Xg, ……., Zb, can be computed using the following formulas.

$$X_r = \int_{300}^{800} I'red(\lambda) \cdot \bar{x}(\lambda)\ d\lambda$$

$$Y_r = \int_{300}^{800} I'red(\lambda) \cdot \bar{y}(\lambda)\ d\lambda$$

$$Z_r = \int_{300}^{800} I'red(\lambda) \cdot \bar{z}(\lambda)\ d\lambda$$

……

(Where I'red(λ) is the spectral power distribution when the drive signal is (R, 0, 0) and $\bar{x}(\lambda)$ is the CIE 1931 colour matching function.)

Therefore, the following equation is drived:

$$X = \int_{300}^{800} I'red(\lambda) \cdot \bar{x}(\lambda)\ d\lambda + \int_{300}^{800} I'green(\lambda) \cdot \bar{x}(\lambda)\ d\lambda + \int_{300}^{800} I'blue(\lambda) \cdot \bar{x}(\lambda)\ d\lambda$$

i.e., hence, (**1**) becomes

$$X = \int_{300}^{800} (I'red(\lambda) + I'green(\lambda) + I'blue(\lambda)) \cdot \bar{x}(\lambda)\ d\lambda \textbf{ (A1)}$$

And same thing also applies for (**2**) and (**3**). Therefore, (A2) and (A3) can be derived:

$$Y = \int_{300}^{800} (I'red(\lambda) + I'green(\lambda) + I'blue(\lambda)) \cdot \bar{y}(\lambda)\ d\lambda \textbf{ (A2)}$$

$$Z = \int_{300}^{800} (I'red(\lambda) + I'green(\lambda) + I'blue(\lambda)) \cdot \bar{z}(\lambda)\ d\lambda$$ **(A3)**

3. The 'maximum' spectral distribution curve shape of Ired(λ) is measured at (255,0,0) and the shape of I'red(λ) corresponds to the corresonding luminance signal Lr. In other words, for one given spectral radiance scan, there is one and only one corresponding luminance. It is a one to one correspondence. Therefore, the ratio of Lr to the maximum luminance (where drive signal is maximum) is the same as I'red(λ) to Ired(λ). Therefore, I'red(λ) can be replaced with Ired(λ), Lr and Lr_max in **A1**, where according to our spectral radiance calibraion, Ired(λ) is already known. If Lr_max and Lr can be calculated, the corresponding Rmax and R that produce the given luminance in the calibration results can be derived. So formula ▲ becomes:

$$(X, Y, Z) \xrightarrow[map]{} (Lr, Lg, Lb) \xrightarrow[map]{} (R, G, B)$$

Where (X, Y, Z) is the desired tristimulus value and (Lr, Lg, Lb) are luminance values which corresponds the desired gun levels (R, G, B).

4. The same rule can also be applied to **A2** and **A3**. Now, these formula become:

$$X = \int_{300}^{800} \left( \frac{Lr}{L_{r\_\max}} Ired(\lambda) + \frac{Lg}{L_{g\_\max}} Igreen(\lambda) + \frac{Lb}{L_{b\_\max}} Iblue(\lambda) \right) \cdot \bar{x}(\lambda)\ d\lambda$$ **(B1)**

$$Y = \int_{300}^{800} \left( \frac{Lr}{L_{r\_\max}} Ired(\lambda) + \frac{Lg}{L_{g\_\max}} Igreen(\lambda) + \frac{Lb}{L_{b\_\max}} Iblue(\lambda) \right) \cdot \bar{y}(\lambda)\ d\lambda$$ **(B2)**

$$Z = \int_{300}^{800} \left( \frac{Lr}{L_{r\_\max}} Ired(\lambda) + \frac{Lg}{L_{g\_\max}} Igreen(\lambda) + \frac{Lb}{L_{b\_\max}} Iblue(\lambda) \right) \cdot \bar{z}(\lambda)\, d\lambda \quad \textbf{(B3)}$$

And, the $\frac{R}{R_{\max}}$ is just a contrast, it can be put outside the integration. And because the following is also known:

$$X_{r\_max} = \int_{300}^{800} Ired(\lambda) \cdot \bar{x}(\lambda)\, d\lambda$$

$$Y_{r\_max} = \int_{300}^{800} Ired(\lambda) \cdot \bar{y}(\lambda)\, d\lambda$$

$$Z_{r\_max} = \int_{300}^{800} Ired(\lambda) \cdot \bar{z}(\lambda)\, d\lambda$$

Hence, the **B1**, **B2** and **B3** become:

$$X = \frac{X_{r\_\max}}{L_{r\_\max}} Lr + \frac{X_{g\_\max}}{L_{g\_\max}} Lg + \frac{X_{b\_\max}}{L_{b\_\max}} Lb \quad \textbf{(C1)}$$

$$Y = \frac{Y_{r\_\max}}{L_{r\_\max}} Lr + \frac{Y_{g\_\max}}{L_{g\_\max}} Lg + \frac{Y_{b\_\max}}{L_{b\_\max}} Lb \quad \textbf{(C2)}$$

$$Z = \frac{Z_{r\_\max}}{L_{r\_\max}} Lr + \frac{Z_{g\_\max}}{L_{g\_\max}} Lg + \frac{Z_{b\_\max}}{L_{b\_\max}} Lb \quad \textbf{(C3)}$$

Because $Y_{r\_max}$, $Y_{g\_max}$ and $Y_{b\_max}$ are luminance values, therefore: $Y_{r\_max} = L_{r\_max}$ ; $Y_{g\_max} = L_{g\_max}$ and $Y_{b\_max} = L_{b\_max}$. In the (C) formulas, there are 3 formulas with 3 unknown varibles Lr, Lg and Lb. According to Kramer's rule (Cramer, 1750), the solution is:

$$L_r = \frac{D_{red}}{D}$$

$$L_g = \frac{D_{green}}{D}$$

$$L_b = \frac{D_{blue}}{D}$$

Where D is the determinate of the matrix.

$$D \equiv \begin{pmatrix} \frac{X_{r\_\max}}{L_{r\_\max}} & \frac{X_{g\_\max}}{L_{g\_\max}} & \frac{X_{b\_\max}}{L_{b\_\max}} \\ 1 & 1 & 1 \\ \frac{Z_{r\_\max}}{L_{r\_\max}} & \frac{Z_{g\_\max}}{L_{g\_\max}} & \frac{Z_{b\_\max}}{L_{b\_\max}} \end{pmatrix}; \quad D_{red} \equiv \begin{pmatrix} X & \frac{X_{g\_\max}}{L_{g\_\max}} & \frac{X_{b\_\max}}{L_{b\_\max}} \\ Y & 1 & 1 \\ Z & \frac{Z_{g\_\max}}{L_{g\_\max}} & \frac{Z_{b\_\max}}{L_{b\_\max}} \end{pmatrix};$$

$$D_{green} \equiv \begin{pmatrix} \frac{X_{r\_\max}}{L_{r\_\max}} & X & \frac{X_{b\_\max}}{L_{b\_\max}} \\ 1 & Y & 1 \\ \frac{Z_{r\_\max}}{L_{r\_\max}} & Z & \frac{Z_{b\_\max}}{L_{b\_\max}} \end{pmatrix}; \quad D_{blue} \equiv \begin{pmatrix} \frac{X_{r\_\max}}{L_{r\_\max}} & \frac{X_{g\_\max}}{L_{g\_\max}} & X \\ 1 & 1 & Y \\ \frac{Z_{r\_\max}}{L_{r\_\max}} & \frac{Z_{g\_\max}}{L_{g\_\max}} & Z \end{pmatrix}$$

5. Once ($L_r$, $L_g$, $L_b$) are solved. the closest real luminance values ($L_{r'}$, $L_{g'}$, $L_{b'}$) from luminance calibration results like shown in (Figure 3-9) can be derived and then the corresponding drive signals (R, G, B) can be calculated.

**2. Calculate phosphor limits**

Because each phosphor's maximum spectral radiance is fixed, when the luminance of a stimulus is increased, the maximum stimulus' CD is reduced. Based on the calibration results, a function of the afterimage program is in charge of calculating the maximum CDs at different background levels. The phosphors' limits for the most

commonly used background luminance levels are calculated in advance for the afterimage program to increase efficiency. However, if a luminance level is not listed, the afterimage system will perform a check when the program starts and do the relative calculation.

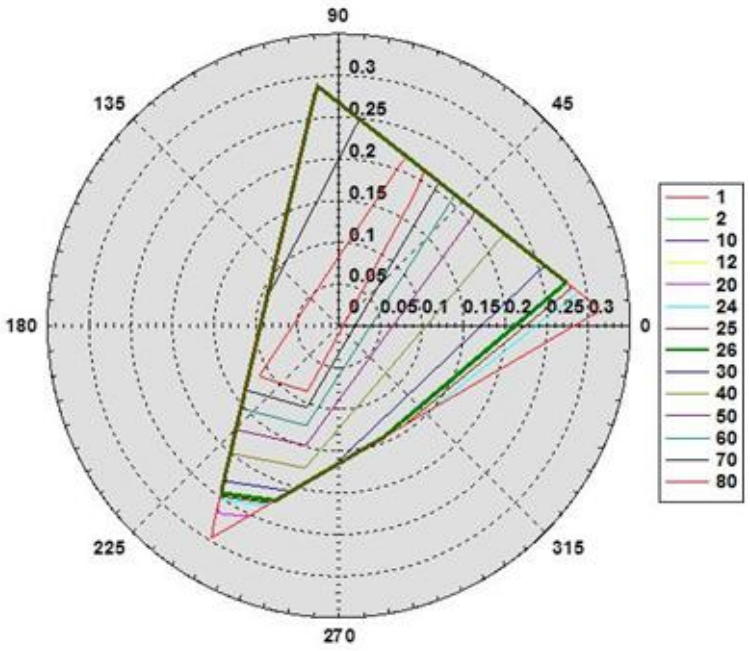


Figure 3-10. The phosphors' limits as a function of the luminance levels.

## 3.6 Summary

In this chapter, the software design and implementation of QAA application is described. A waterfall software design model was employed in the design stage. The first step was to do the requirement analysis, where the functional and non-functional requirements were extracted. Based on the requirement analysis, a detailed software design was produced. The implementation of psychophysics module was discussed and lastly the monitor calibration and its usages were

introduced. In the next chapter, the QAA system is employed to measure the strength and duration of the chromatic afterimages and the measured results are discussed.

# 4 QUANTITATIVE AFTERIMAGE ASSESSMENT

## 4.1 Introduction

Vision starts with light entering the eyes and involves complex mechanisms in the retina and the brain. By exploring and studying visual perception, vision scientists have discovered and studied many visual illusions over centuries. The perception of afterimage is one of the most fascinating effects, and refers to the continued perception of some form of image after the original stimulus disappears. Hence, it is often referred to 'visual afterimage'. Other factors can also cause visual afterimages, such as adaptation to motion, colour, orientation, size change, luminance etc. The current study that is described in this chapter focuses on only colour afterimages (or chromatic afterimages).

Chromatic afterimages fall into two categories, positive afterimages and negative afterimages. Perceptually, positive afterimages have the same colour as the original colour whereas negative afterimages have the complementary colour. The process behind the formation of positive afterimages is less well understood, though some studies suggest that the principle mechanism is mostly related to neural adaptation (Barlow and Sparrock, 1964, Miller, 1966). On the other hand, negative afterimages have been associated mostly with the retina and are likely to be caused when the cone cells are over stimulated and become less sensitive (Shimojo et al., 2001). For example, when looking at a reddish colour stimulus for several seconds, the L cones in the eye become most active and send out a strong signal. Then, if

immediately the gaze is diverted to a uniform spectrally neutral background, the same L-cones generate reduced signals as a result of bleached pigment. But the remaining cone classes were unaffected by bleaching and hence generate normal signals. Since the generated colour will be composed of proportionally 'less' red signal, it will therefore appear to be more greenish.

In primates, the eyes compensate for the effect of afterimages by changing the fixation positions in small amounts (amplitudes vary from ~2 to ~120 arc minutes), but at a fast speed. This process is referred to microsaccades (Darwin and Darwin, 1786). The role of microsaccades in visual perception has been debated and is still largely unresolved. It has been proposed that the main functions of macrosaccades are to prevent the retinal image from fading and weaken the afterimage effect by moving the stimulus in and out of a neuron's receptive field. But, if the stimulus is spatially large and is viewed for a sufficient long time, afterimages will still be produced. Attention also affects the strength of afterimages (Suzuki and Grabowecky, 2003, Tsuchiya, 2005, Wede and Francis, 2007). Suzuki and Graboweeky (2003) reported that an attended inducer stimulus would cause shorter and weaker afterimages than an unattended inducer (Suzuki and Grabowecky, 2003).

Several studies have reported pupillary responses at the stimulus offset in additional to the onset and these secondary responses are referred to as the pupil afterimage responses. The pupil Barbur (1999) used two isoluminant stimuli with opponent colours (reddish and greenish) and he reported that the pupil colour responses were normal in the sighted hemifields of two hemianopia subjects, whereas in their blind hemifields there was only an onset pupil response to the

reddish stimulus and an offset response to the greenish stimulus (Barbur et al., 1999). The pupillary afterimage responses have been observed in many other pupil studies (Kimura and Young, 1995, Kohn and Clynes, 1969, Tsujimura et al., 2001). Although the pupil afterimage responses have been observed in many occasions, the mechanism is still not very well understood.

In this study, the QAA program was employed to investigate the duration and strength of the chromatic afterimages in normal trichromats as well as in subjects with congenital red-green colour deficiency. The pupil colour response has also been measured and compared in these subjects. We show that the afterimage results measured from the normal subjects display consistent results with previous studies; however the results obtained from the colour deficient subjects reveal the importance of cone contrast increments in driving the pupil response.

## 4.2 Methods

The QAA program (described in section 2.7 and 3) was employed to measure the afterimages and P_SCAN system (described in section 2.2) was used to assess pupil responses. 10 normal trichromatic subjects (aged between 23 and 59), six patients with VS syndrome and palinopsia (aged between 24 and 42), 2 deuteranope subjects (23 and 45 years old) and 2 protanope subjects (33 and 35 years old) participated in the study. All subjects were given written informed consent, and the study was approved by the research and Ethics Committee of City University London.

**Pupil measurements**

A uniform background ($30^o$ x $24^o$) with CIE coordinates (0.298, 0.335) and a luminance of 12cd/$m^2$ was used throughout the pupil afterimage studies. The stimulus was a disc of $9.5^o$ in diameter and was presented in the centre of the background for 2.4 seconds. The subjects were instructed to view the screen binocularly and the pupil traces obtained represent the averages of 32 measurements per stimulus. Two chromatic angles were selected, i.e., $118^o$ and $249^o$. Both stimuli had the same photopic luminance as the background, but the individual photoreceptor contrasts generated were different. Figure 4-1 shows the photoreceptors' contrasts calculated along an ellipse contour with the centre chromaticity (0.298, 0.335). The greenish stimulus has an absent rod contrast whereas the bluish stimulus contains a very large rod contrasts.

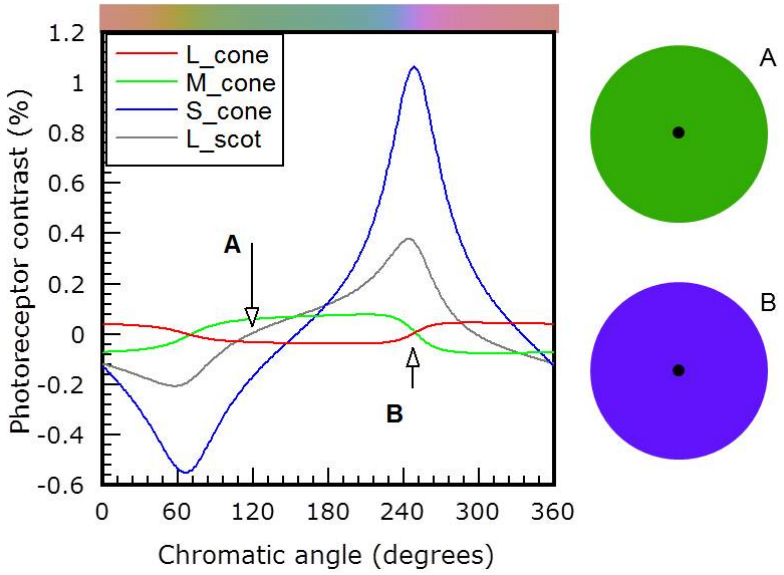


Figure 4-1. Relative photoreceptor contrasts calculated along an ellipse contour with the centre (0.298, 0.335) on the CIE1931 chromatic diagram. A indicates the rod free (0% rod contrast) direction and B indicates the chromatic direction that contains the maximum rods and S-cone contrasts.

**Afterimage measurements**

To investigate the afterimage thresholds in a variety of conditions, we varied one stimulus parameter each time while keeping others fixed. For instance, in one measurement, we keep the properties of both reference stimulus and test stimulus the same and vary only the time between the offset of the reference and the onset of the test. Then we can plot the afterimage threshold as a function of this duration. The five different types of measurements employed are listed below:

1. Afterimage thresholds measured as a function of the time delay between the offset of the reference stimulus and the onset of test stimulus.
2. Afterimage thresholds measured as a function of the duration of reference stimulus.
3. Afterimage thresholds measured as a function of the chromatic signal strength of the reference stimulus (i.e., the CD amplitude).
4. Afterimage thresholds measured for different hue directions in (x, y) chromaticity space.
5. Afterimage thresholds measured for different background luminance levels.

In all conditions, the reference and the test stimulus luminances were kept the same and equal to that of the uniform background.

Apart from experiment 5, the background employed had a fixed luminance of 26cd/m$^2$ and chromaticity (0.305, 0.323). The luminance and the chromaticity of the background were chosen to be the same as the CAD test. Therefore, the measured strength of the chromatic afterimages can be compared with the colour sensitivity. This background chromaticity corresponds to the white point used by MacAdam, which is the centre of the MacAdam ellipse (MacAdam, 1942). Colour sensitivity

measured with respect to this background chromaticity at 26cd/$m^2$ allows the program to generate an optimum number of coloured stimuli for any chromatic directions in the CIE 1931 x,y colour space.

## 4.3 Results from normal subjects

### 4.3.1 The effect of the gap duration

Figure 4-2 shows the afterimage thresholds plotted against the gap time between the offset of the reference stimulus and the onset test stimulus. The mean results from 10 normal subjects illustrate that the strength of the afterimage decays very fast when the gap time is increased and follows an exponential trend ($R^2$> 0.99). In one subject, the thresholds were measured continuously for up to 14 seconds delay. Even after 14 seconds, the thresholds tend to asymptote to a straight line after the first 8 to 10s. To establish the day to day variability, the tests had been repeated on the same subject measured in Figure 4-2 (A) in six consecutive days and the mean average and the corresponding ±σ values were shown in Figure 4-2 (B).

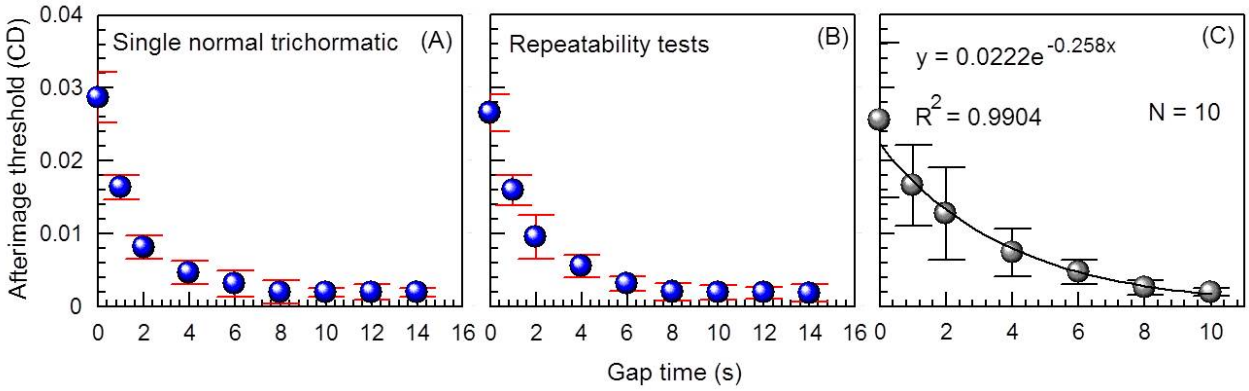


Figure 4-2. Chromatic afterimage strength measured as a function of 'gap time' between the reference and the test stimuli in one normal trichromat with a gap time up to 14s (A) and the average and the corresponding ±σ values for 10 normal subjects (C). (B) showed the mean and the corresponding ±σ values of repeated tests on the same subject measured in A in six consecutive days. The reference stimulus had a chromatic angle of 125 degrees and is presented for 5 seconds. The afterimage was measured after 0, 1, 2, 4, 6, 8 and 10 seconds after the reference stimulus was gone. The error bars in the first diagram plotted 2 standard errors obtained from the last six reversals in the staircase measurement algorithm and in the second diagram showed the standard errors for the group of normal subjects.

### 4.3.2 The effect of reference stimulus duration

Afterimage thresholds were also measured when different reference stimulus durations were employed. According to Figure 4-3, when the gap time is fixed, increasing the duration of the reference stimulus induces stronger afterimages. However, this effect becomes increasingly small as the presentation duration of the reference stimulus becomes large. The thresholds exhibit a maximum for a reference duration of eight seconds and a gap time is one second. As expected, when the reference stimulus duration is fixed, increasing the gap time reduces the strength of corresponding chromatic afterimages.

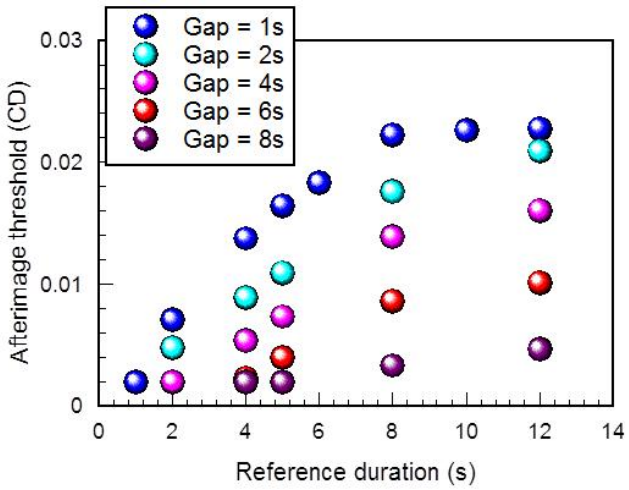


Figure 4-3. Chromatic afterimage thresholds measured for different reference stimulus durations in a trichromat. The gap times employed are shown as different coloured symbols. The data shown are for one subject with normal colour vision.

### 4.3.3 The effect of the chromatic saturation of the reference stimulus

The strengths of the generated afterimages were measured for four reference stimuli that differed in chromatic saturation (i.e. the CD value). The results are shown in Figure 4-4 for 3 normal trichromats. The first subject shows a low initial threshold and then the thresholds increase sharply with increasing CD values. In the second and the third subjects, they exhibit similar increasing trends as the first subject. However, when compared with the first subject, the last thresholds show reduced increment and appear to reach a maximum. The third subject also exhibits a higher initial threshold when compared with the first 2 subjects. The maximum reference stimulus' CD employed (0.12) is limited by the screen phosphors of the display. A maximum chromatic displacement of 0.12 units can be generated for the background chromaticity and the display luminance employed.

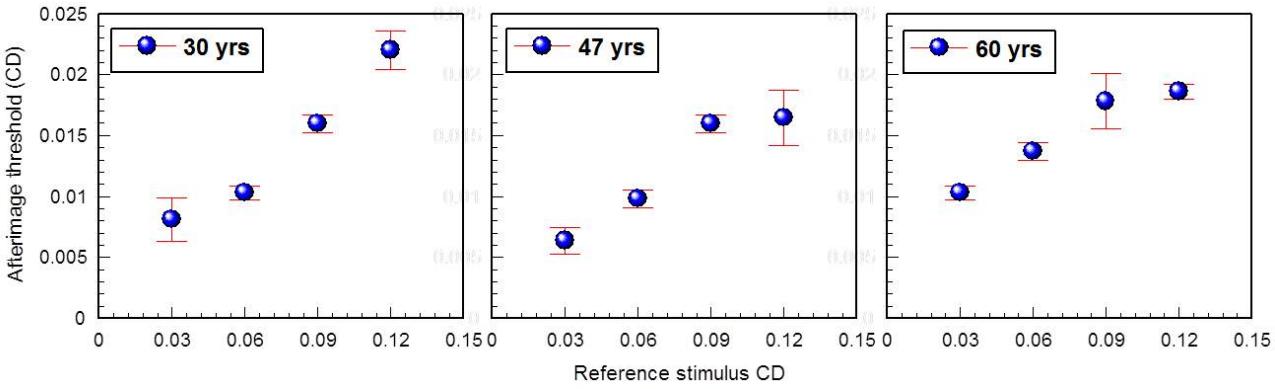


Figure 4-4. Afterimage thresholds measured as a function of chromatic saturation in 3 normal subjects – a 30 year old male subject, a 47 year old male subject and a 60 year old male subject. The reference stimulus has a fixed chromatic displacement orientation of 125$^{o}$, but varies in chromatic displacement. The gap time is fixed at one second.

### 4.3.4 The effect of chromatic direction

In the previous measurements, the reference stimuli employed had a fixed displacement orientation angle of 125$^{o}$. The "greenish" stimulus generated along this direction has 0% rod contrast (as shown in Figure 4-1) and generates relatively large afterimage responses as demonstrated in other studies (Barbur et al., 1999, Tsujimura et al., 2001). If the reference stimulus angle is changed, the rod contrast in the stimulus is no longer 0%. Aguilar and Stiles reported the sensitivity of rod mechanism to stimulus differences begins to fall off rapidly and that at above 2000 to 5000 scotopic trolands (corresponding approximately 120 to 300 cd/m$^2$ daylight luminances) the rods mechanism becomes saturated (Aguilar and Stiles, 1954). Although, the measured afterimage thresholds were carried out in central vision when rod activity is minimal, one cannot guarantee that rod signals do not contribute to the strength of the measured afterimage for other directions of the chromatic displacement.

Figure 4-5 shows the afterimage thresholds measured for a number of chromatic displacement directions for reference stimuli of fixed CD (0.09).

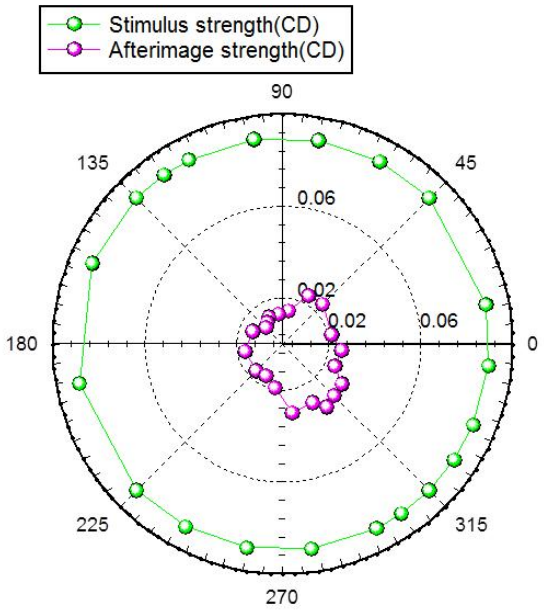


Figure 4-5. The strength of chromatic afterimages measured as a function the chromatic displacement angle of the reference stimulus. The reference stimulus has a fixed chromatic distance (CD = 0.09) and a fixed duration (5s).The pole corresponds to the background chromaticity (0.305, 0.323) (MacAdam white) in the CIE1931 chromaticity diagram. The luminances of the background, the reference and the test stimuli were 26cd/$m^2$. The test stimulus was presented two seconds after the reference stimulus disappeared from the screen.

The threshold contour of the measured afterimages is complex and differs significantly to the threshold detection ellipse reported by MacAdam (Silberstein and MacAdam, 1945). Reddish and greenish displacement directions appear to produce the largest and the smallest afterimage strengths, respectively. The fixed chromatic displacement employed and the nonlinearity of the CIE (x, y) diagram for large chromatic displacement may contribute significantly to the measured afterimage thresholds. In this afterimage test, the reference stimuli had fixed CDs (0.09) and varied in chromatic angles. As discussed in Section 4.3.2, chromatic displacement

of the reference stimulus is a factor that affects the afterimage threshold. Therefore, if the CDs of reference stimuli are changed, the measured afterimage thresholds will change accordingly and so does the 'result shape'.

### 4.3.5 The effect of background luminance

Kelly and Martinez-Uriegas (1993) used a flashed-grating threshold-elevation technique to measure chromatic and achromatic afterimages as functions of the green/red balance of a grating. They found that the threshold only peaked when the test flash was isoluminant (Kelly and Martinez-Uriegas, 1993).

Figure 4-6 shows the afterimage results measured in a normal subject at high mesopic (6cd/$m^2$) and photopic (60cd/$m^2$) range. The tests were repeated six times in each stimulus condition. In the tests, the reference stimuli employed had chromatic angle of 125$^o$, CD of 0.09 and the gap time of 1 second. To obtain the largest threshold at each background luminance level, both the reference and the test stimuli were kept at the same luminance as the background, i.e., either 6 or 60cd/$m^2$. Due to the limit of the screen phosphors and the algorithm employed, the largest luminance that could be measured in the afterimage program was 60cd/$m^2$. Although there is some variance in chromatic afterimage strength between the two stimulus conditions, the variation is not statistically significant ($p = 0.48$).

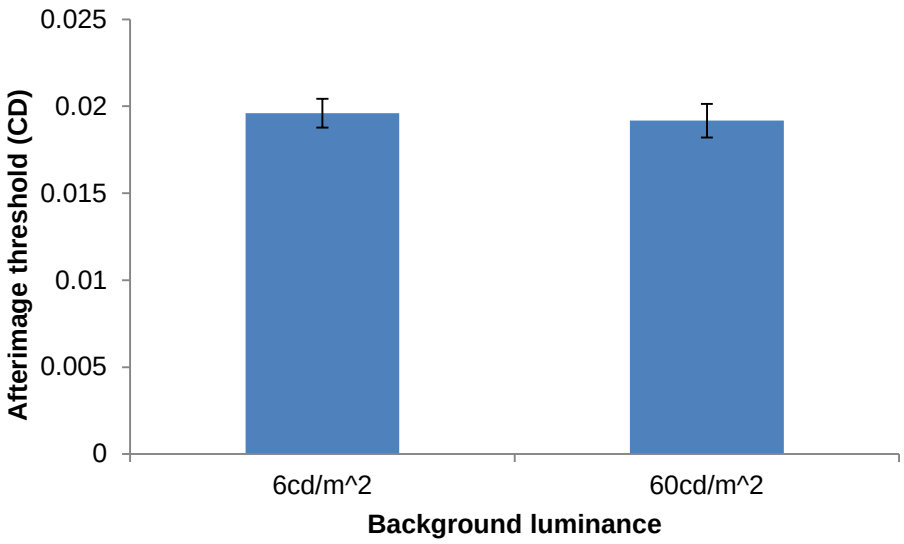


Figure 4-6. Afterimage thresholds measured at 6cd/m$^2$ and 60cd/m$^2$. Tests were repeatedly measured for six times for each stimulus conditions. The mean and one standard deviation values of the six tests were plotted. The stimuli had a chromatic displacement angle of 125$^o$, CD of 0.09 and gap time of 1 second. The luminance of stimuli employed was changed accordingly to have the same luminance as that of the background.

## 4.4 Results from deuteranopes

### Afterimage thresholds measured in two deuteranopes

Preliminary results showed that the deuteranopes exhibited significantly larger afterimage thresholds when measured immediately after the reference stimulus disappeared (gap time = 0s). However, when measured just after the stimulus offset, with delays of 1s, 2s, 4s etc., the thresholds decayed dramatically compared with the initial value, followed by an exponential decrease and then asymptote to a straight line. Student's t tests were computed at each point. The results showed that

there are significantly differences ($p < 0.05$) between the two groups when gap time equals to 0, 1, 4, 6, 8 and 10s. However, the p-value is approximately equal to 0.08 when gap time equals 2s and this may suggest that the measured afterimage strength is not significantly different at this point.

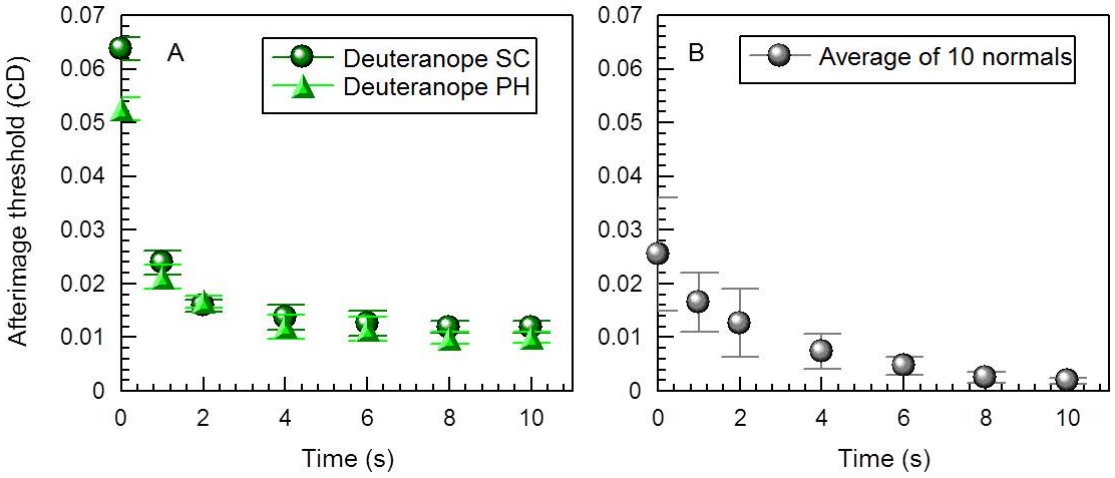


Figure 4-7. (A) Afterimage thresholds measured for two deuteranopes and (B) results for 10 normal subjects with normal colour vision. Both deuteranopes have much larger initial thresholds and the asymptotes are much higher than those measured in normal trichromats.

A comparison of pupil responses to chromatic stimuli measured in one normal subject and one deuteranope is shown in Figure 4-8. Both subjects exhibit very large onset pupil responses to the bluish stimulus and good offset pupil responses to the greenish stimulus. However, the deuteranope subject shows an absent onset pupil response to the onset of the greenish stimulus.

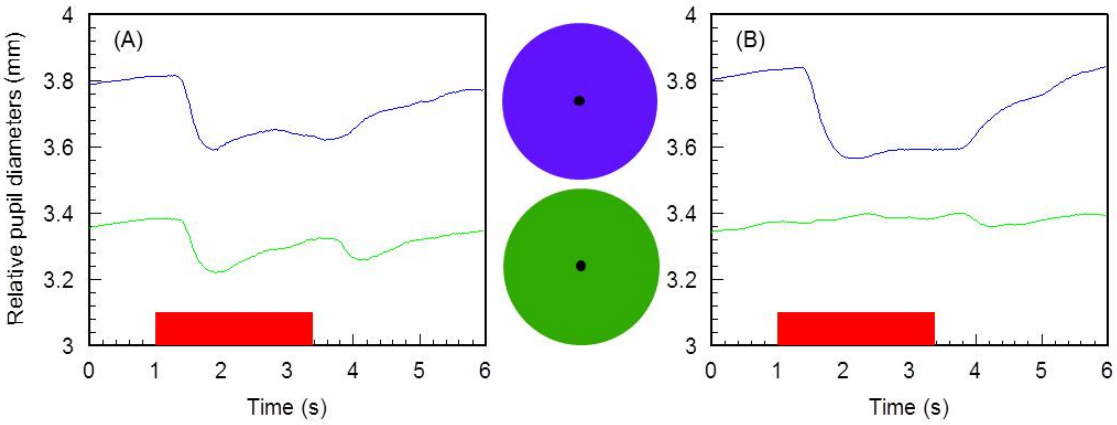


Figure 4-8. Pupil responses in a normal trichromat measured for stimulus colours that correspond to chromatic angles of 125$^{o}$ and 249$^{o}$ (A). Similar data are shown for deuteranope in section (B). The pupil response is absent to the onset of the stimulus but is present at the offset of the d-isoluminant greenish stimulus. Significant pupil constrictions can however be observed at the onset of the bluish stimulus which contains a large rod contrast component. The subject was aware of both colours, although the perceived colours were undoubtedly different to those experienced by a normal trichromat.

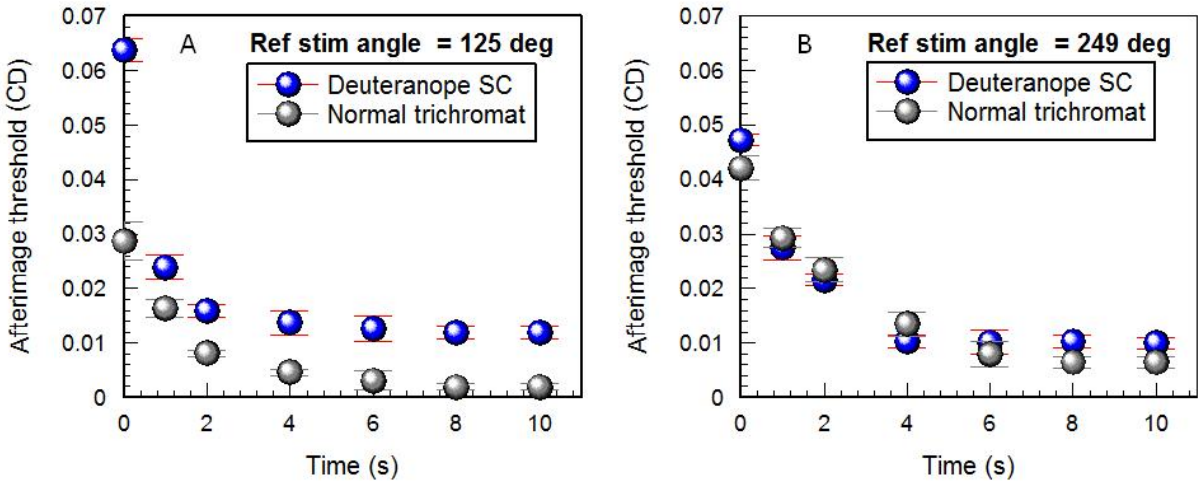


Figure 4-9. A comparison of the measured afterimage strength to two chromatic stimuli between a deuteranope and a normal trichromat. Two reference stimuli corresponding to angles of 125$^{o}$ (A) and 249$^{o}$ (B) were employed. The deuteranope yielded very similar results to the normal trichromat to in response to the bluish stimulus (B), but shows quite different results to the greenish stimulus (A).

## 4.5 Results from subjects with palinopsia and visual snow

The Red/Green and yellow/blue chromatic sensitivity, visual acuity, chromatic afterimage strength and duration and pupil colour responses were measured in the six subjects with visual snow syndrome. The tests were carried out in collaboration with Ruba Alissa.

All of the six visual snow (VS) subjects exhibited both normal visual acuity and colour detection thresholds. Figure 4-10 (A & B) shows typical results from one VS subject. His visual acuity measured binocularly yield slightly lower threshold (~0.25 arc min) than that measured with each eye separately and his R/G and Y/B chromatic sensitivity results are within the normal range.

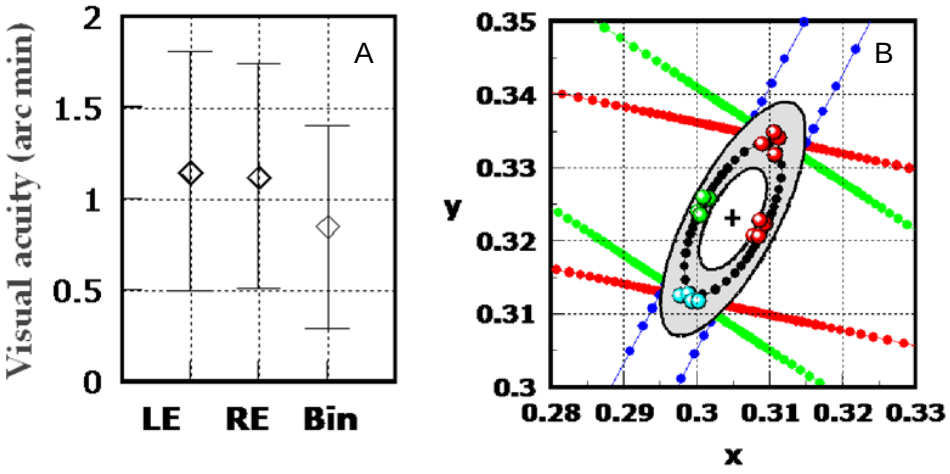


Figure 4-10. (A) Example of visual acuity (A) and chromatic sensitivity (B) measured in a subject with VS syndrome. The error bars plot ±2 standard errors that were obtained from the visual acuity staircase algorithm.

A comparison of the measured afterimage strength and duration between 10 normal trichromats and 6 VS subjects is shown in Figure 4-11. Because the error bars in

Figure 4-11 show standard errors for the groups, the VS subjects do not exhibit significantly different results from those obtained from the normal trichromats.

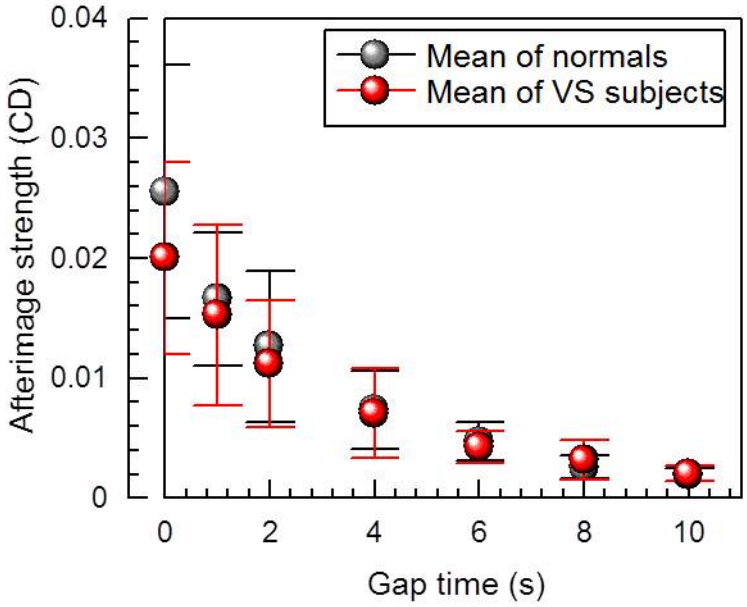


Figure 4-11. Chromatic afterimage strength and duration results measured in 10 normal subjects and in 6 VS subjects. The error bars plot the standard errors for the groups of VS and normal trichromats. The difference between the two groups at each point is not statistically significant ($p > 0.05$).

Pupil responses to chromatic stimulus have also been measured in 9 normal subjects and in 6 VS subjects (Figure 4-12). The chromatic stimulus employed had 0 rods contrast in addition to being photopically isoluminant (shown in Figure 4-1A). Both normal subjects and 2 VS subjects exhibited initial pupil constrictions to the onset of the coloured stimulus, with a latency of 320ms, followed by recovery during the stimulus and a secondary pupil constriction at the stimulus offset with latencies at approximately between 320 and 420ms. The secondary pupil responses can be attributed to the perceived red afterimages, which were reported to be seen by every subject at the stimulus offset. However, the pupil responses in the other 4 VS

subjects lacked the rapid recovery phase following the initial pupil constriction to the stimulus onset.

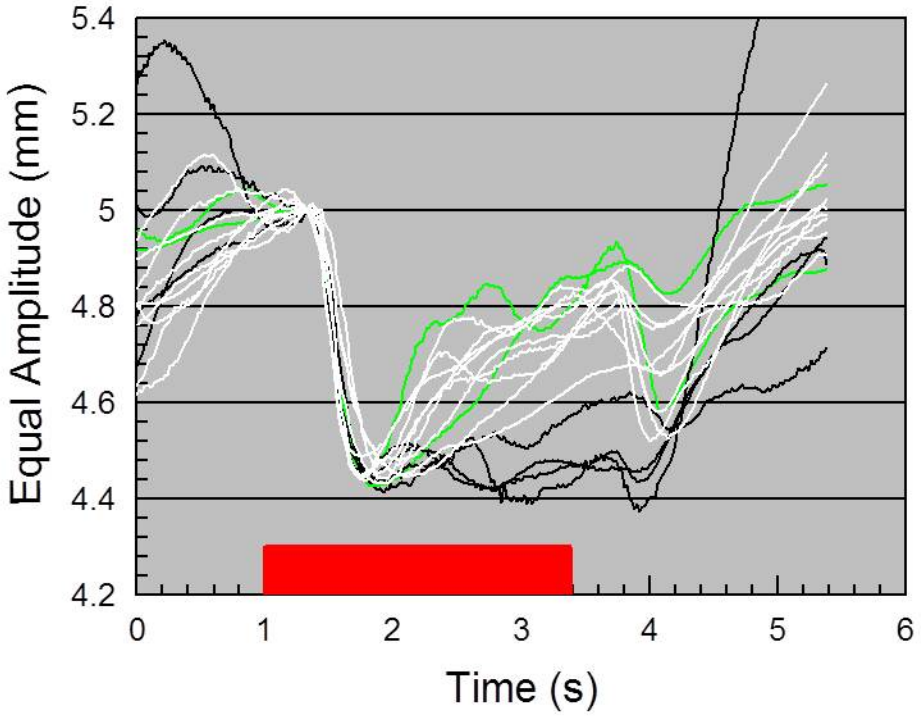


Figure 4-12. Pupil responses to chromatic stimulus measured in 9 normal subjects (white curves) and in 6 VS subjects (green and black curves). All subjects exhibited pupil constrictions to the stimulus onset and further constrictions at stimulus offset. The pupil recoveries rapidly following the initial constrictions in the normal subjects and 2 VS subjects. However, 4 of 6 VS subjects showed absent or slow recovery during the stimulus.

All the 9 normal subjects showed rapid recovery during the stimulus following the initial constriction. However, 3 of the 6 VS subjects exhibited completely absence of the rapid recovery. This result suggests the presence of a more sustained retinal afferent signal that may drive the pupil response in some of the VS patients and this may be linked to differences in retinal processing of visual signals that cause the perception of visual snow/prolonged afterimages when coloured stimulus is viewed against a uniform background.

## 4.6 Mechanisms for chromatic afterimages

### 4.6.1 Normal Trichromats

The chromatic afterimage thresholds corresponding to the d-isoluminant stimulus measured in normal trichromats reveal an exponential decay. These results are consistent with those reported in previous studies (Kelly and Martinez-Uriegas, 1993). Other studies have argued for possible mechanisms that drive the afterimage responses based on the colour opponent theory (Thompson and Burr, 2009, Mollon, 1974, Francis, 2010). Using the same theory, a simple model was derived to explain the results obtained in the current study.

Figure 4-13 shows the perceived afterimage as the opponent colour of the reference stimulus. This decays exponentially and after 10s the threshold is very close to the expected threshold for colour detection in normal subjects. Because the "greenish" reference stimulus is designed to be d-isoluminant according to the standard observer model, only the chromatic channel exhibits response signals to the reference stimulus. Therefore the afterimage is also likely to reflect any changes in the same chromatic channel as the reference stimulus. This argument is the basis of the schematic diagram.

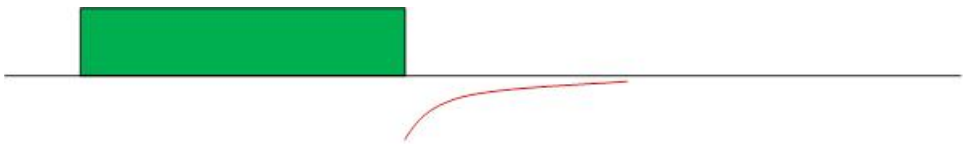

Figure 4-13. A schematic diagram shows the perceived reference stimulus and the opponent colour seen by a colour normal observer. The green rectangle shows the reference stimulus, the black line in the middle displays the time line and the red curve illustrates the perceived afterimage strength. It is drawn in the opposite side of the line to show the perceived afterimage as the opponent colour of the reference stimulus.

The subjects in Figure 4-2 have normal colour vision. Their colour vision thresholds fall in the gray region (Figure 4-14). The gray region shows the mean data obtained from 330 normal trichromats in the CAD test and the data was collected by Rodriguez-Carmona in 2005 (Rodriguez-Carmona et al., 2005). The colour vision results suggest that, in order to distinguish the employed greenish colour ($125^o$) from the background, even the most sensitive normal subject (e.g., result shown in Figure 4-14(A)) will need a CD with at least 0.003 to detect moving target in that chromatic displacement direction. This value is much larger than the smallest afterimage thresholds (<0.002) obtained from the normal trichromats but much smaller than the smallest afterimage thresholds (0.012) obtained from the deuteranope (Figure 4-2(C)). Similarly, when a bluish stimulus ($249^o$) is employed (Figure 4-9(B)), the smallest afterimage threshold is approximately 0.008 in the normal subject and this is larger than the normal trichromats smallest afterimage thresholds (~0.006) but less than deuteranope's chromatic threshold of this chromatic displacement direction (~0.011).

In fact, for the largest delay times investigated (when t = 8s or 10s), one reports seeing no chromatic afterimages. Then, the task becomes to match the test stimulus to background, which is equivalent to measuring one's chromatic discrimination threshold with respect to the achromatic background. Because the stimulus is designed to be isoluminant for the standard observer, a threshold of approximately ~ 0.004 is expected for the $125^o$ directions. The 0.004 is the medium

value from the normal trichromats colour vision results, but at that specific chromatic displacement direction, results obtained from normal trichromats can vary from ~0.003 to ~0.005.

The fact that the afterimage threshold is smaller than the actual measured chromatic threshold with the CAD suggests that either the subjects tested might be more sensitive than the standard median observer or that other channels might be involved. Since normal subjects may differ significantly from the standard observer, the “isoluminant” stimulus might not be exactly isoluminant to every normal subject investigated. In this case, one could rely on the residual luminance signal to detect the luminance contrast difference between the stimulus and the background when the colour signal becomes really weak. The detection of small luminance contrast signals may therefore be lower than the final thresholds when afterimage signals are negligible. This also explains why modern colour vision tests employ some dynamic luminance mask technique to minimize the detected residual luminance signal (Barbur et al., 1993, Mollon and Regan, 1999).

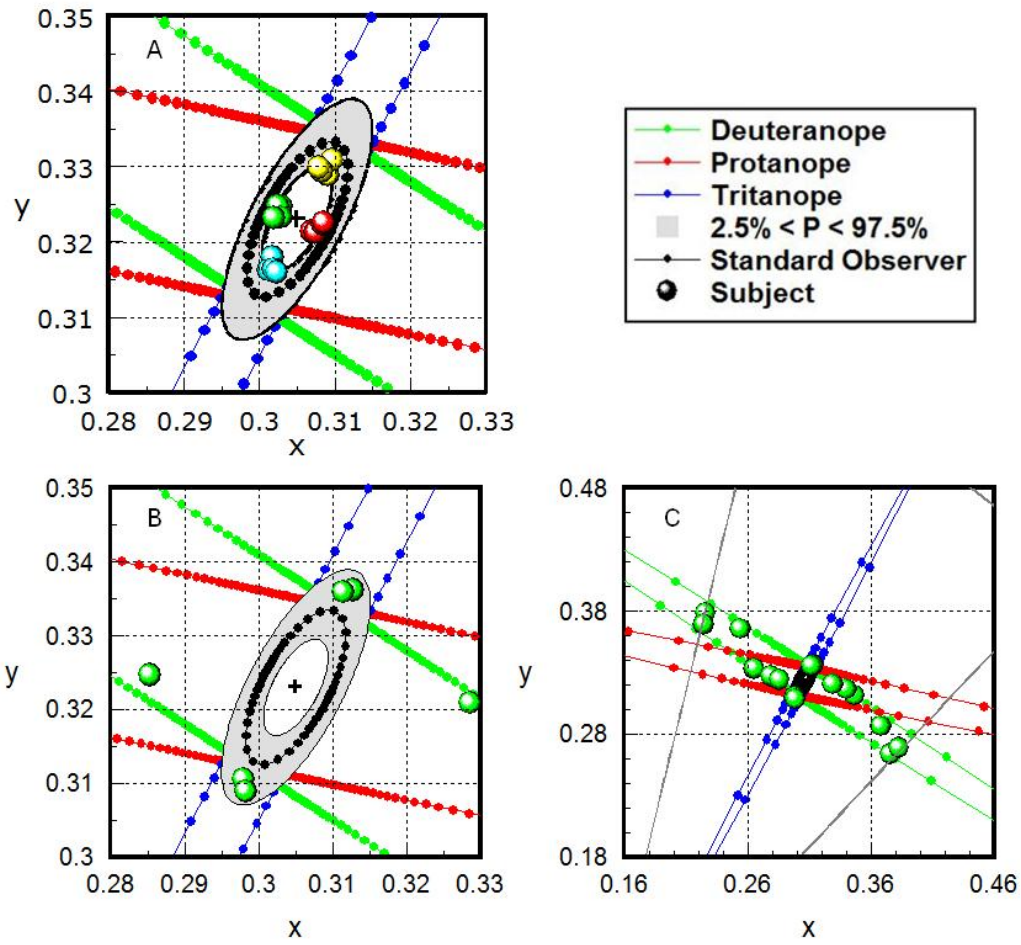


Figure 4-14. Chromatic thresholds measured in a subject with normal colour vision (A) and a deuteranope (B & C). In the normal subject, the measurements were carried out in 16 different directions. However in the deuteranope, 12 angles were measured in the red and green directions.

### 4.6.2 The afterimage thresholds reveal dichromacy

The deuteranope shows similar pupil responses to the bluish stimulus, but very different responses to the greenish stimulus when compared to the normal subject. This suggests that the deuteranope might use the same chromatic mechanism for

the bluish stimulus, but very different mechanism for the greenish stimulus. Figure 4-7(A) shows that the measured afterimage thresholds for the deuteranopes are different when compared to results for normal subjects in two ways – a very large initial afterimage threshold when t = 0 and abnormal high thresholds following an exponential trend for the rest (t = 1, 2 … 10).

**Possible mechanism for the large initial afterimage threshold**

Due to the lack of M cones, the stimulus is no longer d-isoluminant to a deuteranope. In fact, to generate the isoluminant greenish stimulus in a normal trichromat, the M cone signal is increased whereas the L cone signal is decreased to balance the overall luminance change. Because the deuteranope subject only has L- and S-cones, he only responds to L- and S- cone signals. When the stimulus is presented, the deuteranope detects L-and S- cone signal decrements and the offset of the stimulus causes L- and S- cone increments. The L cone increment may well result in an overall luminance increment at stimulus offset.

Figure 4-15. A schematic diagram shows perceived reference stimulus from the deuteranopes. The gray rectangle shows the L cone signal decrement and the red arrow indicates the sudden increment at stimulus offset.

For the standard observer, the luminance signal is defined as the sum of the L and M cone signals (L+M) and the yellow-blue colour signal is defined as the difference between the S cone signal and the sum of L and M cone signals (S - (L+M)). Due to the absence of M cones in deuteranopes, both the (L+M) and S - (L+M) signals yield different results. Therefore, the gray rectangle shown in Figure 4-15 can

indicate either a luminance decrement, a yellow blue colour signal or the combination of the two.

Nevertheless, in all these cases, the reference stimulus can be viewed as two components (the gray region and the red arrow in Figure 4-15). So the generated afterimage can also be modelled as two stages.

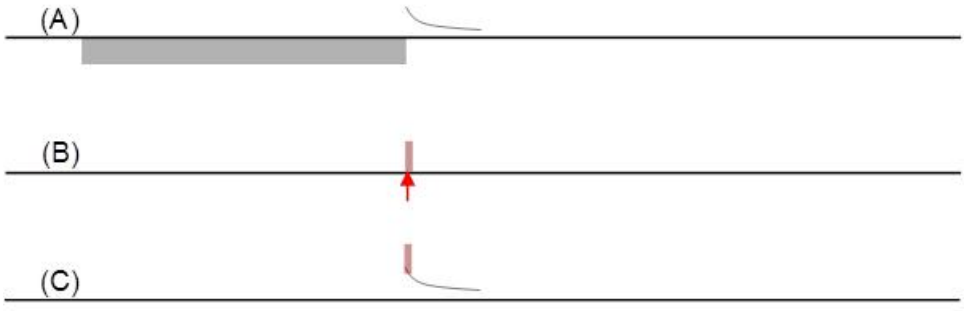


Figure 4-16. A deuteranope may well match the perceived 'afterimage' in two stages – (A) the curve shows the match of the afterimage created in the gray rectangle and (B) the red rectangle illustrates the matching signal of the impulse signal. (C) The final result is the sum of the signals produced by the two mechanisms. Notice that, the test stimulus is the exact opponent colour of the reference stimulus, i.e., the chromatic angle is reversed by $180^{o}$. Therefore, a deuteranope subject only responds to the L-cone increment in the test stimulus. Both colours are seen the same by the deuteranopes. The colour used in the figure is intended only for illustration purposes.

Figure 4-16 (A & B) shows how the afterimage perceived by a deuteranope can be modelled and separated in two parts – one part to match the afterimage caused by a stimulus (either a luminance decrement, a blue colour signal or the combination or the two) and one part to match the offset increment signal. The final outcome is the sum of the two matches shown in Figure 4-16(C). The model therefore explains the large initial afterimage threshold shown in Figure 4-7(A) and Figure 4-9(A) for the deuteranope. When the bluish stimulus ($249^{o}$) is employed (Figure 4-9(B)), the deuteranope subject yields just a little higher initial threshold than the normal

trichromat. This is because for this particular angle, the L and M cone contrasts are approximately equal to 0%. Therefore, it is much more isoluminant to the deuteranope. Also, the yellow-blue chromatic sensitivity is very similar between a normal subject and a deuteranope. Hence, the measured thresholds have similar values and shape.

**Mechanism for the abnormally high final thresholds**

Figure 4-9 (B) shows that along the chromatic displacement of 249$^{o}$, the results for the normal subject are similar to the deuteranope. The deuteranope's final threshold is, however, higher than the corresponding threshold in a normal trichromat. The deuteranope's colour thresholds are shown in Figure 4-14 (B & C) and his yellow-blue threshold is approximately 0.015 which is only slightly more than his smallest afterimage thresholds (around 0.011). This suggests that the deuteranope may also use some luminance signal to match the test stimulus with the background.

A similar pattern is observed for the greenish stimulus (125$^{o}$) in Figure 4-9(A), where the normal's thresholds are much lower than that of the deuteranope's. However, the deuteranope shows very similar thresholds (within 1 standard deviation) in both figures in the tail part of the curves ($x > 6s$). This suggests that the deuteranope uses the same mechanism for both stimuli. Because they only have two types of cones, the signal generated provide the inputs to all three channels – red-green, yellow-blue and luminance channel.

As demonstrated in Figure 1-22, Brown reported that the luminosity functions from deuteranopes are very similar to those of normal trichromats in the long wavelength

region (>590nm) whereas in the short wavelength region (<590nm), the deuteranopes are less sensitive to luminance (Brown and Wald, 1964). This is not surprising since the luminance channel depends only on L cone signals in deuteranope. These findings confirm these expectations and also show that the afterimage results for the deuteranope subjects can be accounted for using a single system colour discrimination, that is S – L.

### 4.6.3 Pupil colour responses in dichromacy depend on signal difference from the two types of cones

A comparison of pupil responses to stimuli that have $125^{o}$ and $249^{o}$ between dichromats and normal subjects is also shown in Figure 4-8. A more extensive study in pupillometry with stimuli that can have specific angles can be used to confirm the deduced results in the last section. Three possible outcomes can also be used to explain the results measured in deuteranopes for chromatic displacement directions that yield Zero S-cone signals (i.e., $155^{o}$ and $335^{o}$ shown in Figure 4-17).

(1) Pupil constriction caused by an increment in L cone signal.

(2) Pupil responses due to a difference (S – L) in cone signals.

(3) A combination of the above signals.

In the last section, the results suggested that an increment in L cone signal contributes to luminance detection in the deuteranope, and that the effectiveness of this luminance signal can be reduced by burying the stimulus in dynamic random luminance noise. Therefore, it is of interest to compare the pupil responses between

the tests that incorporate high levels of luminance noise and the tests that do not. On the other hand, we would expect that pupil responses to stimuli that have chromatic angles of $70^{o}$ and $249^{o}$ to be always present, due to the large S-cone contrasts which initiate a colour signal that is not affected by the luminance contrast noise. 2 normal trichromats, 2 protanope and 2 deuteranope subjects have been tested in this section. The chromatic displacement angles of interest and the corresponding cone contrasts generated in the stimuli are shown in Figure 4-17 and in Table 4-1, respectively.

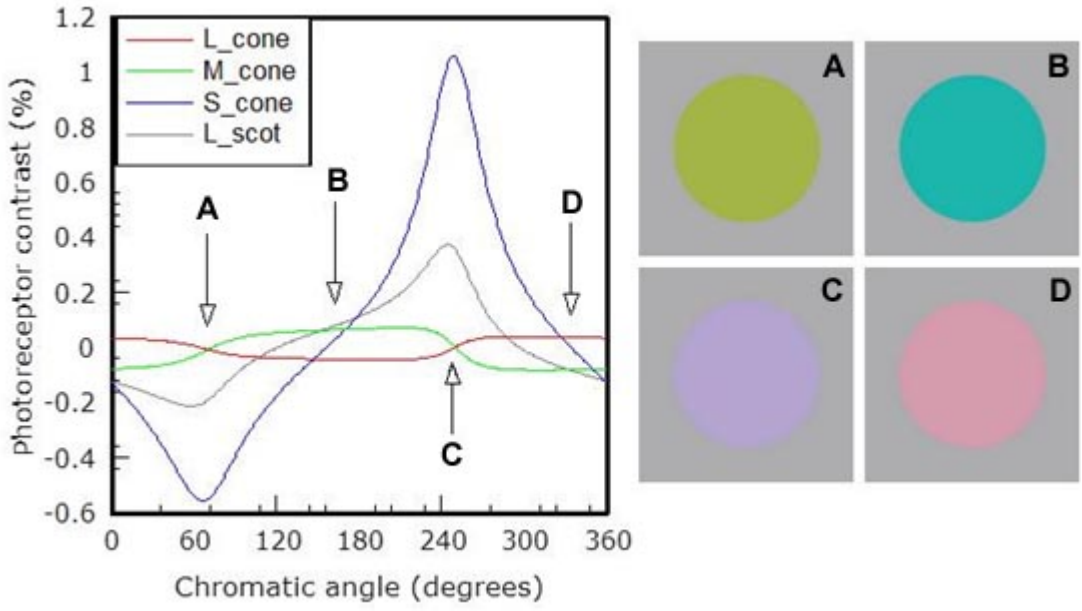


Figure 4-17. The graph shows selected chromatic displacement angles that have minimum and maximum S-cone contrasts. Examples of the corresponding visual stimuli are also shown – chromatic angle equals $70^{o}$ (A); $155^{o}$ (B); $249^{o}$ (C) and $335^{o}$ (D).

| Chromatic angles (deg) | Photoreceptor contrast (%) | | | |
|---|---|---|---|---|
| | L | M | S | Rods |
| 70 | -0.2 | -1.0 | -81.7 | -28.4 |
| 155 | -6.5 | 11.8 | 0.4 | 12.55 |
| 249 | 0.9 | -0.2 | 86.80 | 28.90 |
| 335 | 10.55 | -19.19 | -0.74 | -20.36 |

Table 4-1. Selected photoreceptor contrasts generated by the coloured stimuli employed in pupil studies.

Two types of dynamic luminance contrast noise were employed (Figure 4-18) – the Spatial Random Luminance Masking (RLMs), a technique that masks the detection of "local" luminance contrast signals generated by the coloured stimulus, and the Temporal Random Luminance Masking (RLMt) that masks the spatially pooled component of luminance contrast change.

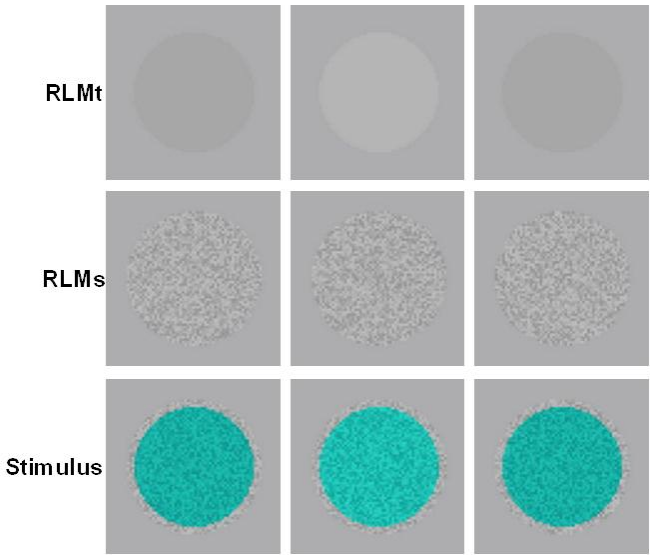


Figure 4-18. Dynamic luminance contrast noise employed in pupil studies. RLMt – luminance noise that masks components that have large spatial luminance summation, RLMs – noise that masks components that have local spatial summation and example stimulus with noises.

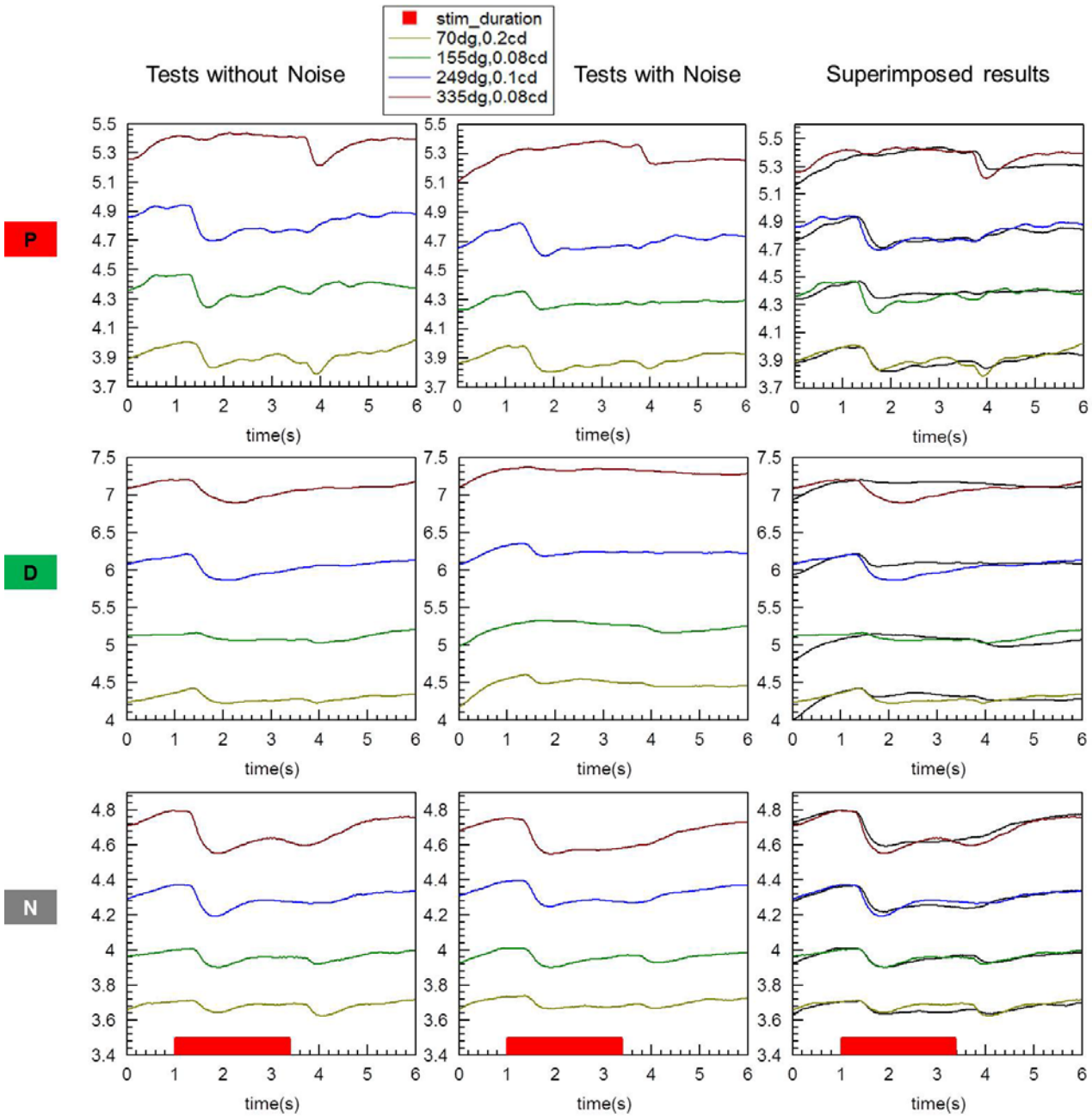


Figure 4-19. Example pupil responses measured in a protanope - P, a deuteranope - D and a normal trichromatic - N. Results in the first and second columns are shown for stimulus conditions with and without the dynamic luminance contrast noise (RLMs & RLMt). Results in the third column showed the superimposed result – the coloured traces were kept the same from the tests that did not have the noises whilst the black traces were the results from the corresponding stimulus conditions from the tests with the noises.

Figure 4-19 shows pupil responses measured in one normal trichromat, one deuteranope and one protanope subject. Student's t tests were carried out for the pupil response latencies at stimulus onset and offset between the two tests within same group and between groups for the same tests and the results showed no significant differences (p values > 0.05). The pupil response latencies can also be seen clearly in the superimposed diagrams in third column of Figure 4-19.

Although, both normal and deuteranope groups are likely to use the same pupil pathways (Figure 1-24), the two groups exhibited different pupil responses.

The normal subject produces very similar pupil responses between the tests without noises and the tests with noises. Only the pupil response to the offset of the yellowish ($70^o$) stimulus is reduced. This pupil response may be attributed to rod stimulation (increment) at stimulus offset. The results suggest that the rapid luminance contrast noise does not have obvious effects on the pupil response and that when the noise fails to mask pupil responses, the latter can be attributed to colour signals.

Unlike normal trichromats, in the absence of noise, the protanopes show large pupil responses to the offset of the reddish stimulus ($335^o$) and the onset of the greenish stimulus ($155^o$). In the presence of the noise, the pupil responses to the offset of the reddish stimulus and to the onset of the greenish stimulus are reduced. However, these pupil responses are not eliminated. On the other hand, the pupil responses to the yellowish and bluish stimuli are similar to those measured in the normal subject. The deuteranope shows completely opposite results to the reddish and greenish stimuli, but with much smaller response amplitudes. The response amplitudes are also different, primarily because of the different cone contrasts employed. The

observed responses show large differences partly due to the natural variation in pupil response amplitudes between individuals (Alexandridis et al., 1985).

In order to show these pupil response amplitudes are significant, statistics was carried out on the pupil response traces of interest. These pupil response amplitudes range from 0.051mm to 0.3mm. The smallest pupil response amplitude of interest shown in Figure 4-19 (diagram in the middle) is the pupil response to reddish stimulus (chromatic angle= 335, CD= 0.08). The noise level in the pupil trace was estimated by measuring the changes in pupil diameter at two points in time t1, t2 (see Figure 4-20) estimated from the average pupil response traces. The average pupil response was obtained by average 32 pupil traces. The noise standard deviation was computed from the values extracted from individual pupil traces. This was found to be ~0.016. The pupil response amplitude for the trace is 0.051mm and this pupil response amplitude is significant since the probability of measuring a pupil response amplitude larger than 0.051mm is extremely small ($p < 0.001$).

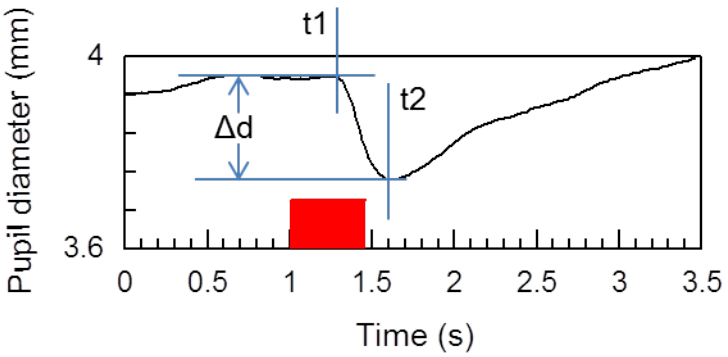


Figure 4-20. Example of pupil response diagram showing how the pupil response amplitude was extracted.

The pupil responses to the reddish and greenish stimuli measured in dichromats are reduced, but not eliminated, even when the amplitude of luminance contrast noise is high. This suggests that these responses combine a colour response and a luminance increment response. The luminance response is eliminated by the noise and leaves only the colour response. This finding supports the conclusions deduced from the afterimage test: that the deuteranope uses signals from the L cone only for the luminance channel and S – L for their chromatic channel. This result should also apply to protanopes who use M-cone signals only for detection of luminance and rely on the S – M signal for their colour channel. Tritanopes, on the other hand, use (L+M) for the luminance channel but can only discriminate red / green (L – M) colour differences.

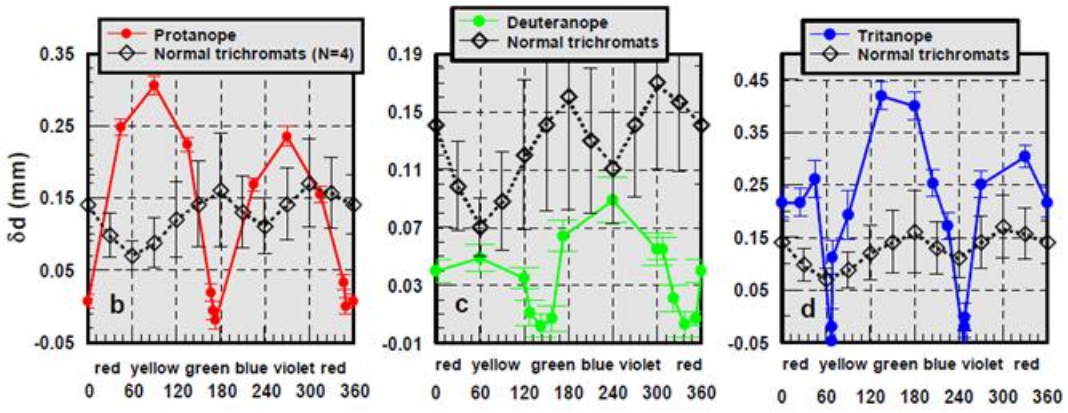


Figure 4-21. Pupil responses to isoluminant chromatic stimuli in protanopes, deuteranope and tritanopes. The direction of chromatic displacement was varied systematically from $0^o$ to $360^o$. (Adapted with permission from Barbur (2004)).

Barbur (2004) published a comprehensive review on pupil response components (Barbur, 2004b). The studies involved the use of grating-like colour stimuli, but similar luminance masking techniques to minimize the detection of luminance contrast signal. Pupil responses were measured for stimuli that varied from $0^o$ to

360$^{o}$ in each class of dichromat. The author found that the maximum and minimum responses for the three groups of subjects were shifted for dichromats along the chromatic axis, and these minimum values corresponded to the colour confusion bands.

In these studies, not only earlier results were confirmed, but we could also measure and predict more accurately the angles that yield zero response in dichromats.

For the protanope, the colour discrimination mechanism relies on different signal from the S and M cones, i.e., S – M. Therefore, when the signals from these two types of cones are equal, the colour signal will be minimized and pupil colour responses will be absent. These chromatic angles can be found in Figure 4-17 when the S cone and M cone have the same contrast value, i.e., 169$^{o}$ and 349$^{o}$. Similarly for the deuteranope, the angles are 147$^{o}$ and 326$^{o}$ and in the tritanope 70$^{o}$ and 249$^{o}$. These angles match well the minimum pupil responses shown in Figure 4-21.

Using the same approach, the chromatic angles that yield the maximum pupil response correspond to the largest colour signals for each group. For protanopes and deuteranopes, these angles are 70$^{o}$ and 249$^{o}$, respectively. Tritanopes have two ranges of angles (120$^{o}$ and 220$^{o}$) and (300$^{o}$ to 370$^{o}$), because in these two ranges the different contrasts between L and M cones are similar when the signals are localised on the ellipse contour. Tritanopes show a ‘narrowed’ range of maximum values, partly because the stimuli employed had a constant chromatic displacement (along a circular contour shown in Figure 4-17).

The angles that produce minimum pupil colour responses for the dichromats are the angles of the protan-, deuteron- and tritan- confusion lines for the same background

chromaticity, in this case (0.298, 0.335). Using the same approach, we can predict the colour confusion lines for different background chromaticity and hence predict the maximum and minimum colour signals and the corresponding pupil responses.

# 5 A STUDY OF PUPIL RESPONSE COMPONENTS IN NORMAL SUBJECTS AND IN PATIENTS WITH CONGENITAL OR ACQUIRED HEMIANOPIA

## 5.1 Introduction

Unilateral destruction of the primary visual cortex causes loss of conscious visual perception in the counterlateral hemifield. Damage to the right side of the posterior portion of the brain or right optic tract can cause a loss of the left field of view in both eyes and vice versa. Homonymous hemianopia refers to a condition in which a person can see only to one side and it is usually secondary to stroke, head trauma or localised tumors (Zhang et al., 2006).

Although the retina geniculostriate pathway (from retina to lateral geniculate nucleus of the thalamus to striate cortex) is the most thoroughly understood and studied visual pathway, the primary visual cortex is not its only target in the primate brain (Cowey and Stoerig, 1991). Cowey and Stoerig showed that there are at least 10 pathways from the retina to the brain, and that the LGN also sends very small projections to prestriate cortical areas that survive damage to V1 (Cowey and Stoerig, 1992).

A number of studies (Sahraie and Barbur, 1997, Barbur et al., 1994a, Weiskrantz et al., 1998, Barbur, 1996) have shown that pupil responses elicited with small stimuli

of low contrast (<40%) are normally absent in subjects with acquired damage of the primary visual cortex. The same studies also show that when large, high contrast stimuli are employed, there is no difference in pupil response between the sighted and the corresponding blind regions of the visual field. These studies also demonstrate a clear cortical contribution to the pupillary response because removal of V1 in monkeys also diminishes the pupil light reflex response (Weiskrantz et al., 1998). However, other reports show that the pupil continues to respond to spatial structure and colour even in patients with loss of V1 (Weiskrantz et al., 1999). These observations suggest that specific stimulus attributes processed by extrastriate visual areas can influence the midbrain.

The majority of subjects involved in the studies mentioned above had dense homonymous hemianopia from acquired unilateral occipital damage. These subjects were aware of their visual deficit and received medical care and training. However, those with congenital homonymous hemianopia who were born with the symptom are usually not aware of the visual deficit and are usually identified as abnormal via routine eye examination. Brain plasticity and development in early life (Kolb, 1995) may play an important role in determining the observed differences between acquired and congenital types. To understand more about the visual processing mechanisms in these subjects, we investigated and compared pupil responses to visual stimuli that isolate either photopic luminance or colour signals both in the sighted and in blind region of the visual fields.

## 5.2 Methods

### 5.2.1 Subjects

10 normal trichromats (aged between 28 to 55 years with a median of 32 years), 11 subjects (aged between 44 and 72 years with a median of 53 years) with acquired homonymous hemianopia and four subjects (aged between 22 to 33 years with a median of 28 years) with congenital homonymous hemianopia caused by unilateral post-geniculate lesions participated in the study. The acquired group consists of 10 subjects with occipital lesions and one subject with optic radiation. The subjects do not show any other functional loss as a result of cortical damage. All subjects were given written informed consent, and the study was approved by the research and Ethics Committee of City University London.

| Sex | Cause | Location of damage | Age(years) | Duration |
|---|---|---|---|---|
| Male (JS) | Infarct | Occipital lobe & optic radiation | 66 | 1 |
| Male (GY) | Head injury | Occipital lobe | 53 | 40 |
| Male | Surgery | Occipital lobe | 72 | 18 |
| Male | Infarct | Occipital lobe & optic radiation | 67 | 3 |
| Female | Infarct | Occipital lobe & optic radiation | 44 | 1 |
| Male | Infarct | Occipital lobe & optic radiation | 46 | 5 |
| Male | Head injury | Occipital lobe | 44 | 34 |
| Male | Infarct | Occipital lobe & optic radiation | 62 | 1 |
| Male | Haemorrhage | Occipital lobe | 50 | 1 |
| Male | Infarct | Occipital lobe & optic radiation | 63 | 2 |
| Male | Haemorrhage | Optic radiation | 49 | 2 |

Table 5-1. Summary of subjects with acquired homonymous hemianopia.

| Sex | Age(years) | Detected | Past medical history |
|---|---|---|---|
| Male (RC) | 22 | Routine eye check up | None |
| Male (AA) | 33 | Routine eye check up | None |
| Female (NS) | 28 | Routine eye check up | None |
| Male (NJ) | 33 | Routine eye check up | Illness at birth, required to wear a respirator for several months. |

Table 5-2. Summary of subjects with congenital hemianopia.

### 5.2.2 Apparatus & pupillometry stimuli

The P_SCAN system (introduced in section 2.2) was employed to generate appropriate stimuli, to measure the pupil responses and to monitor the subject's point of regard. Stimuli were presented on a uniform background field either in the sighted or blind hemifields according to the visual field results for the hemianopia subjects or left or right visual field for the control subjects.

Two types of stimuli were produced to isolate either chromatic or luminance channels. The stimuli were presented for 480ms in a 3.5s presentation, in which the size of pupil was measured continuously. The achromatic stimuli have fixed sizes but varied in contrast (20%, 100% and 400%). The choice of luminance, contrasts within a large range was based on findings from a previous study (Barbur, 2003). These earlier results show that two components (transient & sustained) are likely to be involved in the control of the PLR response. One component involves a direct projection to the striate cortex, and exhibits response saturation at large contrast (>40%). The second component exhibits low contrast gain, extensive spatial summation and is likely to reflect the properties of midbrain projections. The chromatic stimuli consist of one greenish stimulus and one reddish stimulus. The latter can have one of two chromatic saturations (Figure 5-1). The chromatic stimuli

were designed to be both photopically and scotopically isoluminant and were buried in dynamic contrast random luminance noise so as to minimize the detection of any possible residual luminance signals. The uniform background field had CIE chromaticity: 0.298, 0.335 and a luminance of 3cd/m$^2$ for the pupil light reflex tests and 12cd/m$^2$ for the pupil colour response tests.

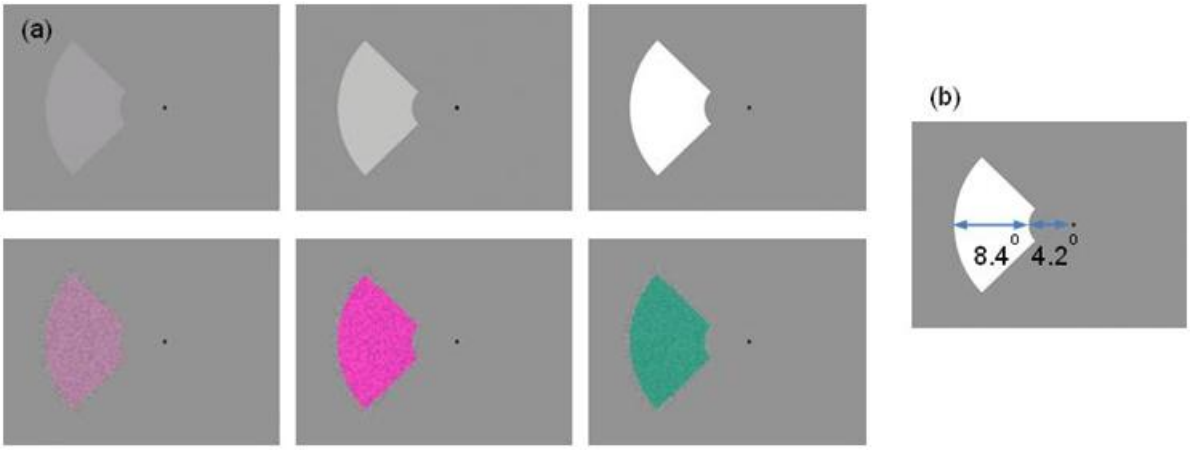


Figure 5-1. (a) Illustration of the visual stimuli designed to isolate luminance and chromatic channels. The chromatic stimuli were buried in RLM noise to minimize the detection of any residual luminance signal. (b) The angle of the sector (section b) subtends 92$^o$ and they were presented 4.2$^o$ away from fixation, along the horizontal meridian. The uniform background field subtended a visual angle of 30$^o$x24$^o$.

In the subjects with visual field loss, the locations of stimuli were restricted in the affected hemifield only. The affected hemifields were based on the parametric plots which we were informed by the ophthalmologists. Not all the visual field data was available to us, however, in parametric tests carried out by the ophthalmologists, they have demonstrated absence of residual vision in the affect areas of visual fields. The stimuli were then restricted to these locations. Figure 5-2 and Figure 5-3 shows the examples of visual fields results superimposed with the stimuli employed in the acquired and congenital subjects.

When tested with our stimuli in the affected visual fields, the acquired subjects show no conscious perception of anything presented in the visual field whilst some of congenital cases were aware of something presented in their affected visual fields although they could not report the structure, colour or any other details of the stimulus. Stimuli were moved to different part of visual field was to ensure that any conscience perception of the stimulus when presented in the affect visual field was minimized.

For all the participants with acquired damage, almost all of them showed dense and severe damage in their blind hemifields. Figure 5-2 shows the superimposed picture of the stimuli employed and the visual field result from one subject with acquired visual field loss in the right hemifield (subject GY).

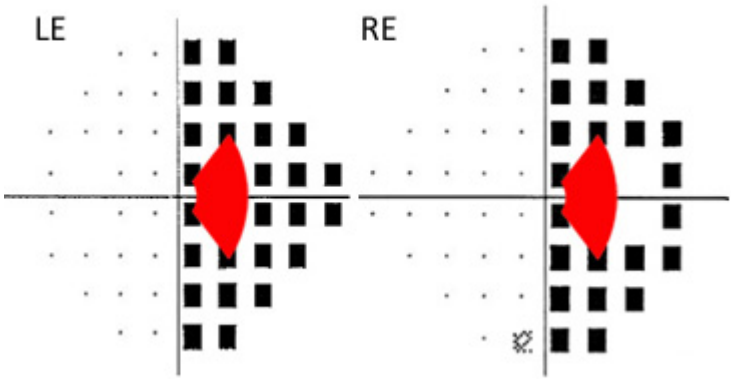


Figure 5-2. Humphrey Visual Field 24-2 results from subject GY superimposed with the stimulus employed. The stimulus was located 4.2$^{o}$ in the right hemifield.

In the subjects with congenital visual field loss, however, the visual field loss is always not symmetrical or complete in the two eyes. Three of these participants showed a severe visual field loss in their blind hemifield and one of them (NJ) exhibited a large spare vision in the vertical pole. The stimulus was shifted 9$^{o}$ into the periphery in order to be restricted to his blind hemifield.

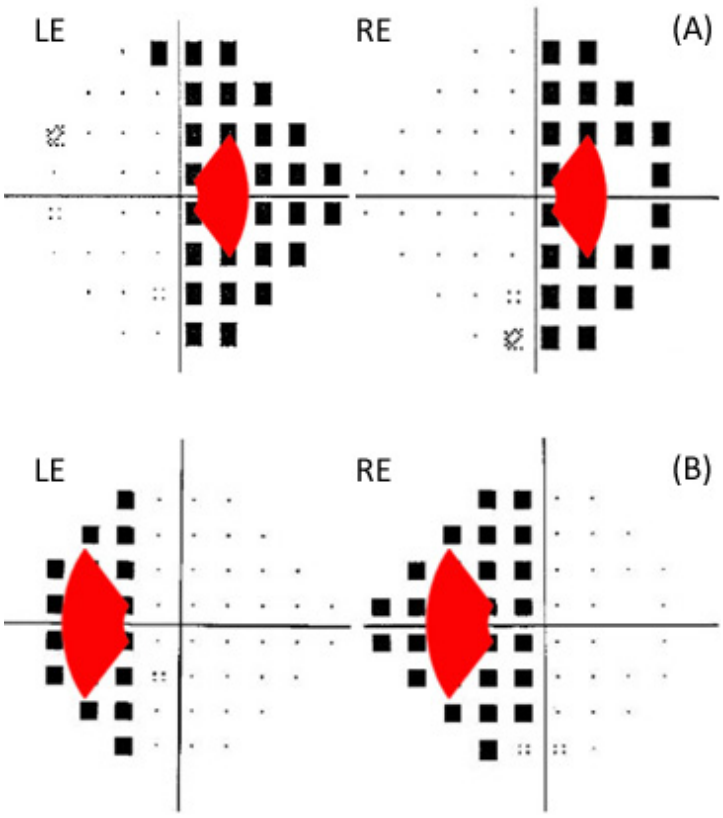


Figure 5-3. Superimposed visual field results and the stimulus employed from two subjects with congenital visual field loss – RC (A) and NJ (B).

## 5.3 Results

### 5.3.1 Pupil light reflex response measurements

Pupil responses to light flux stimuli measured in a 30 years old subject with normal colour vision and in two subjects with acquired hemianopia subjects are shown in Figure 5-4. In the normal subject, the pupil responses measured from either the left hemifield or the right hemifield show almost no difference, and the light flux stimuli

produce a classic pupillogram with a latency of 280ms and with the largest pupil constriction to the stimulus that has the largest luminance contrast, i.e. 400%. The sighted hemifield yields PLR responses of similar response latency and amplitude in acquired hemianopia subjects, but are almost absent in the blind hemifield, especially when the stimulus has small luminance contrast. In the subject with acquired hemianopia – GY, the pupil starts responding to blind hemifield stimulation for luminance contrast greater than 100%. GY's response latency to the largest contrast light flux stimulus employed is about 20ms longer in the blind hemifield than in the sighted hemifield. Pupil responses in subject JS are completely absent to both the 20% and 100% contrast light flux stimuli.

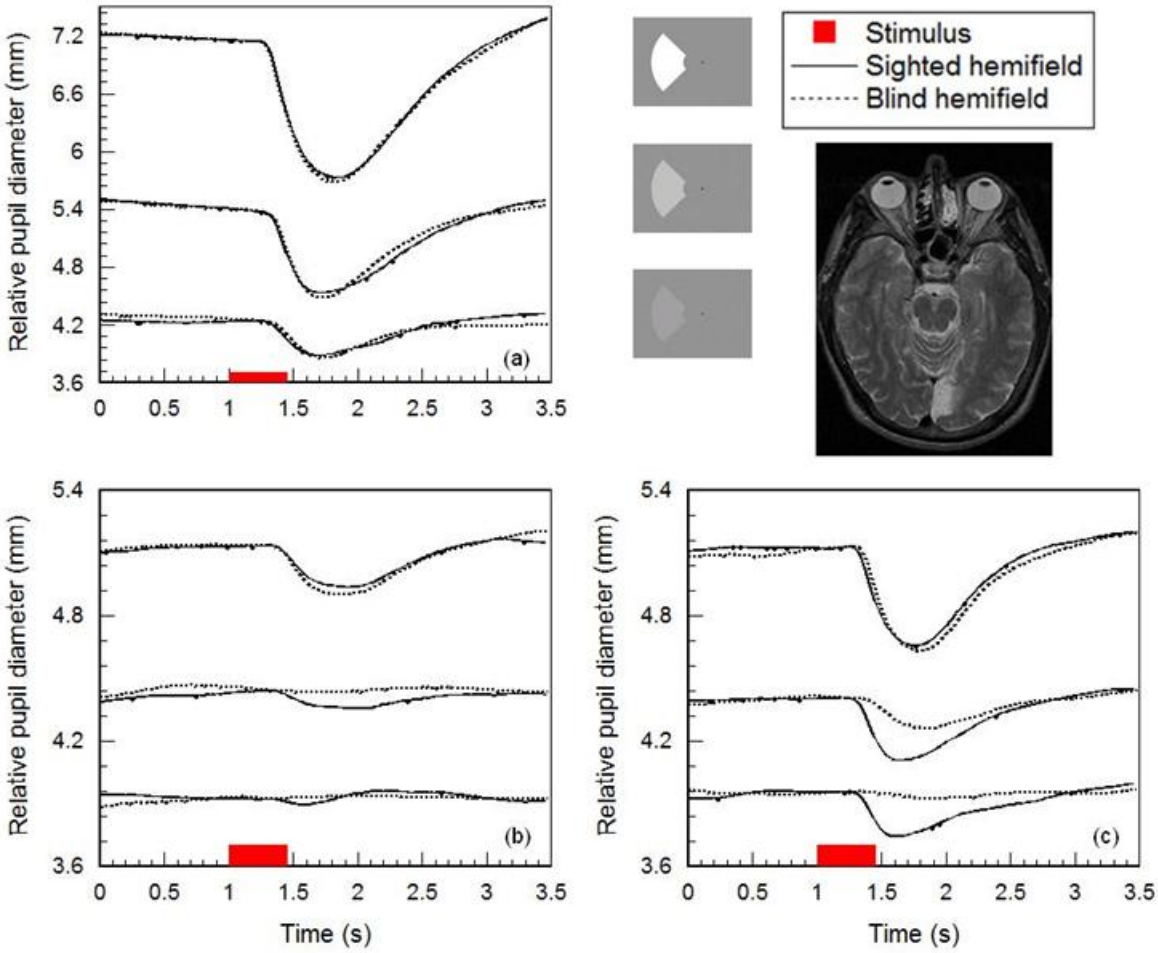


Figure 5-4. Pupil responses to light flux from a typical normal trichromat (a) and two subjects with acquired hemianopia – JS and GY (b & c). The MRI scan shows that subject GY has significant damage in the left primary visual cortex with sparing at the pole (Barbur et al., 1993). GY is clinically blind in the right hemifield, but exhibits small (~3.5$^{o}$) macular sparing (Barbur et al., 1980). The pupil responses for the normal subject were measured either in the left hemifield (solid line) or the right hemifield (dotted line). In the case of hemianope, pupil responses were measured both either in the sighted and the blind hemifields. In each diagram, the lowest pupil responses traces were the raw response traces and the base lines reflect the steady-state pupil sizes. The other traces were shifted up vertically for clarity of presentation and analysis purposes.

Unlike the subjects with acquired hemianopia, all the four patients with congenital loss of visual field show good PLR responses to all 3 stimuli (Figure 5-5). Subject NJ and NS (Figure 5-5 (c & d)) shows enhanced pupil responses in the blind

hemifields compared to the sighted hemifields, even to the stimulus that only has 20% luminance contrast. Pupil response latencies to all stimuli are the same (approximately 280ms) for all congenital subjects.

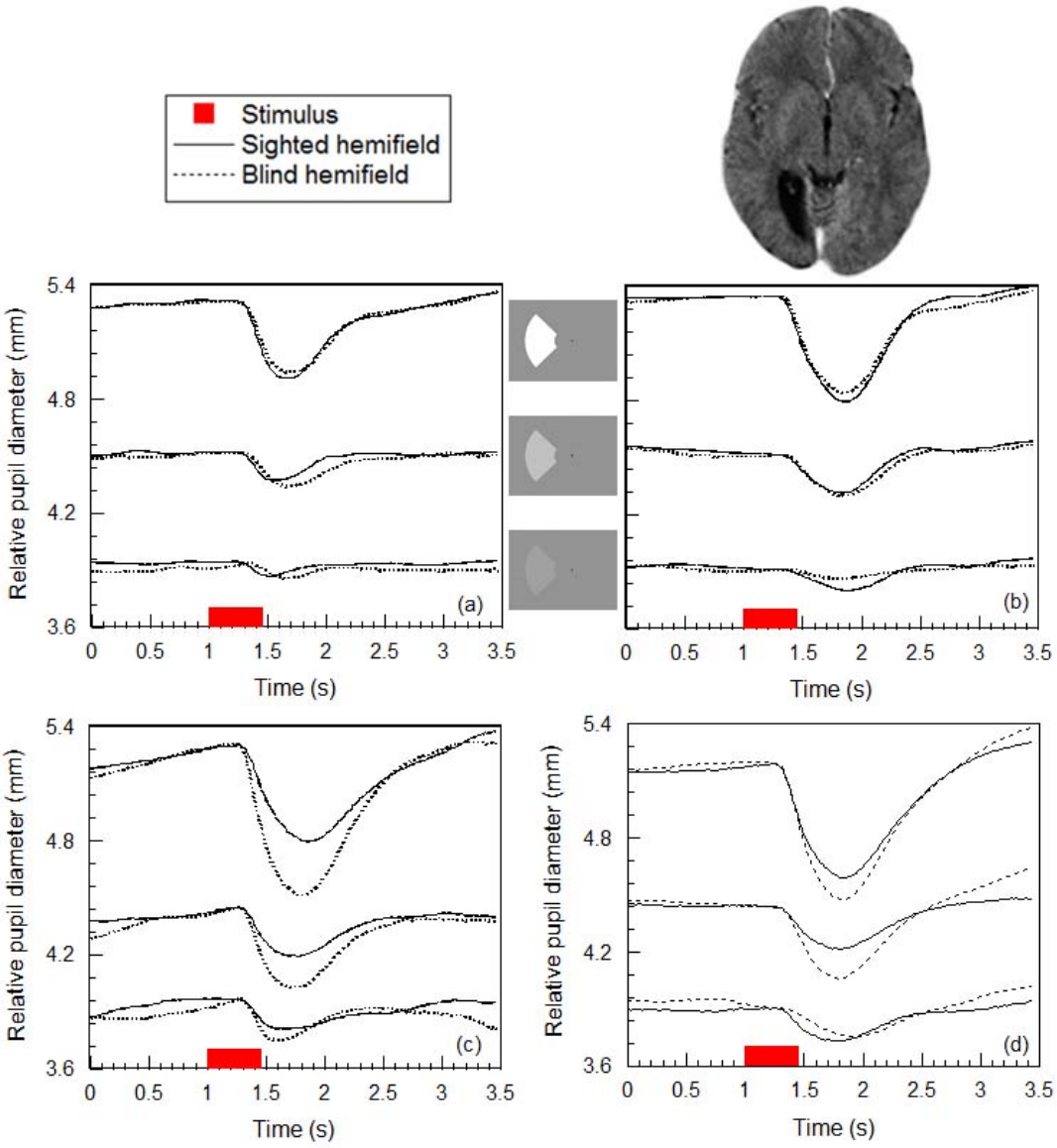


Figure 5-5 (a, b, c & d). Pupil responses to light flux changes in four congenital hemianopia subjects – RC, AA, NJ and NS. The MRI scan result is from subject AA (b) and it shows significant damage in the right primary visual cortex.

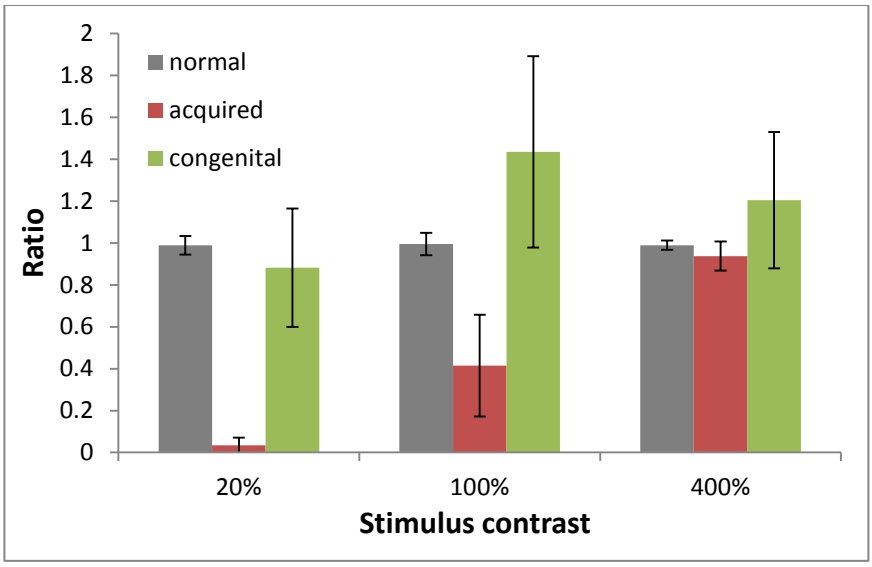


Figure 5-6. The mean and the corresponding 1 ±std for the ratios of pupil responses from the stimuli in the blind hemifields to those in the sighted hemifields in subjects with normal vision, acquired visual field loss and congenital visual field loss in the achromatic tests. The ratio from the normal group was calculated using the pupil amplitudes from the left hemifield divided by that of the right hemifield.

Figure 5-6 shows the ratios of pupil responses from the stimuli in the sighted hemifield to those in the sighted hemifield for the three groups. The normal subjects exhibited very similar ratios (~1) to all the three achromatic stimuli. Patients with acquired loss of visual field showed absent pupil response to the stimulus that had the lowest luminance contrast (20%). However, when the contrasts of the stimuli were increased, they exhibited an increased ratio. The ratios from patients with congenital visual loss showed larger values than the other groups, but the standard deviations were also much larger. Student's t tests were carried out to compare the results in respect to the normal subjects. When compared with the normal subjects, the patients with acquired visual loss showed significant different responses ($p<0.05$) to the stimuli that were of 20% and 100% whilst the patients with

congenital visual field loss exhibited significant difference ($p < 0.05$) to the stimulus that was of 100%.

### 5.3.2 Pupil colour responses measurements

Figure 5-7 (a, b, c) shows a comparison of pupil responses to chromatic stimuli measured in a normal trichromat and in two subjects with acquired hemianopia. In normal subjects, both hemifields elicit pupil responses with very similar amplitudes and latencies. The largest response corresponds to the most saturated “red” stimulus. These responses are, however completely absent when the stimulus is presented to the blind hemifields in the subjects with acquired hemianopia. When the sighted hemifield is stimulated, both subjects with acquired hemianopia show relatively good pupil responses, with the largest response amplitude corresponding to the reddish stimulus of larger saturation.

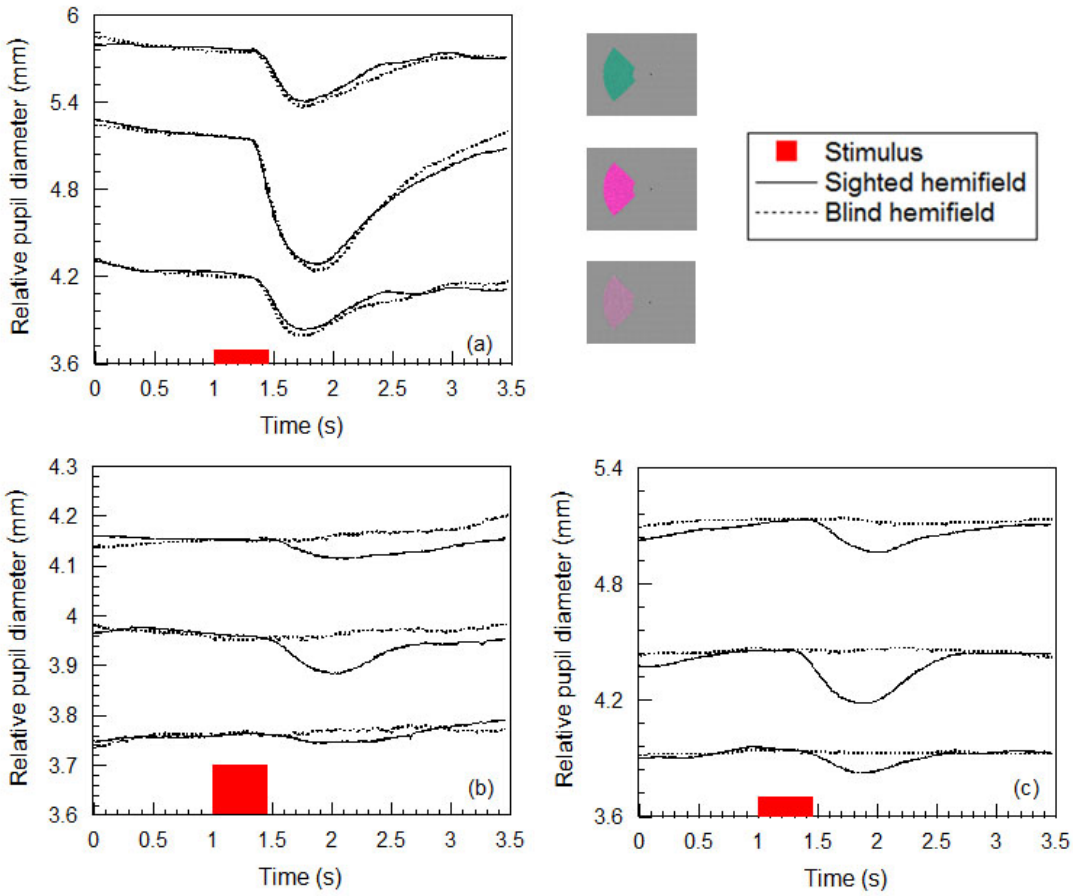


Figure 5-7. Pupil responses to chromatic stimuli in a normal trichromat (a) and in two subjects with acquired hemianopia – (JS & GY) (b & c).

The congenital hemianopes (Figure 5-8) show very different results when compared to the subjects with acquired hemianopia. The latter do not exhibit pupil responses when the stimulus is presented to the blind hemifield. In the sighted hemifield, all four congenital hemianopes exhibit pupil responses that are similar to those measured in the normal trichromat. Apart from subject AA showing an absent pupil response to the reddish stimulus that has a smaller CD in the blind hemifield, relatively good pupil responses can be observed in all congenital hemianopes. When compared to the sighted field, the response amplitudes are much reduced in the blind hemifield in subject RC (a) and AA (b). Subject NJ (b), on the other hand,

shows comparable pupil responses to the 1st and 3rd stimuli but an enhanced pupil response in the blind hemifield to the 2nd reddish stimulus that has the larger CD. Subject NS (d) also exhibit enhanced pupil responses to the two reddish stimuli.

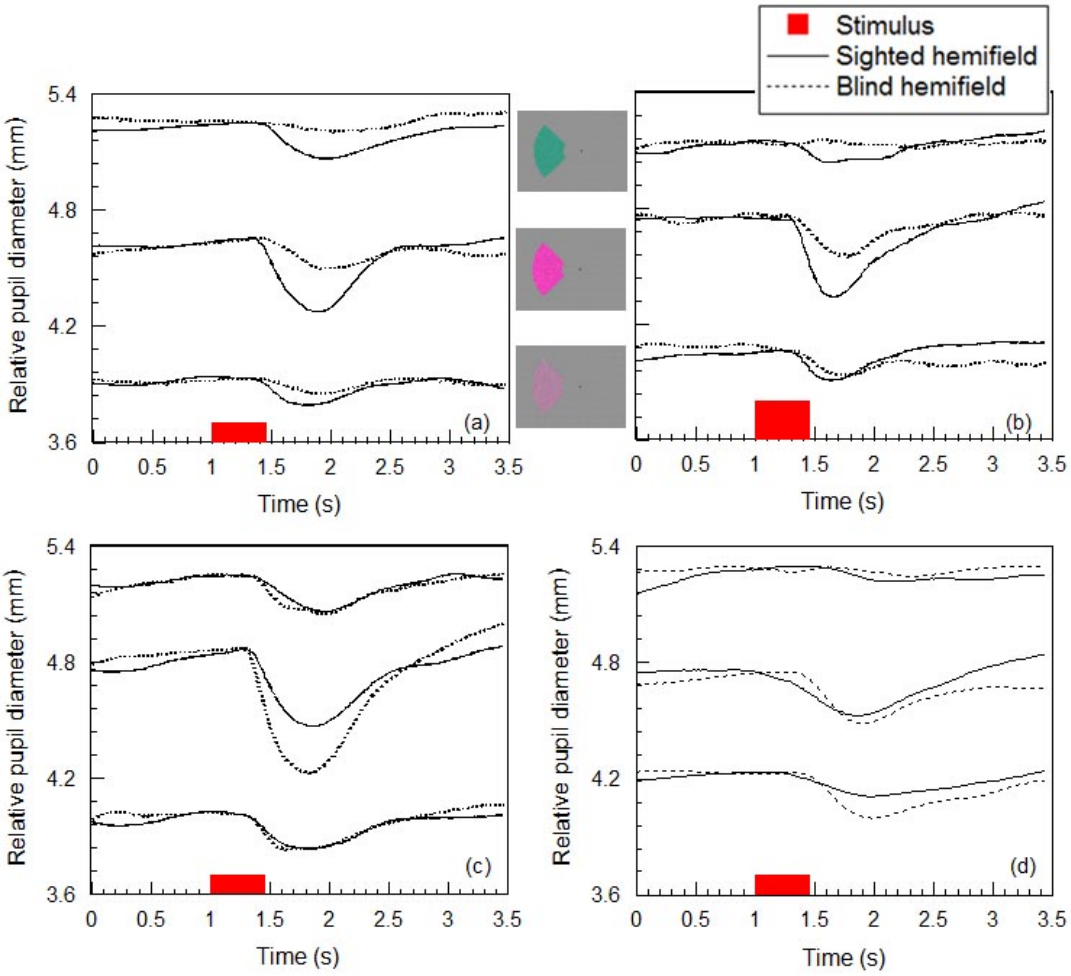


Figure 5-8 (a, b, c & d). Pupil responses to chromatic stimuli measured in four congenital hemianopes – RC, AA, NJ and NS.

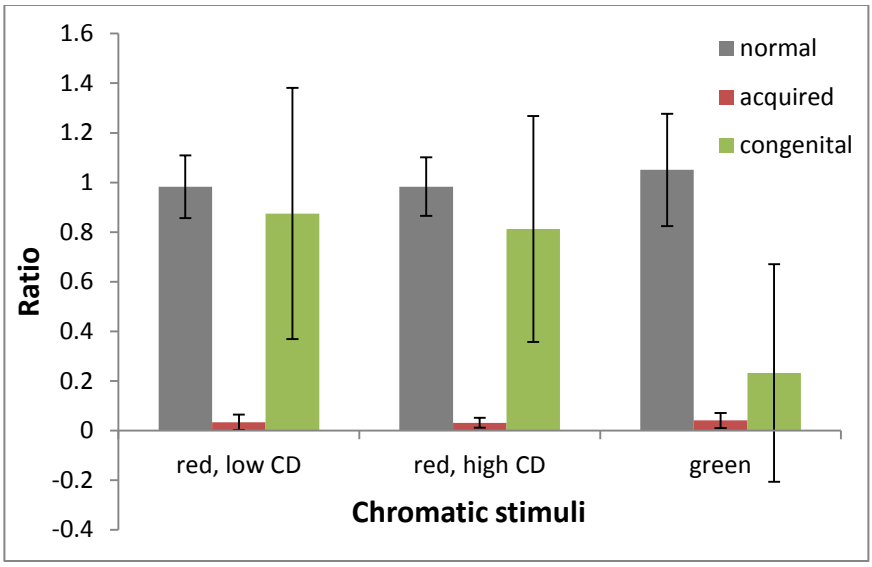


Figure 5-9. The mean and the corresponding 1 ±std for the ratios of pupil responses from the stimuli in the blind hemifields to those in the sighted hemifields in subjects with normal vision, acquired visual field loss and congenital visual field loss in the chromatic tests. The ratio from the normal group was calculated using the pupil amplitudes from the left hemifield divided by that of the right hemifield.

Figure 5-9 shows the ratios of pupil responses from the stimuli in the sighted hemifield to those in the sighted hemifield for the three groups in the tests with chromatic stimuli. The normal subjects exhibited very similar ratios (~1) to all the three achromatic stimuli. When compared with the normal subjects, patients with acquired loss of visual field showed absent pupil responses to all coloured stimuli which is significant from the normal group ($p<0.05$). The results from patients with congenital visual loss showed almost similar mean pupil response amplitudes to the reddish stimuli ($p>0.05$), significant smaller pupil responses to the greenish stimulus ($0<0.01$), but with much larger standard deviations.

## 5.4 Discussion

Normal subjects show similar pupil responses to both light flux and chromatic stimuli with little or no difference between the two hemifields. Pupil responses measured in the blind hemifield of patients with acquired cortical damage are either absent or much reduced in response to both chromatic stimuli and luminance stimuli of low contrast. When the contrast of the light flux stimulus is increased, pupil responses increase in the blind hemifield and they yield similar responses for stimulus contrast above 400%. The absence of pupil responses to stimuli that are of low contrast (20%) are likely to be linked with cortical projections whilst the increased pupil responses to stimuli that are of large contrasts (100% & 400%) are likely to be associated with subcortical projections (Figure 1-24). Previous studies on patients with damage to the geniculostriate projections have revealed similar results (Barbur, 2004b, Brindley et al., 1969, Cibis et al., 1975, Harms, 1951, Kardon, 1992).

Pupil responses measured in patients with congenital loss of visual field are, however, exhibited different results when compared to the acquired group. Unlikely the patients with acquired visual field loss who show no pupil responses to achromatic stimuli that are of low contrast or to chromatic stimuli, the patients with congenital loss showed relatively good PLR and PCR responses in their blind hemifields. In two subjects (NJ & NS), the pupil responses in the blind hemifields are greater than those measured in the sighted hemifields. The existence of a separate afferent pupil pathway associated with subcortical projections provides an explanation for the pupil responses that can be elicited with the light flux stimuli of high contrast. It cannot, however, explain the PCR responses, the PLR responses

to 20% light flux stimulus and the enhanced responses in the blind hemifield in the congenital subjects. For the congenital hemianopia group, these observations suggest that, in the absence of normal functioning of the direct geniculostriate projection, other enhanced projections to midbrain nuclei or to the extrastriate region of the brain (that bypass the primary visual cortex) may exist and that these projections are reflected in the pupillary pathways (Figure 1-24), however, why these signals are enhanced in the damaged visual fields is not clear.

Using diffusion-weighted MRI techniques, Bridge (2008) reported that there was evidence suggesting there might be different connections between patients with cortical damage in childhood and normal subjects and the former might even have strengthened connections (Bridge et al., 2008). The enhanced neural activities are also evident in other studies. Results showed that individuals with Autistic Spectrum Disorders (ASD) exhibit superior skills in perception and attention, such as motion perception, relative to the general population (Milne et al., 2002, Plaisted Grant and Davis, 2009, Mottron et al., 2006). Studies that also show pupil responses are also affected in autistic subjects, but the mechanisms involved remain poorly understood (Anderson and Colombo, 2009, van Engeland et al., 1991).

The subjects with congenital homonymous hemianopia are often unaware of their visual loss since this is always present in the absence of preceding normal visual experience. Any early changes in visual function as a result of plasticity during early development remain largely undetected. The enhanced subcortical function and/or functions that do not require a direct geniculo-striate projection are poorly understood and require further multidisciplinary studies.

# 6 MELANOPSIN SIGNALS AND THE PUPIL RESPONSE

## 6.1 Introduction

Since the discovery of the intrinsically photosensitive retinal ganglion cells (ipRGCs) (Berson et al., 2002), there has been a huge effort to study the extent to which melanopsin signals drive vision related mechanisms such as the pupil response. Rodless and coneless mice still show normal circadian patterns and pupillary responses in response to light stimuli. In humans, ipRGCs innervate the circadian pacemaker – the suprachiasmatic nucleus (SCN) and synchronize the circadian rhythms (Berson et al., 2002). Recent studies have shown that the steady-state size of the pupil during long exposure to intense stimuli and the corresponding sustained constriction in darkness following the offset of the stimulus (Gamlin et al., 2007) are likely to involve melanopsin signals through intrinsically photosensitive retinal ganglion cells. These cells also receive spatially pooled signals from rod and cone photoreceptors (Dacey et al., 2005), but the extent to which melanopsin contributes to rapid pupil responses elicited with brief stimuli remains unclear.

This chapter examines and establishes the contribution that ipRGCs make to the dynamic pupil light reflex responses based on results from two different studies.

In the first study, 10 normal trichromats, two subjects with rod deficiency, one rod monochromat and one subject with Optic Neuritis were investigated. When carefully interpreted, the findings from this study suggest that pupil responses to briefly presented stimuli are mediated largely by rod and cone signals with no contribution

from melanopsin. The results also suggest that, although more sluggish, rod signals remain unsaturated and can contribute to dynamic pupil responses at much higher light levels.

Findings from some studies suggest that Leber's Hereditary Optic Neuropathy (LHON) subjects lose visual function as a result of significant damage to the principal classes of ganglion cells and the ipRGCs can be preferential spared (Sadun et al., 2000, La Morgia et al., 2010). In order to examine such findings, we investigated a number of visual functions in LHON subjects. These included colour vision, motion perception and pupil responses to stimuli that isolate colour and grating responses. In addition, we also measured pupil responses to stimuli that isolate luminance, colour and combined rod/melanopsin signals. Four LHON subjects with different levels of damage and five normal subjects took part in the study. The results suggest that, in Leber's disease, the pupil responses to the achromatic and rod stimuli are selectively spared.

## 6.2 The contribution of the rod / Melanopsin driven ganglion cells to the dynamic pupil light reflex responses

### 6.2.1 Introduction

The discovery of the intrinsically photosensitive retinal ganglion cells (ipRGCs) (Berson et al., 2002) and their unique photopigment melanopsin (Provencio et al., 2000, Provencio et al., 1998) significantly changed the classical view that rods and cones are the only photoreceptors in the eye and led to a reassessment of the non-

image forming processing systems, such as the circadian photoentrainment and pupillary light reflex response (Hattar et al., 2002, Panda et al., 2002, Ruby et al., 2002, Lucas et al., 2003, Mrosovsky and Hattar, 2003). It is well established that most of ganglion cells project to the visual cortex via the lateral geniculate nucleus (LGN) (Barbur et al., 1992), but a small number of fibres project to the Olivery Pretectal Nucleus (OPN), which is the main component in the brain that provides input signal to the Edinger-Westphal (EW) nucleus, which in turn controls the constriction of the sphincter muscle through parasympathetic innervation. Since the ipRGCs comprise 0.2 percent of approximately 1.5 million retinal ganglion cells in the human eye (Markwell et al., 2010, Dacey et al., 2005), it is of great interest to establish the extent to which intrinsically photosensitive retinal ganglion cells contribute to the control of the pupillary light reflex response in human vision.

Previous reports have used experimental conditions where functional rods and cones are believed to be absent in order to isolate the ipRGCs component, for example, in transgenic animals lacking rods and cones (Lucas et al., 2001, Lucas et al., 2003, Panda et al., 2002, Ruby et al., 2002), in blind subjects (Zaidi et al., 2007) and in monkeys by pharmacological blockade of rods and cones (Gamlin et al., 2007). Using transgenic animals, Lucas et al. (Lucas et al., 2003) measured pupil light reflex as a function of irradiance level and showed that rods and cones contribute to the pupillary control mechanism mainly under low irradiance levels, but melanopsin was required for the full pupil constriction at high irradiance levels. Other studies showed that the steady-state size of the pupil (Tsujimura et al., 2010) during long exposure to intense stimuli and the corresponding sustained constriction in darkness following the offset of the stimulus (Gamlin et al., 2007) are likely to involve melanopsin signals through ipRGCs. Berson also showed that the

Melanopsin signals are very sluggish and respond best only at very high light level conditions, usually orders of magnitude above rod threshold (Berson et al., 2002).

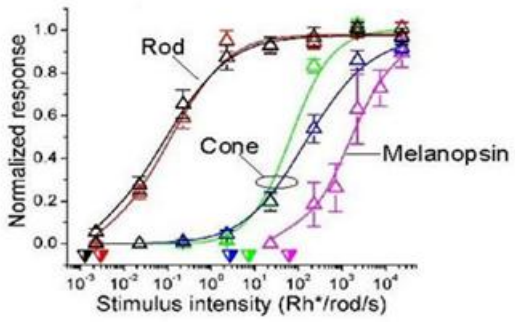


Figure 6-1. Schematic diagram shows that the melanopsin only starts to respond when the light level is high, which rods approximately saturate (adapted from David Berson 2002).

The ipRGC cells also receive spatially pooled signals from rod and cone photoreceptors and the extent to which melanopsin contributes to rapid pupil responses elicited with brief stimuli remains less clear. The purpose of this study was to examine how the dynamic pupil light reflex response changes with the level of light adaptation for stimuli that isolate luminance, colour or combined rod and melanopsin. The results obtained suggest that the dynamic pupil light reflex response in human vision involves mostly rod and cone signals, with little or no input from melanopsin derived signals.

### 6.2.2 Methods

Pupil responses, colour sensitivity and visual acuity were measured in this study. The general techniques of these tests have already been described in chapter 2. In addition to the description provided in the chapter 2, more information and details

are provided on the properties of visual stimuli employed for the pupil response tests and visual acuity tests.

**(a) Measurement of pupil size**

The pupil measurement was collected using the P-SCAN system (described in section 2.2). In this study, two P-SCAN systems were employed. One was connected to the four-primary illumination system (see Figure 6-2(a)), so that the pupil responses to stimuli generated in the four-primary illumination system could be measured. The other P-SCAN system was used independently to generate two stimuli that were both scotopically and photopically isoluminant and these stimuli were used to investigate pupil responses in the rod monochromat.

**(b) Stimuli designed to elicit pupil responses**

The principle pupil experiment employed three stimulus conditions – luminance, colour and rod/melanopsin. Each of these stimulus conditions was then measured against 3 different light levels and this was achieved by using two spectrally calibrated neutral density filters (0.8 and 2.0 OD). For the luminance and colour stimulus conditions, the background light levels were 438, 70.1 and 4.55 cd/m$^2$ whereas for the rod/melanopsin stimulus condition, the background light levels were 456, 74.4 and 4.76 cd/m$^2$. All stimulus conditions had an (x, y) - background chromaticity of (0.565, 0.390).

Under the luminance stimulus condition (L + M stimulus), we varied the L and M cone modulation whilst the other photoreceptor signals (S-cone, rods and melanopsin) remained unchanged. The modulation of the luminance stimulus was 28%.

Under the colour stimulus condition (L – M stimulus), the luminance modulation remained unchanged and the stimulus was defined purely as RG chromatic change. This was achieved by increasing the M cone contrast and decreasing the L cone contrast, so that the sum of the L and M signals or the luminance signals remains unchanged. The RG colour signal consists of ~ -6% L cone and 12% M cone modulation to reflect the average L:M ratio in the human eye.

Under the rod/melanopsin stimulus condition (rod/melanopsin stimulus), the L, M and S cone signals were kept unchanged, but had ~50% and ~60% rods and melanopsin modulation, respectively.

| Contrast Measured from Spectral Scans | | Photorector Excitation (%) | | | | |
|---|---|---|---|---|---|---|
| **Condition** | **Modulation amplitude (%)** | L | M | S | Melanopsin | Rods |
| L+M | **25.70** | 25.4 | 25.8 | -0.1 | -0.6 | 3.1 |
| Mel / Rods | **56.4 & 47.4** | -0.5 | -0.9 | 3.7 | 56.4 | 47.4 |
| L-M | **-6.8 & 12.6** | -6.8 | 12.6 | 0.2 | -0.4 | 1.8 |

Table 6-1. The measured photoreceptor contrasts for luminance, colour and rod/melanopsin stimulus conditions with the spectral radiance distribution results.

### (c) Measurement of contrast acuity (CAA test)

Figure 6-2(c) shows an example of stimuli that were employed in the high contrast acuity test. The details of the CAA test have been described in section 2.3. In this study, the stimulus had the maximum, negative contrast of -100%. The background field subtends a visual angle of $20^o$ x $16^o$ and was generated on a LaCie electronblue 22" CRT display (LaCie Ltd, London, UK). The chromaticity of the background was (0.2868, 0.3309) and four different background luminance were employed, i.e. 65, 26, 7.8 and 2.8 cd/$m^2$.

**(d) Subjects**

The studies reported here were carried out in ten control subjects (all wearing appropriate refraction and in the age range of 23 to 65 years; 6 males and 4 females), one mild rod deficient, male subject (age 25), one retinitis pigmentosa, male subject (age 23), one rod monochromatic, male subject (age 55) and one subject with Multiple Sclerosis (MS) and related Optic Neuritis (age 52). All subjects were given written informed consent, and the study was approved by the research and Ethics Committee of City University London.

The mild rod deficient subject has completely normal visual performance at high light levels, but is handicapped in the mesopic/scotopic range. The subject complains of poor visual acuity at night, e.g. this subject reports that he cannot see things clearly on the street or pavement at night even when the same conditions pose no problems to normal subjects. In order to confirm his potential rod deficiency, we measured his ability to resolve fine spatial details in the fovea as well as in the periphery and compared his results with normal trichromat subjects.

The subject with retinitis pigmentosa was diagnosed with RP autosomal recessive inheritance in 2002. But, he reported that he actually had problems with his vision throughout his childhood. When he was young, he always found it difficult playing outdoors at night, which may have been caused by his rod deficiency. He also had a cataract surgery in late 2002 which improved his vision significantly and since then he became aware of his reduced field of view.

The rod monochromat's best corrected vision was 6/60 for the right and 6/36 for the left eye. He was diagnosed with vision problems at high light levels from childhood and prescribed dark glasses. In 1990, the subject was diagnosed to have congenital

nystagamus, ocular albinism and total colour blindness. In 1999, he reported that he noticed a dark area in his central visual field and was diagnosed with cone dystrophy. In 2001, he was diagnosed with ocular cutaneous albinism, bilateral foveal aplasia, bilateral posterior vitreous detachment and bilateral posterior polar lens opacities. A retina examination revealed that he had no obvious fovea. In 2004, the subject had a cataract surgery.

**(e) Procedure**

Firstly, colour sensitivity and contrast acuity tests were carried out in all subjects. Then, we used the 4-primary illumination system to carry out melanopsin pupillometry tests. Lastly, we also carried out the modified contrast acuity experiments for the mild rod deficient subject, the pupillometry experiments for the rod monochromat subject and for the Optic Neuritis subject and their results were compared with the corresponding results obtained in normal trichromats.

In the melanopsin pupillometry tests, subjects fixated a black cross (subtended $1^{o}$ and always presented in the centre of the background field). The disc stimulus subtended 17 degrees in diameter and was viewed binocularly as shown in Figure 6-3(a). The fixation stimulus was well defined so as to minimize fluctuations of accommodation.

Three stimuli and three background levels were employed in the study. Therefore, nine pupil tests were carried out with each subject. Each of these tests started after 5 minutes adaptation to the corresponding background and involved the measurement of 32 pupil responses. Each presentation lasted 6 seconds and the stimulus was modulated in a half cycle sinusoidal envelope for 2 seconds and presented 1 second after the start of each presentation (see Figure 6-3(b)). The

measured 32 pupil traces were then averaged to obtain the mean pupil response trace. For each subject, the tests were interleaved using a latin-square design.

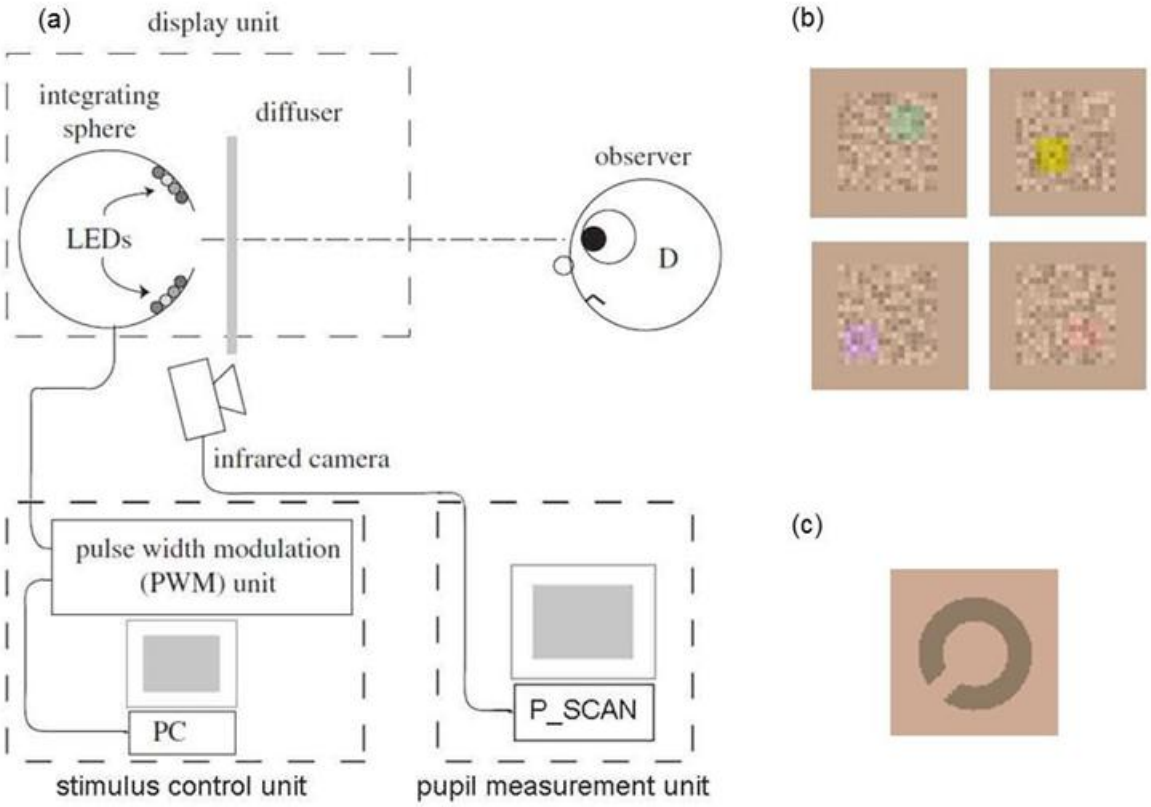


Figure 6-2. (a) Schematic diagram of the primary experiment set-up. A personal computer and an interface board controlled a four-primary illumination system which was connected with the P-SCAN system for the pupil measurement. The illumination system consisted of an optical diffuser and an integrating sphere which presented 17$^{o}$ circular onto the optical diffuser. (b) An example of the colour-defined stimuli in the CAD test. Random luminance noise was employed to minimize the luminance signal detection from the colour-defined targets. (c) An example of a visual acuity test stimulus.

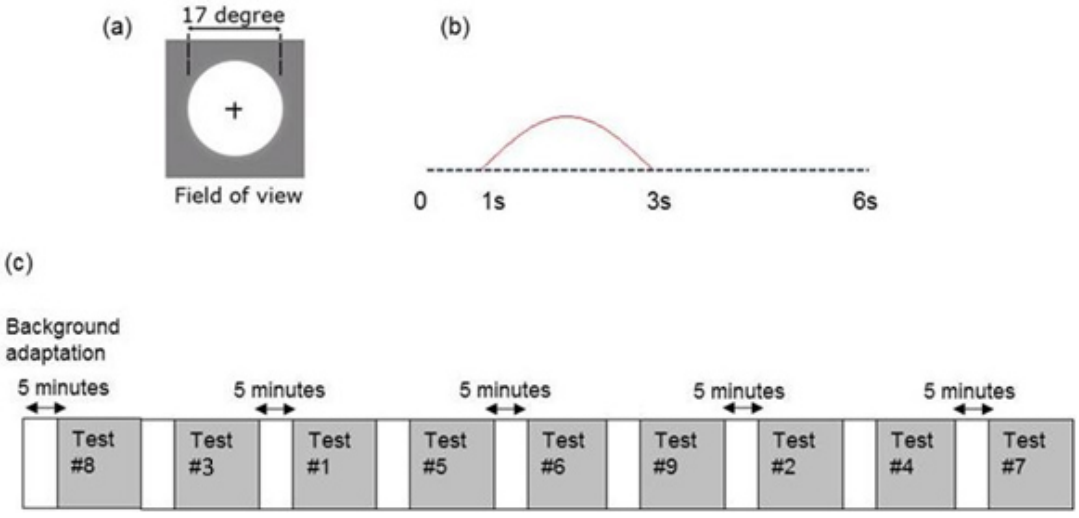


Figure 6-3. (a) The stimulus was a disc of $17^{o}$ in diameter. (b) The pupil was continuously measured for 6 seconds. The stimulus was modulated as a two second half-cycle sinwave and its onset was delayed by one second with respect to the beginning of the pupil trace. (c) An example of an experiment test sequence. The 9 tests (3 stimulus conditions and 3 light levels) were interleaved and subjects were given at least 5 minutes to adapt to the background before each test.

### 6.2.3 Results

Figure 6-4 (a - h) shows pupil traces plotted as a function of time in seconds for a typical normal subject and one subject with mild rod deficiency. The two diagrams on the top row show the relative pupil diameters for the subjects, in which the pupil traces are shown on the original scale. For each screen luminance the mean responses to the three stimulus conditions were shifted vertically to ensure the same initial starting diameter. This makes it easier to observe the original pupil response amplitudes and latencies. In order to make comparisons amongst subjects, the pupil constrictions in bottom diagrams were scaled with respect to the largest pupil response amplitude among all the nine tests in one subject. This

makes it possible to compare the response amplitudes and latencies generated by the three stimuli.

In the normal subject Figure 6-4 (a - d), each of the three stimuli produced brief pupillary constrictions at stimulus onset, with larger response amplitudes at lower light levels, which is consistent with previous studies (Barbur et al., 1992, Barbur et al., 1999). The colour modulation also produced a small pupil afterimage response at stimulus offset, especially at the highest light level. The rod/melanopsin stimulus condition yields larger response latencies, with the largest difference observed at the lowest light level.

Unlike the typical normal subject, Figure 6-4 (e - h) shows the result in one subject with mild rod deficiency who shows normal responses to the colour and luminance modulation, but much reduced pupil constriction to rod/melanopsin modulation at each light level. In the normalized diagrams, when compared to the normal subject's results (b-d), the mild rod deficient subject shows reduced pupil responses to the rod/melanopsin stimulus (blue traces in Figure 6-4 (f-h)), but this pupil responses are comparable for luminance and colour modulation.

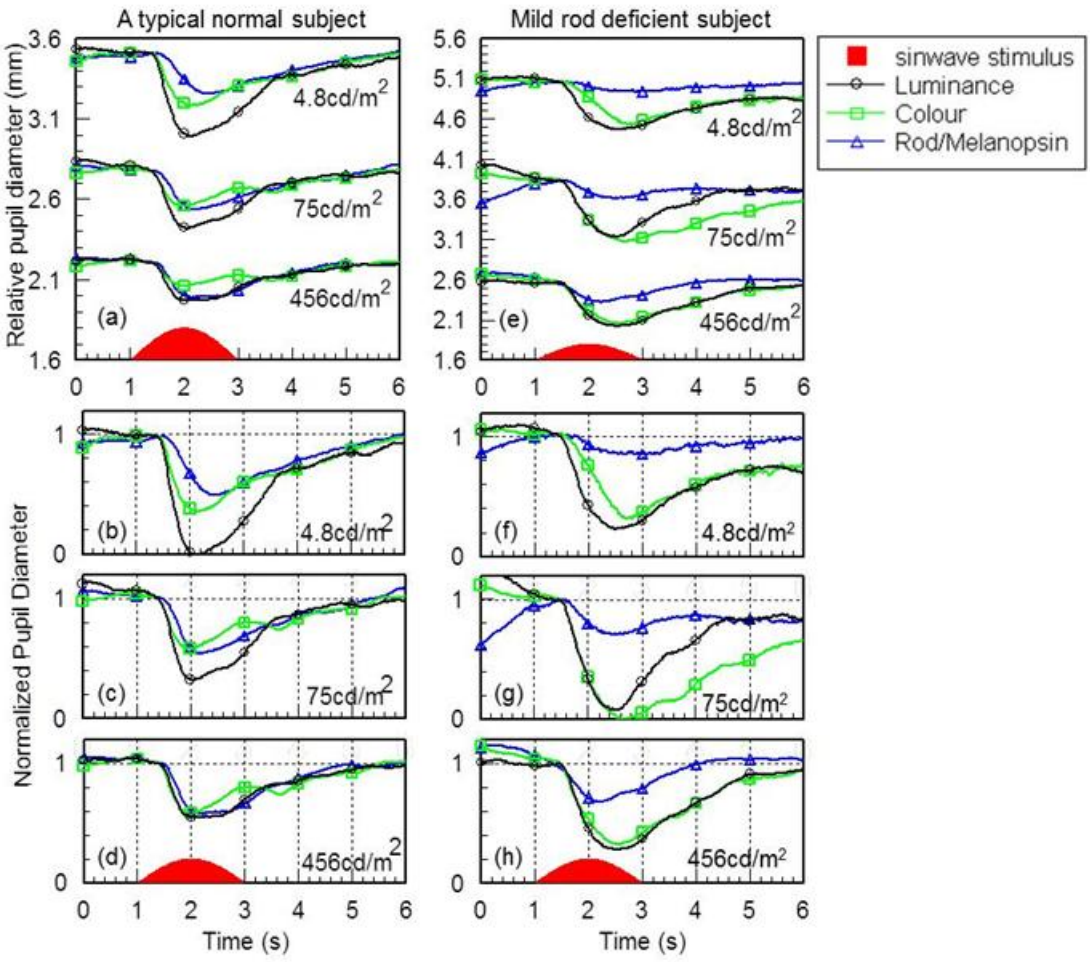


Figure 6-4. Pupil response results from (a – d) a typical normal subject and (e – h) a subject with mild rod deficiency (e-h). The horizontal axis represents time in seconds and the vertical axis plots the pupil diameter. The black circled traces, the green rectangled traces and the blue triangled traces show the pupil responses to luminance, colour and rod/melanopsin modulation, respectively. Diagrams (a & e) in the top row show pupil responses on the original mm scale. The baselines in these traces show the corresponding steady-state pupil sizes and the absolute pupil constriction amplitude and latencies can be compared easily for each stimulus condition. The pupil constrictions in the bottom diagrams (b, c, d, f, g and h) have been normalized with respect to the individual subject's largest pupil response amplitude among all the 9 traces, so that each pupil trace would have a maximum pupil constriction of 1. Each trace illustrates a mean pupil response trace of 32 measurements for each stimulus condition (i.e., luminance, colour and rod/malanopsin stimulus modulation) at each light level. The 3 rows (b & f, c & g and d & h) in the bottom diagram section correspond to the pupil response measurements at the lowest light level (4.8cd/$m^2$), the mid light level (75cd/$m^2$) and the highest light level (456cd/$m^2$), respectively. Diagrams f, g

and h show pupil responses for the mild rod deficient subject. The traces reveal much reduced pupil response amplitude to the rod/melanopsin stimulus when compared to his pupil response amplitudes to the luminance and colour stimuli, especially at the lowest light level. However, in the normal subject (b, c and d), the pupil response amplitude to the three stimuli are very similar.

The normal subject's result shown in Figure 6-4 (a - d) is redrawn in Figure 6-5 (a - d) together with a Retinitis Pigmentosa subject who doesn't have functioning rods in the eye and a rod monochromat subject who relies entirely on rod photoreceptors, so that we can compare the different pupil responses between the normal subject, the RP patient and the rod monochromat.

The Retinitis Pigmentosa subject shows abnormal pupil responses to the luminance and colour stimuli at the middle and high light levels, but absent pupil responses to all stimuli at the lowest light level. These abnormal pupil responses are consistent with his poor acuity results shown in Figure 6-7 (c). However, the rod monochromat subject yields almost completely opposite pupil responses when compared to the Retinis Pigmentosa subject. He doesn't show any pupil responses to the luminance and colour stimuli at any light level and his pupil response latency to the rod/melanopsin stimulus is similar to those measured in normals, but the response amplitude increases when light level is reduced. Even when the background luminance is 456cd/$m^2$, which was previously believed to be well above the threshold for rod saturation, he still shows good pupil responses to the rod/melanopsin stimulus.

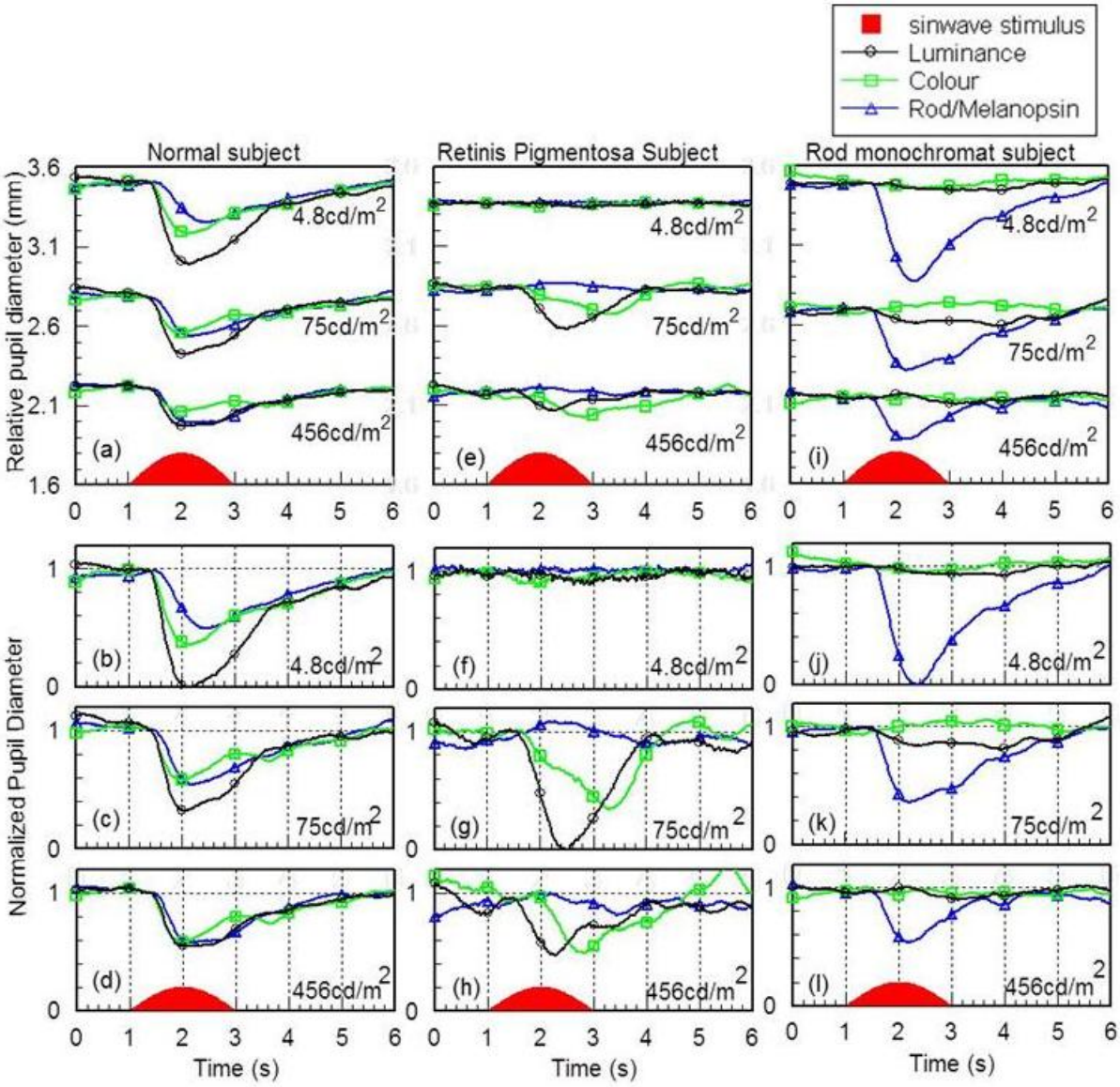


Figure 6-5. Pupil response results from (a – d) a normal subject, (e – h) the Retinitis Pigmentosa subject who has no functioning rods and (i – l) the rod monochromat subject who only functioning rods in the eye. The results from the Retinitis Pigmentosa and the rod monochromat subject have been shifted down so that they share the same vertical coordinates with the normal subject, but the scale has been kept the same. The Retinitis Pigmentosa subject and the rod monochromat yield almost completely opposite pupil response results.

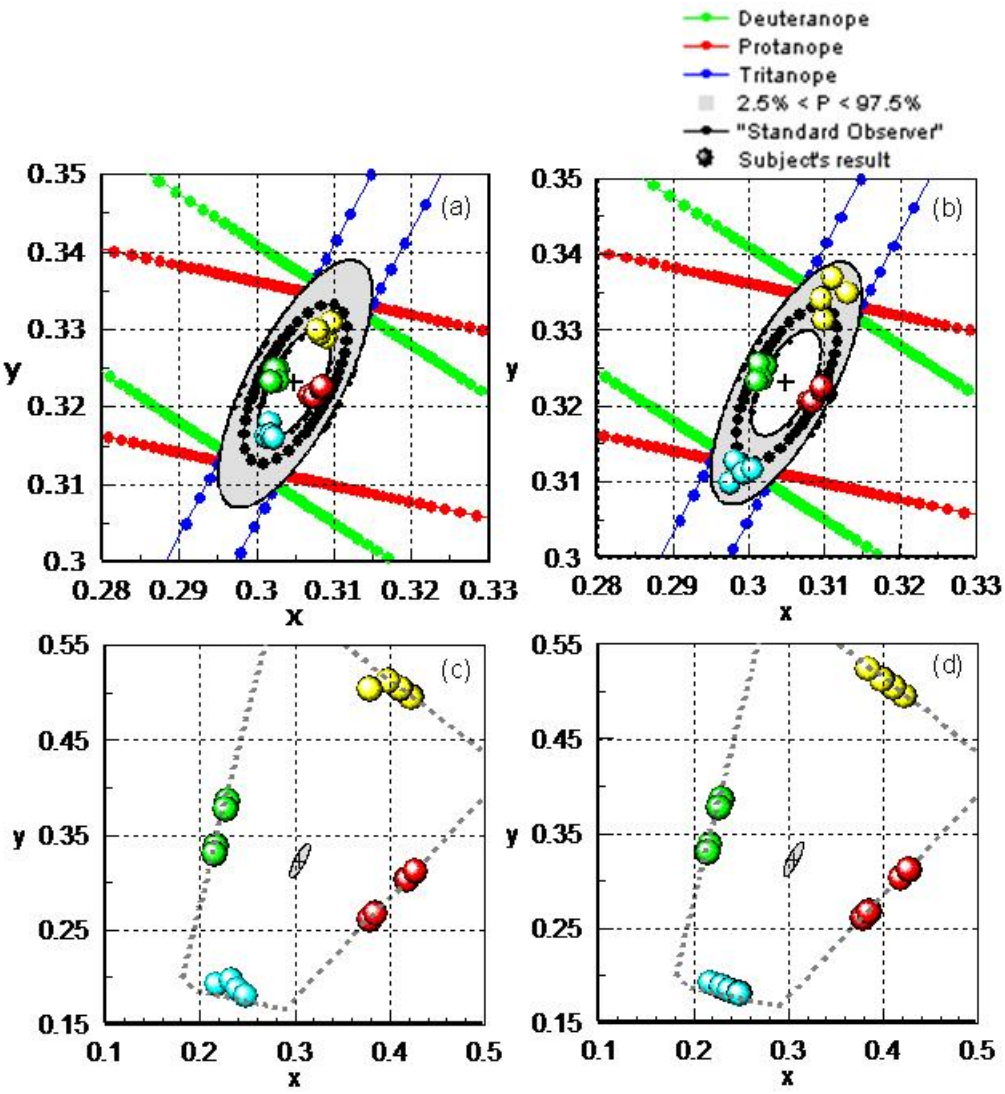


Figure 6-6. CAD test results in the normal tricrhomat (a), in the mild rod deficient subject (b), in the retinis pigmentosa subject (c) and in the rod monochromat (d). The colour vision tests are carried out with a background of 26cd/m$^2$. The mild rod deficient subject has excellent colour vision whereas neither the RP subject or the rod monochromat show any sign of colour vision and are unable to see or detect the presence of the colour defined targets even for chromatic saturations that are limited only by the phosphors of the display.

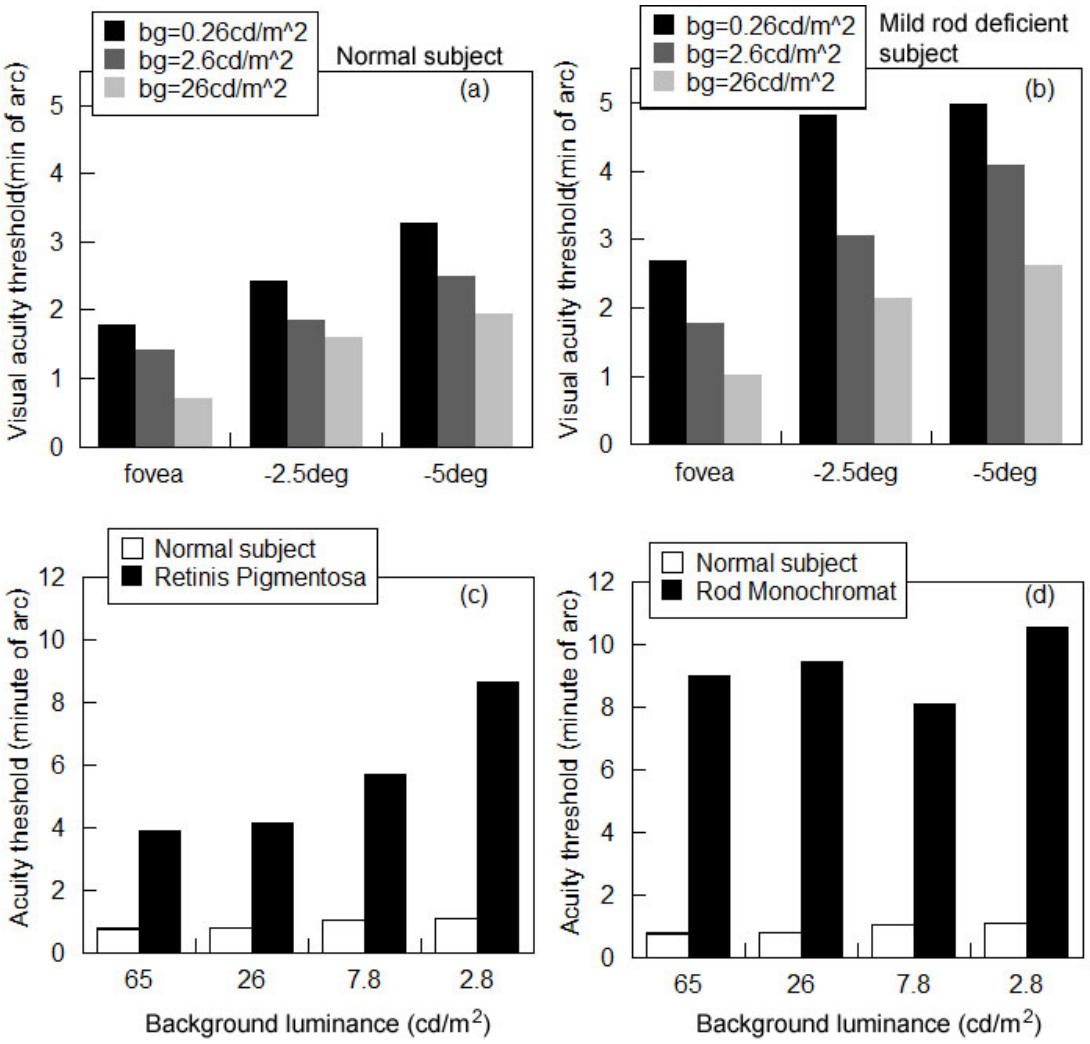


Figure 6-7. Contrast acuity results from a normal subject (a) compared with the mild rod deficient subject (b) measure in the fovea, -2.5$^{o}$ and -5$^{o}$ eccentricity when at 3 different background levels (26, 2.6 and 0.26cd/m$^{2}$). The rod monochromat shows similar visual acuity threshold at the fovea when light level is high, but shows a much higher threshold in the periphery especalliy when light level is low and the rods are more dominate in visual performance. c & d show the contrast acuity results for the RP subject (c) and the rod monochromat (d) measured in the foveal region at each of four different background luminance levels (65, 26, 7.8 and 2.8cd/m$^{2}$).

In order to ensure that the pupil responses measured in the rod monochromat were attributable entirely to rods, we employed the P-SCAN system to generate two double isoluminant stimuli (scotopically and photopically isoluminant) (see Figure

6-8 inset). Disc stimuli were presented in the centre of a uniform background field of 12cd/m$^2$ and subtended a visual angle of 9.5$^o$. The photoreceptor contrasts were calculated along an ellipse contour Figure 6-8 (a) (origin at (0.298, 0.335)) in the CIE1931 chromaticity diagram as a function of chromatic angle as shown in Figure 6-8 (b). Points A and B have zero-rod contrast and correspond to a chromatic displacement angles of 118$^o$ and 298$^o$. Both stimuli correspond to a chromatic displacement of 0.1 units, as measured with respect to background chromaticity. The colour stimuli generated for these two directions are designed to have the same luminance as the background and this was achieved by increasing or decreasing the L or M contrast, because luminance signal is defined to be the sum of the L-cone and M-cone signal. The pupil was continuously measured for 6 seconds in this experiment and the stimulus duration was 2.4 seconds. In order to minimize the pupil responses that might be triggered due to any residual luminance signal in these stimuli, dynamic random luminance masking of the checks was used to mask any local luminance contrast signal. The luminance of the whole stimulus also varied randomly within ±20% mean background luminance to mask any spatially pooled luminance signal.

Figure 6-8(c & d) shows results for a normal subject and for the rod monochromat. Unlike the normal subject who had very good pupil responses to the double-isoluminant stimuli, the rod monochromat failed to show any pupil responses to these two stimuli. This ensured that the rod monochromat doesn't respond to a stimulus that doesn't have a rod contrast and hence provided further evidence that he does not have functioning cones in the eye. Since the melanopsin signal is not completely absent in the absence of rod modulation, the results suggest that the modulation signal either too weak or simply unable to drive the pupil response.

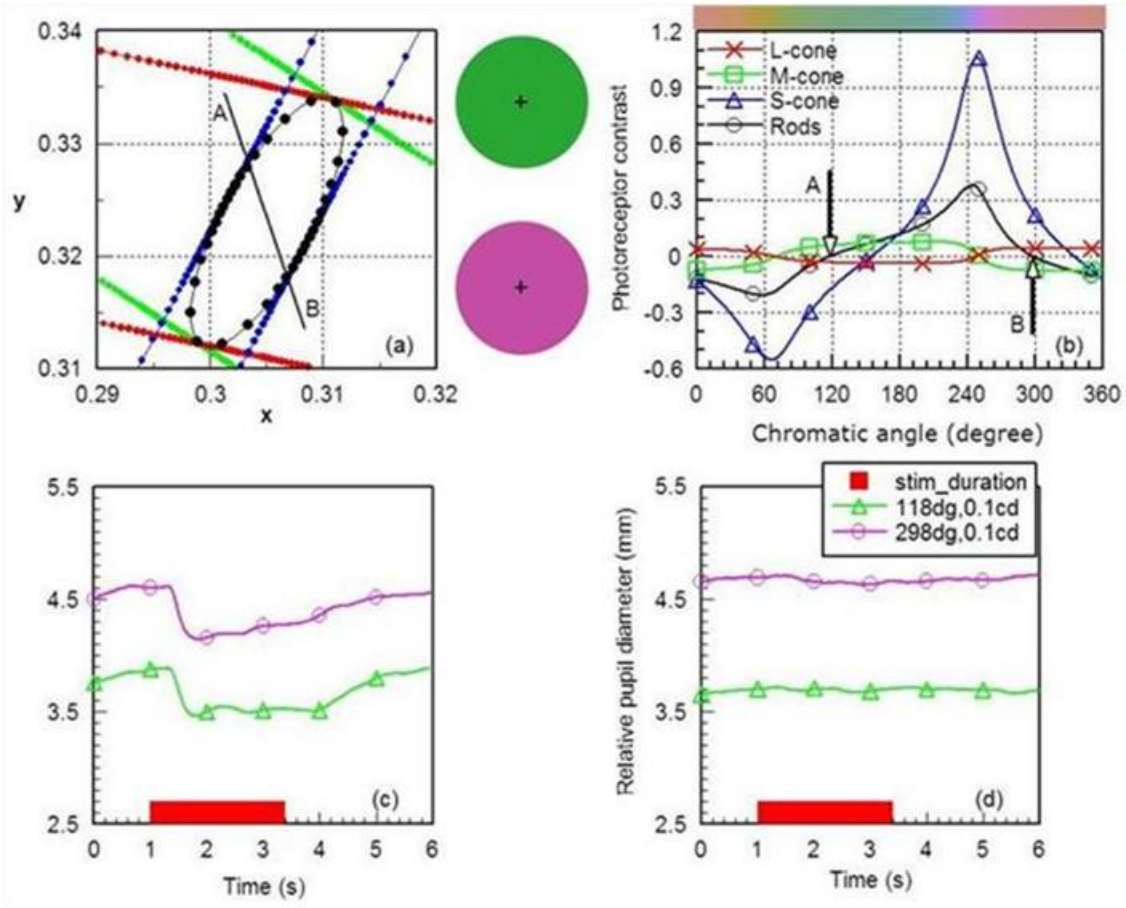


Figure 6-8. Double-isoluminant stimuli employed to test for pupil responses in the rod monochromat. Diagram (a) shows the d-isoluminant stimulus directions in the CIE 1931 chromatic diagram. The stimuli were discs of 9.5$^{o}$ in diameter and presented in the centre of a uniform background of luminance 12cd/m$^{2}$. The red, green and blue dot lines represent the colour confusion lines. The black dotted ellipse shows the colour thresholds for an average of 330 normal trichromats (Rodriguez-Carmona et al., 2005). The photoreceptor contrasts are calculated along this ellipse contour and are drawn in diagram (b) as a function of the chromatic displacement angle in degrees. The dots, crosses, squares and triangles show the contrasts generated in rods, L-cones, M-cones and S-cones, respectively. Point A has a chromatic angle of 118$^{o}$ and B has angle of 298$^{o}$ and both of them have 0 rod contrast for 0.1 chromatic displacement (CD) from the background chromaticity (0.298, 0.335) in the CIE – (x,y) chromaticity chart. (c) Pupil responses to the d-isoluminant stimulus in a normal subject. The red dotted curve shows the pupil response to the reddish stimulus (i.e., $\theta$ = 298$^{o}$, CD = 0.1) and the green curve is for the greenish stimulus (i.e., $\theta$ = 118$^{o}$, CD = 0.1). (d) Pupil responses to

the d-isoluminant stimulus shown for the rod monochromat. Unlike the normal subject who shows good pupil responses to the d-isoluminant stimuli, there are no pupil responses for these stimuli in the rod monochromat.

### 6.2.4 Discussion

(a) Contribution of ipRGCs via melanopsin derived signals to the pupil control pathway.

This study employed four primary lights to generate photoreceptor specific pupil stimuli using the silent substitution technique (Smith et al., 1995, Pokorny et al., 2004). The aim was to measure pupil responses to brief stimuli that isolate luminance, colour and rod / melanopsin signals. The completely opposite pupil response patterns to the rod / melanopsin stimulus measured in the rod monochromat and the severe rod deficient subject (or the retinitis pigmentosa subject) suggest that the pupil responses to the rod / melanopsin stimulus are mediated largely by rod signals and that melanopsin via the ipRGCs does not contribute significantly to the dynamic pupil light reflex response in human vision. These findings suggest that the dynamic pupil light reflex response in human vision involves mostly rods and cone signals, with little or no input from the ipRGCs.

Furthermore, Figure 6-8 (b) shows that the d-isoluminant stimulus fails to elicit pupil responses in the rod monochromat. Although the d-isoluminant stimulus fails to stimulate rods and the subject has no functioning cones, the stimulus does, however, generate a small melanopsin signal, but this signal fails to drive the dynamic pupil light reflex response.

Previous reports indicate some involvement of melanopsin signals in the control of the steady-state pupil size at much higher light (Tsujimura et al., 2010) and the

sustained constriction in darkness following the offset of long exposure to intense stimuli (Gamlin et al., 2007). These results are not, however, in conflict with the findings that emerge from the current study. The absence of detectable melanopsin signals in the dynamic pupil light reflex response may be due to the sluggish properties of the melanopsin signals.

The number of classical photoreceptors (i.e., rods and cones) and the corresponding ganglion cells are significantly larger than the ipRGCs. There are approximately 90 - 120 million rods and 4.5 - 7 million cones in the eye which connect to ganglion cells. The ipRGCs comprise only 0.2 percent of retinal ganglion cells in the human eye. The cone signals are optimized for spatial and temporal visual acuity whilst the rods respond well at lower light levels. The melanopsin signals are sluggish and the ipRGCs can integrate the light irradiance information over long time intervals, which provides a measure of exposure to light. The main function of these sluggish melanopsin signals is therefore to photoentrain the circadian rhythm (Ruby et al., 2002). These cells also have longest dendrites and largest fields of all known ganglion cells, with diameters of 305 to 1200 μm increasing with eccentricity (Dacey et al., 2005). Apart from the intrinsically photosensitive properties, the large receptive fields indicate that they also receive signal input from a large number of classical photoreceptors, especially from rods. Hence, it is not too surprising to discover that in the rod / melanopsin stimulus condition, the ipRGCs do not contribute to the dynamic pupil light reflex and that the only significant contribution to the pupil response is from rods and perhaps through the rods that innervate with the ipRGCs (see section 6.3).

(b) Rod contribution to the pupillary pathway at high light levels.

The results from the rod monochromat also suggest that, although more sluggish, rod signals remain unsaturated and contribute to the dynamic pupil responses at much higher light levels. Previous studies have shown that rods can produce large pupillary responses when large stimuli are involved (Alpern and Ohba, 1972). Based on previous results and the current findings, it is reasonable to conclude that in normal subjects pupil responses to the rod / melanopsin stimulus are the result of stimulation of rods, and that rod signals are also effective at higher light levels. The fact that the rod monochromat exhibited even bigger pupil response amplitudes than those from normal subjects, especially from the lowest light levels, suggest that in normal vision rod signals may be inhibited or partially blocked by the cone signals. When light level was reduced, in normal subjects, the dynamic pupil responses to luminance, colour and rods stimulation tended to increase. This increase may however be caused, at least in part, by the increased steady-state pupil size, and the corresponding change in the operating range of the iris. This result is also consistent with previous findings (Winn et al., 1994).

(c) Pupil responses in the MS (Optic Neuritis) subject

MS is an inflammatory disease in which the fatty myelin sheaths around the axons of the brain and spinal cord are damaged, leading to demyelination and scarring as well as a broad spectrum of signs and symptoms (Compston and Coles, 2008). Optic Neuritis is used to describe the inflammation of the optic nerve. The MS is the most common etiology for Optic Neuritis (Beck and Trobe, 1995).

In 1986, Mullen and Plant reported that patients with optic neuritis showed greater loss of chromatic sensitivity when compared to luminance sensitivity (Mullen and Plant, 1986). Another study from Wall (1990) showed that the ON patients could

have similar contrast sensitivity from the affected and unaffected eyes, however the Farnswarth-Munsell 100 Hue colour testing was found to be very abnormal in the affected eye. The author suggested that the P cells experienced greater damage when compared to the M cells (Wall, 1990). Moro et al measured pupil responses and assessed visual performance in 14 patients with a history of unilateral optic neuritis. The authors showed dissociation between visual acuity and colour sensitivity as well as between pupil responses to light flux and chromatic stimulus. These and other studies suggest that some degree of selective damage of ganglion cells may occur in ON (Flanagan and Zele, 2004, Moro et al., 2007).

It is not known how ipRGCs are affected in ON subjects. Due to the special role that these cells play, they might be spared in ON. It is therefore of interest to carry out the rod/melanopsin experiment on a typical ON subject.

The majority of the above studies have been carried out on patients with ON that were secondary to MS. So, we recruited an MS related ON subject (with No Perception of Light or NPL in the affected eye). In December 2008, the subject experienced sudden loss of vision in his right eye. In May 2009 the patient suffered a heart attack and lost control to the entire right side of his body in July 2009. He had been placed on Azathioprine treatment at a daily dose 150mg. He experienced a second attack of ON and as a result lost vision in his right eye, but the left eye is unaffected with a -2.5D refractive error.

We examined his pupil responses using the four-primary system and his results are shown in Figure 6-9.

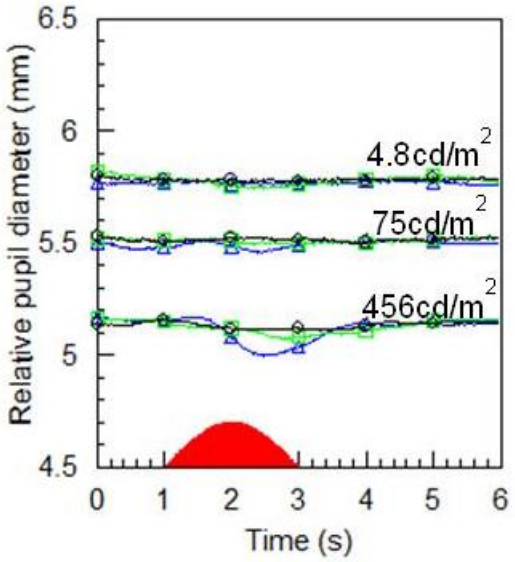


Figure 6-9. Pupil responses measured following stimuluation of the affected eye in the ON subject. The responses to the luminance and colour stimuli are almost absent. However, when light level is increased, the subject shows some pupil responses but only to rod/melanopsin stimulus.

The pupil responses to photopic luminance and colour signals are very small under all conditions. However, when the light level is increased, the subject shows an increased pupil response but only to the rod/melanopsin stimulus. Our findings from the rod monochromat and the rod deficient subject suggest that only the rod signals generated by the rod/melanopsin stimulus are likely to drive the pupil response. This increased response might due to the fact that the rod/melanopsin stimulus has the largest rod signals at the highest light level condition, whereas in the lowest light level, the rod signals are not large enough to drive a pupil response through the residual ganglion cells that the ON subject may still have. In order to examine this hypothesis, a new pupil test was designed to stimulate rods effectively, but at a lower retinal illuminance.

The new test employs a background and luminance of 1 cd/m$^2$. Seven achromatic stimuli with a fixed contrast 10,000% (i.e., 101cd/m$^2$) were employed and the parameter varied was the size of the stimulus. The area of the stimulus changed approximately by 0.6 log units from one size to the next. The arrangement of the stimulus takes advantage of rod photoreceptor properties (highly sensitive at low light levels and large spatial summation).

| Stimulus number | Width x height (degree$^2$) | Log(area) |
|---|---|---|
| 1 | 0.6 x 0.4 | -0.6 |
| 2 | 1.2 x 0.9 | 0.02 |
| 3 | 2.4 x 1.8 | 0.6 |
| 4 | 4.7 x 3.5 | 1.2 |
| 5 | 9.3 x 7 | 1.8 |
| 6 | 18.5 x 13.9 | 2.4 |
| 7 | 36 x 27 | 2.9 |

Table 6-2. Pupillometry tests with fixed stimulus contrast and variable size.

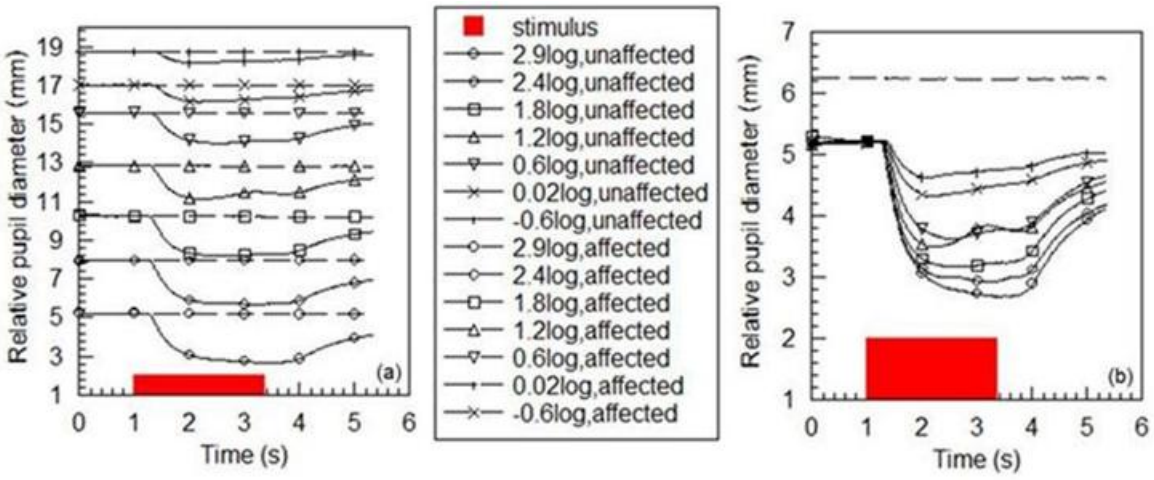


Figure 6-10. Pupil responses measured in the ON subject. Tests were done monocularly in each eye. The dotted lines are responses from the affected eye and the solid lines are from the unaffected eye. The pupil responses are completely absent from the affected for all stimuli. (a) shows a comparison of pupil responses between the affected and unaffected eye. In (b), the pupil responses from the individual eye have been moved together. When the stimulus size increases, the pupil constriction amplitude increases. We can also observe an increase in latency as the size of the stimulus decreases. Each trace represents an average of 32 pupil response measurements.

The results shown in Figure 6-10 show that the pupil responses from the unaffected eye increase in amplitude with the size of the stimulus. In contrast, there are no responses from the affected eye. This suggests that the pupil responses in the affected eye do not reflect spatially summed rod signals, which is contrary to our expectation. The conditions between the two experiments were examined carefully and we found that, in the new test, the unaffected eye was covered with a new eye patch, which ensured that no residual light could reach the retina in the unaffected eye. If the pupil responds to light flex change on the retina as detected by the most common photoreceptor (i.e., rods), then even small amounts of diffuse light that end up stimulating mostly the dark adapted peripheral retina in the normal patched eye may be sufficient to drive the pupil response. Figure 6-9 shows that some pupil response can be elicited when stimulating the affected eye but only for the highest background luminance. Although the rod/melanopsin modulation is the same for all three background luminance levels employed, the net “light flex” change as detected by the rod/melanopsin system is largest for largest luminance. The amount of stray light that may end up stimulating the dark adapted normal eye (and particularly the peripheral retina) also corresponds to the largest background luminance employed. In order to test for this alternative hypothesis, the earlier pupil measurements were repeated using the new eye patch which ensured that there was no stray light entering the unaffected eye.

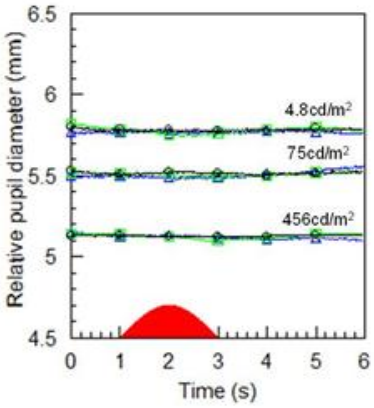


Figure 6-11. Pupil responses in the ON patient measured in repeated tests when stimulating the affect eye. When great care is taken to ensure that no stray light can reach the unaffected eye, there are no pupil responses at any light level.

The results show that the pupil responses are absent to all stimuli at all light levels when stimulating affected eye in the ON subject. The possible damage of ipRGCs in the ON subject is not known. The results obtained in the RP subject and the rod monochromat suggest that the rod contrast is the only signal that drive the pupil response in the rod/melanopsin condition. If the ON subject has any spared ganglion cells that can carry the rods signals to the brain, one can reasonably expect to elicit some form of pupil response, especially when the maximum rods signal is used. But, the pupil responses are completely absent when stimulating the affected eye. This finding suggests that all ganglion cell nerve fibres are severely damaged in the affected eye with no sparing of ipRGCs.

## 6.3 Select sparing of visual pathways in Leber's disease

### 6.3.1 Background

Leber hereditary optic neuropathy (LHON) or Leber optic atrophy is a mitochondrially inherited form of vision loss, which is caused by degeneration of retinal ganglion cells and their axons. Patients with this disease usually suffer a large decrease of visual acuity and colour vision, as a result of acute loss of ganglion cells that mediate central vision. Males are affected much more than females whereas mothers who have LHON pass it to all offspring, but fathers don't.

Sadun's group (2000) showed that in LHON there can be selective dissociation damage in different types of neurones. The authors suggested that parvocellular neurones might be affected more than magnocellular neurones (Sadun et al., 2000). A more recent study on a post-mortem examination provided first evidence suggesting the existence of preferential sparing of ipRGCs in LHON patients (La Morgia et al., 2010).

The purpose of this study was to examine whether pupil response components are linked to different classes of ganglion cells and whether the Magnocellular, Parvocellular or the ipRGCs pathways are equally damaged in LHON.

### 6.3.2 Methods

(a) **Subjects**:

The study was carried out in three LHON patients selected to reflect different stages of visual disability and five normal age and gender-matched control subjects. All of the LHON subjects have good photoreceptor function based on the results obtained from electrodiagnostic testing. However, Goldmann perimetry results showed all LHON subjects had central visual field loss and that the damage affected at least the central 10 degrees.

| | Age | Gender | Onset | Visual Acuity |
|---|---|---|---|---|
| Patient 1 (mild) | 19 | Male | 6 months ago | 6/36 |
| Patient 2 (moderate) | 61 | Female | 21 months ago | 1/120 |
| Patient 3 (severe) | 58 | Male | 48 months ago | Hand movement |

Table 6-3. Summary description of LHON subjects. Subject 1 has shortest duration and best visual acuity whereas subject 3 has the longest duration and worst visual acuity.

(b) **Apparatus**:

In each subject, a number of aspects of visual performance including colour sensitivity, high contrast acuity, contrast sensitivity and first order motion sensitivity were measured. Pupil responses to colour and grating stimuli as well as light flux changes that stimulate preferentially rods and melanopsin were also measured. All tests were carried out monocularly. In the LHON subjects, the most affected eyes were always tested.

***Measurement of chromatic sensitivity***

The standard CAD test with a background luminance of 26cd/m$^2$ was employed (see Chapter 2.4).

***Measurement of coherent motion threshold***

The motion test was also carried out using the CAD program. But instead of defining the moving stimulus as a colour signal, the stimulus was achromatic and defined by luminance contrast. The test measures the contrast of the stimulus needed to detect motion when buried in the dynamic luminance contrast noise of 6%, 12% and 24%.

***Measurement of contrast sensitivity and contrast acuity***

The CAA test was used to measure the contrast sensitivity and also the subject's high contrast acuity. The stimulus was presented in the centre of a uniform background field (26cd/$m^2$) for 600ms in both tests. The observer's task was to press one of the four buttons located on the corners (top left, top right, bottom left and bottom right) of a button box to indicate the location of the gap in the stimulus. In the contrast sensitivity test, the stimulus had a fixed size of 73.2 arc min and a staircase method was employed to measure the threshold of the stimulus contrast that an observer needs to detect the gap of the Landolt ring. But, in the high contrast acuity test, the stimulus was fixed in contrast (-100%) and the measurements variable was the size of the stimulus.

***Pupillometry***

The P-SCAN system was employed in this study. The stimulus was a circular disc of $10^o$ diameter (example stimuli are shown in Figure 6-12). The stimulus was presented in a uniform background field as a rectangle pulse of duration 400ms. The luminance of the background was 12 cd/$m^2$ and the chromaticity was (0.298,

0.335). Each test required the continuous measurement of the pupil for 6 seconds. Four different stimuli were employed:

1. An achromatic light flux increment that had a contrast of 171% with respect to the uniform background (Figure 6-12 (a)).
2. A coloured stimulus that is photopically and scotopicolly isoluminant (i.e., d-isoluminant) (Figure 6-12 (b)). The stimulus is defined by its colour contrast to in a normal trichromat. The stimulus is also buried in a 30% random luminance mask (RLM) which reduces/eliminates the detection of any residual luminance signal that may trigger a pupil response. Unlike the stimulus, the dynamic RLM noise is presented for all 6 seconds of the test.
3. A photopically isoluminant stimulus that has the maximum rod contrast (171%). This stimulus also has a 30% dynamic RLM (Figure 6-12 (c)).
4. A square-wave grating stimulus that has the same luminance as the background. The spatial frequency was 5.5 cycles/degree (Figure 6-12 (d)).

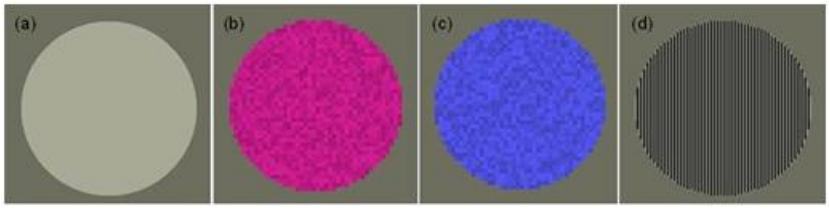


Figure 6-12. Examples of visual stimuli employed to trigger pupil responses. (a) light flux stimulus; (b) d-isoluminant colour stimulus; (c) stimulus that has the same photopic luminance as the background, but has maximum rod contrast, and (d) an achromatic grating stimulus that has the same luminance as the background.

### 6.3.3 Results

It is well established that the P-pathway exhibits chromatic opponency and responds optimally to gratings of high spatial frequency and low temporal frequency (Lennie and Movshon, 2005, Merigan and Maunsell, 1990). Therefore colour and grating stimuli were employed. The M-pathway on the other hand, responds optimally to chaos grating and moving stimuli. It is of interest to examine the extent to which these pathways contribute to the pupil response.

**Colour vision and high contrast acuity results: P-pathway assessment**

Figure 6-13 (b) shows the CAD test results for all 3 LHON subjects. All of their colour thresholds reach the limits imposed by the phosphors of the display. The high contrast acuity results are shown in Figure 6-14. The high contrast acuity thresholds in LHON subjects are also much higher than the corresponding thresholds measured in normal trichromats. The large colour sensitivity and acuity loss in LHON subjects suggests extensive damage to the P-pathway.

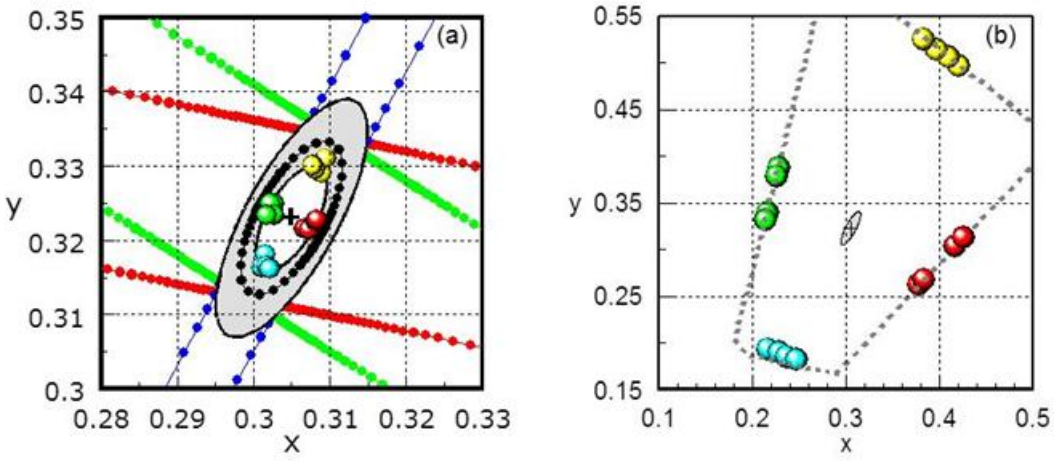


Figure 6-13. Colour vision results for (a) a normal trichromat subject and (b) the 3 LHON subjects. None of the LHON subjects were able to detect the presence of the colour defined stimulus,

even for the largest chromatic saturations possible on the visual display.

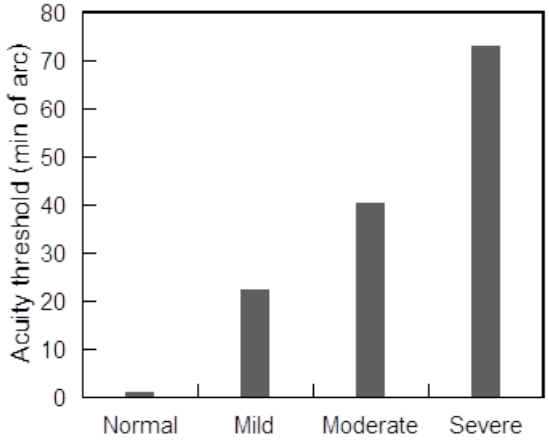


Figure 6-14. High contrast acuity results measured using a Landolt C stimulus for a normal trichromat and for the three LHON subjects. The normal subject needs about one min arc to detect the gap of the Landolt ring while the thresholds of the mild and moderate LHON subjects are approximately 22 and 40 times higher than that of the normal subject. The severe LHON subject was unable to detect direction of the gap in the stimulus even for the largest stimulus sizes (73.2 arc min) possible on the visual display.

**Motion sensitivity and contrast acuity results: M-pathway assessment:**

Figure 6-15 and Figure 6-16 show motion and contrast acuity thresholds for the LHON subjects and a typical normal trichromat. The subject with moderate loss was unable to participate in the contrast acuity test and soon after the initial study he was no long available. Apart from that particular test, subjects perform worse as the severity of LHON increases. LHON subjects thresholds were much larger than those measured in the normal trichromat. The severe LHON subject failed to detect the stimulus, even for luminance contrasts limited only by the visual display. The poor results from the LHON subjects suggest that the M-pathway is also heavily damaged.

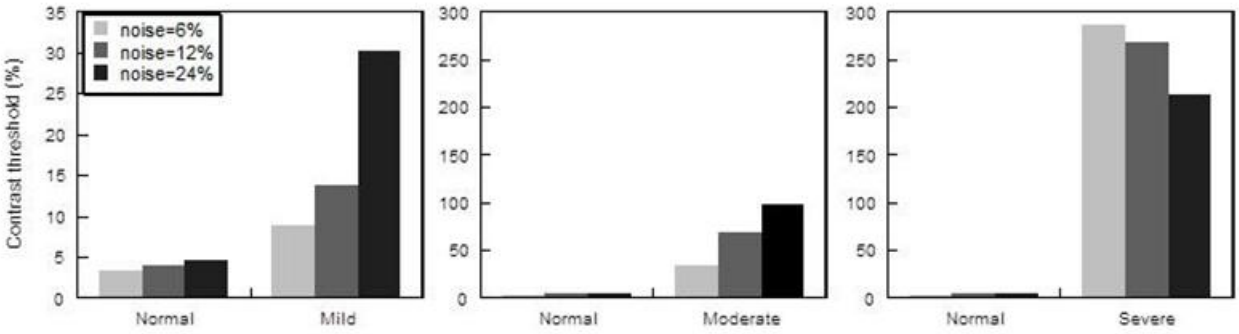


Figure 6-15. Motion tests results for the LHON subjects. The target was buried with the dynamic luminance mask (6%, 12% and 24%). The normal subject shows a small increase in thresholds with level of RLM. The LHON subjects show much higher thresholds than that of the normal subject and the severe LHON subject's thresholds reach the limits imposed by the phosphors of the display. Interestingly, the moderate subjects show a larger increase in thresholds with increasing RLM. This observation suggests that although both P and M neurons are damaged. The largest loss corresponds to the P pathway.

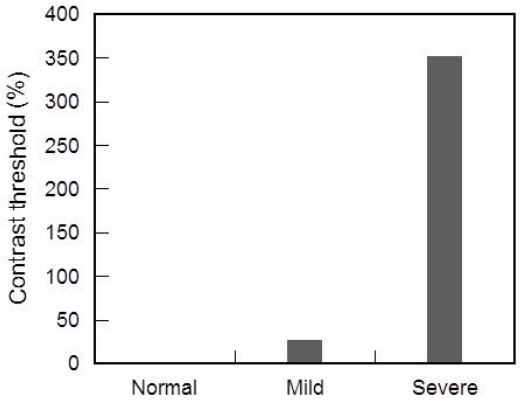


Figure 6-16. Contrast sensitivity results for the mild and severe LHON subjects and a normal trichromat. The normal subject's threshold is approximately 1.7% while the threshold for the mild LHON subject is about 27 higher than that of the normal trichromat. The severely affected LHON subject cannot carry out the test even for the highest thresholds set by the limits of the visual display.

**Pupillometry results: Pupil pathways assessment**

The normal subject showed good pupil responses to all four stimuli Figure 6-17 (a).

The latencies to the d-isoluminant and grating stimuli were approximately 40 –

60ms longer than that of the light flux stimuli (the achromatic and the blue stimulus which has the largest rod contrast components). Similar latency measurements have also been reported in earlier pupil studies (Barbur et al., 1992, Alexandridis et al., 1991, Tsujimura et al., 2001). Because the blue stimulus is photopicly isoluminant, the pupil response to the blue stimulus reflects changes in the contribution that rod signals make to the PLR response (Barbur, 1996). Unlike the pupil colour and grating responses, the faster pupil response latencies to blue and achromatic stimuli suggest that the dominant component that drives the pupil response is the pupil light reflex rather than the colour responses caused by S-cone excitation.

Not only are the latencies the same, but the pupil light reflex responses to both the achromatic and the blue stimulus from the normal subject also yield similar response amplitudes. The two response curves seem to be identical. This may suggest that both responses are driven by one similar pupil component. Because both stimuli have exactly the same rod contrast (171%), these large rod components mainly drive the pupil responses.

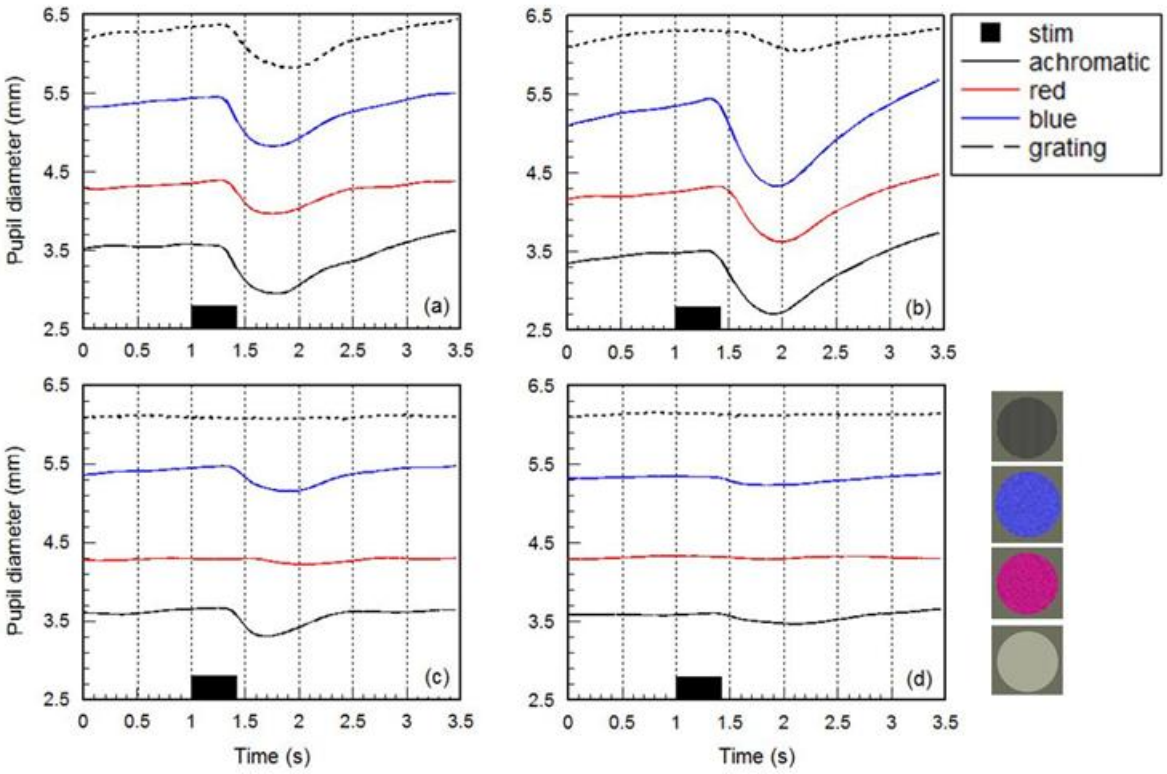


Figure 6-17. Pupillometry results from (a) a typical normal subject, (b) the mild LHON subject – patient one, (c) the moderate LHON subject – patient two, and (d) the severe LHON subject – patient three.

As the severity of the LHON disease increases, the pupil response amplitudes to d-isoluminant colour and grating stimuli decrease and the latencies increase. In the case of the severe LHON subject, the pupil responses to d-isoluminant colour and the grating stimulus are completely absent. The pupil light reflex response measured in response to short wavelength stimuli that trigger large rod signal increments in normal eyes also shows a large decrease in LHON, but the responses are not completely absent but similar in amplitude to those elicited by achromatic stimuli of equivalent rod contrast.

### 6.3.4 Discussion

This study demonstrates selective loss of pupil responses in Lebers disease that are generally in good agreement with the corresponding visual loss.

The patients show complete absence of colour vision (both for RG and YB discrimination). As the severity of LHON disease increases, their motion detection, high contrast acuity and contrast sensitivity also decrease. These results suggest significant damage to the parvocellular and magnocellular cells in LHON and as a result, the pupil colour and grating responses are also very small or absent.

However, the pupil light reflex response remains normal in the mild LHON subject when compared to the normal trichromat except for the grating stimulus is also reduced. In the case of the severe LHON subject, the response latencies are increased and amplitudes are significantly reduced, but these responses are not completely absent.

As discussed earlier in section 6.2, rod signals can contribute significantly to the pupil light reflex response in the rod monochromat. In LHON, the ipRGCs may be spared or less affected (La Morgia et al., 2010). These findings suggest that the dynamic pupil light reflex response pathway rely largely on the rod signals and that this pathway is spared in Lebers disease. Since the P and M pathways are heavily damaged, these findings suggest that the melanopsin labelled ganglion cells which receive a large rod input can be less affected in LHON.

### 6.3.5 Future work

In the motion test, when both the dynamic luminance mask and the static luminance mask are used in a normal trichromat, the modulation amplitude of the static luminance mask doesn't affect one's threshold. An increase in the amplitude of dynamic luminance masking produces corresponding increase in motion threshold in a normal subject.

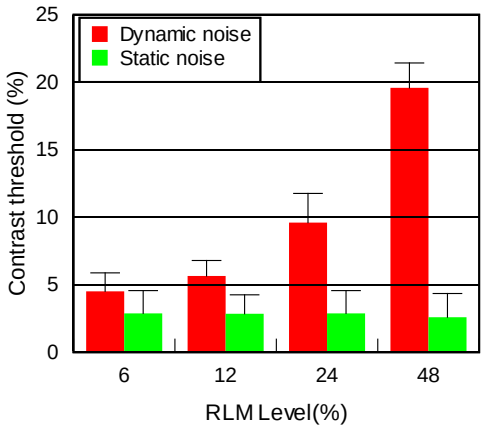


Figure 6-18. Motion thresholds in a normal trichromat. The Y-axis plots the threshold contrast the subject needs in order to detect the moving target. The results reveal a systematic increase in thresholds with increasing levels of dynamic luminance contrast noise. When static luminance noise was employed, the thresholds remain unchanged.

The motion tests with the LHON subjects employed only dynamic luminance contrast noise. Results show increased thresholds when the RLM noise amplitude is increased, with higher thresholds, but similar trends to those measured in normal trichromat. Coherent first order motion relies on the M-pathway which is heavily desensitized by the presence of dynamic RLM noise (Barbur, 2004a, Lu and Sperling, 1995). Consequently, a normal subject shows increasing thresholds with increasing levels of dynamic luminance contrast noise. In LHON subjects, earlier

studies have suggested that the M-pathway is more damaged than the P-pathway (Sadun et al., 2000). If the M-pathway is damaged much more extensively in LHON, the subjects must rely more on their P-pathway to detect the motion. But, because the Pavocellular cells have reduced sensitivity for detection of moving stimuli, it is expected that the use of static contrast noise would also cause an increase in threshold with the level of the noise. This observation/prediction requires further experimental studies.

# 7 SUMMARY AND DISCUSSION

This thesis combines together a number of studies designed to investigate pupil response components and colour perception mechanisms, with emphasis on the measurement of chromatic afterimages.

A complete description of the implementation of a new psychophysics afterimage measurement application has been given. This application includes a number of highly abstracted and extendable functional modules like a front-side GUI, a front-side psychophysics program, a server-side database and a server-side web portal (a design that follows the classic waterfall software engineering model). Detailed display calibration methods and usage were also given. This application was then used to measure the strength of perceived afterimages in both normal trichromats and colour deficient subjects. In normal trichromats, a number of stimulus parameters that affect the strength and duration of afterimages were varied. Results in the normal subject group revealed the same trends and are consistent. The deuteranopes yielded significantly different results from those obtained from the normal subjects when using d-isoluminant colour stimuli, whereas when the stimulus employed had a large S-cone contrast, the results revealed a smaller difference. A model was derived to account for the significant difference between the two groups. The analysis based on the measured afterimage results and the model developed suggest that in deuteranopia, the signals from the L cones are used for the luminance channel and the signal between L and S cones (S – L) is used for the colour channel. It is also assumed that the same theory also applies to

protanopia and tritanopia, in which it is M and (L+M) for luminance and (S – M) and (L – M) for the colour.

Although these findings are consistent with other earlier studies, the outcome also accounts for the findings obtained in the pupil studies. Objective pupil afterimage responses were also investigated to compare with the measured strength and duration of perceived afterimages thresholds. We designed the pupillary stimuli based on their S-cone contrast values (either maximum or minimum) and we found that the results from pupil measurements showed consistency with the measured perceived afterimage results and hence confirmed the theoretical predictions. Furthermore, the simple model proposed here can also be used to predict the pupil responses observed, such as the maximum and minimum pupil responses in dichromats and the colour confusion lines for any given background, provided one is also to compute the corresponding photoreceptor contrasts.

In this study, pupil response differences between subjects with either congenital or acquired hemianopia were compared. Stimuli that isolated photopic luminance and colour signals were employed to compare the pupil responses elicited in the sighted and the blind hemifields. Pupil colour responses and the pupil light reflex responses to stimuli of low contrast were absent in the blind hemifield in the acquired group. In the congenital group, some of these responses were similar and even enhanced when compared to those elicited in the sighted hemifield. The results obtained in the subjects with acquired hemianopia were consistent with earlier findings (Alexandridis et al., 1985, Barbur, 2003) and also confirmed the pupil pathways (Figure 1-24). The differences in results when comparing acquired and congenital

hemianopes suggest that considerable reorganisation of neural projections and function occur during early visual development (Bridge et al., 2008).

Lastly, we investigated whether ipRGCs and melanopsin make a significant contribution to the dynamic pupil light reflex response by investigation both normal subjects as well as selected patients with damaged visual pathways. The properties of the ipRGCs and its contributions to pupil responses have been investigated mostly in mice (Berson et al., 2002, Lucas et al., 2003, Panda et al., 2002). These studies reveal a contribution ipRGCs make to the control of pupil response, but the extent to which this also happens in man remains controversial.

The light stimulator apparatus developed by Tsujimura (Tsujimura et al., 2010) employs a four primary system to generate stimuli that isolate luminance, colour or rods/melanopsin signals. We found that the mild rod deficient subject showed relatively smaller pupil responses to the rod/melanopsin stimulus when compared to that of normal subjects. The RP subject displayed absent pupil responses to the rod/melanopsin stimulus, but good responses to the luminance and colour, whereas the rod monochromat subject yielded completely opposite results. These findings suggest that only rods contribute to the pupil response when the stimulus isolates rod/melanopsin pigment.

We also compared other stimulus properties, such as modulation types – sinwave, squarewave or sawtooth modulation and different stimulus durations, amplitudes and frequencies in a number of preliminary studies in normal subjects. None of the results obtained suggest that melanopsin derived signals contribute to the dynamic pupil light reflex response. Because the rod/melanopsin stimulus generates both a melanopsin and rod pigment modulation, we wanted to recruit a rod deficient

subject to do the test. Previous studies suggest that rods saturate at higher light levels (Aguilar and Stiles, 1954) and it is therefore reasonable to assume that rod signals do not contribute to visual function at high light levels and that any pupil responses reflect either cone or melanopsin based signals. Three light adaptation levels were employed that would be optimum for either the rods component, the melanopsin component or a mixture of the two. After testing a rod deficient subject, we found his responses to the rod/melanopsin stimulus are totally consistent with rod responses. We therefore recruited and tested a subject with RP and a rod monochromat, and their results showed that the pupil responses were only from the rods and that melanopsin doesn't contribute to the dynamic pupil response. Moreover, our rod monochromat continued to respond well to the rod/melanopsin stimulus even at 456 cd/$m^2$. This suggests that the rods do not saturate completely and continue to respond at high luminance levels in the periphery of the visual field.

Colour vision, visual acuity, contrast acuity, motion and pupillometry tests were designed to investigate a group of subjects with Leber's Hereditary Optic Neuropathy. The results show that as the level of disease severity increases, the responses linked to Parvocellular- and Margnocelluar- pathways decrease, but the pupil light reflex responses mediated by rods remain less affected. These results suggest that in LHON, some ganglion cells classes are less affected and that the remaining pupil light reflex response may well be linked to rod signals that drive ipRGCs.

In conclusion, this thesis describes findings from several studies in pupillometry and links the results to the measurement of chromatic afterimages. The work leads to new findings by combining a number of visual psychophysical studies with

measurement of pupil responses to stimuli that isolate photoreceptor signals both in normal subjects and in patients with damaged visual pathways. Overall, the findings from these investigations provide improved understandings of chromatic processes and stimulus specific pupil responses. In addition, a versatile visual psychophysics platform has been developed with its first application in the measurement of chromatic afterimages.

# APPENDIX - A GUIDE OF THE QAA APPLICATION

To start the QAA application, we can simply double click the shortcut icon on the desktop. This actually runs the “Front-end GUI” module.


Then the application checks if the experimenters want to run the application with a database support.


By clicking the “yes” button, the GUI then comes up. The GUI consists of 4 tabs: “Porgram settings”, “Background & fixation”, “Stimulus Options” and “Help page”. These tabs are separated by the stimuli properties. By clicking the “Use default settings to all pages” button, the most commonly used stimuli information will be selected in all tabs. The following figure shows “Program Settings” tab.

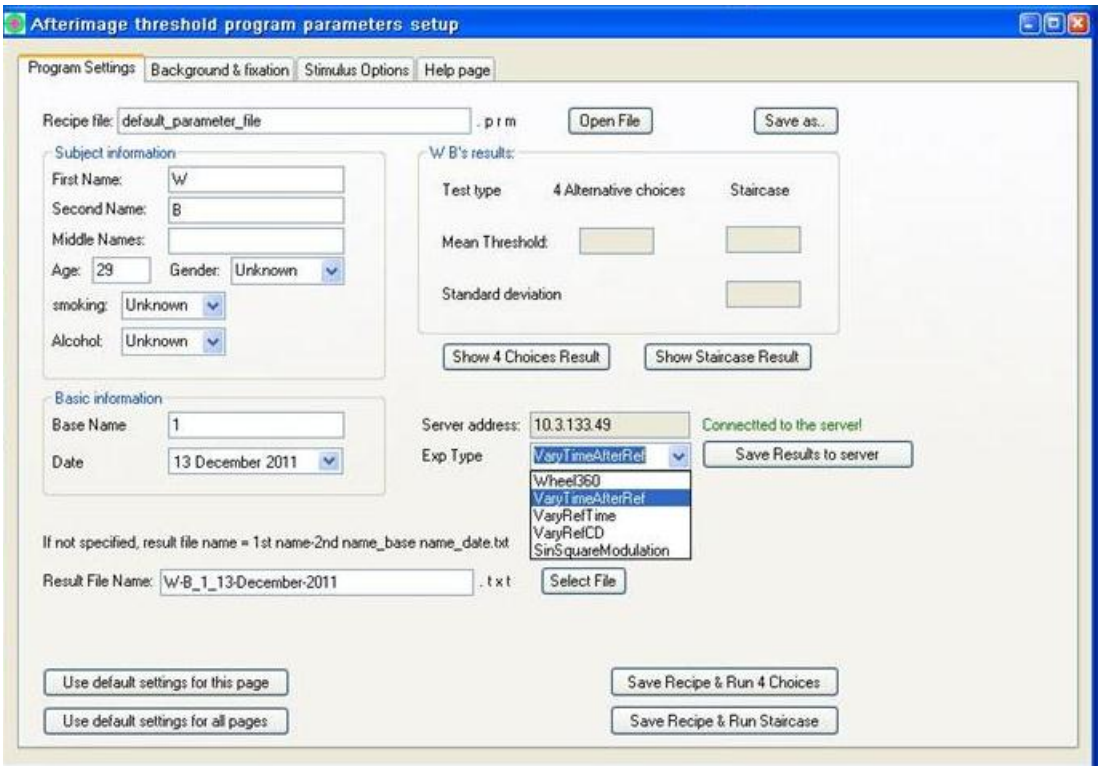
Afterimage threshold program parameters setup
Program Settings
Background & fixation
Stimulus Options
Help page
Recipe file: default_parameter_file
. p r m
Open File
Save as..
Subject information
First Name: W
Second Name: B
Middle Names:
Age: 29
Gender: Unknown
smoking: Unknown
Alcohol: Unknown
W B's results:
Test type
4 Alternative choices
Staircase
Mean Threshold:
Standard deviation
Show 4 Choices Result
Show Staircase Result
Basic information
Base Name 1
Date 13 December 2011
Server address: 10.3.133.49
Connectted to the server!
Exp Type
VaryTimeAfterRef
Save Results to server
Wheel360
VaryTimeAfterRef
VaryRefTime
VaryRefCD
SinSquareModulation
If not specified, result file name = 1st name-2nd name_base name_date.txt
Result File Name: W-B_1_13-December-2011
. t x t
Select File
Use default settings for this page
Use default settings for all pages
Save Recipe & Run 4 Choices
Save Recipe & Run Staircase

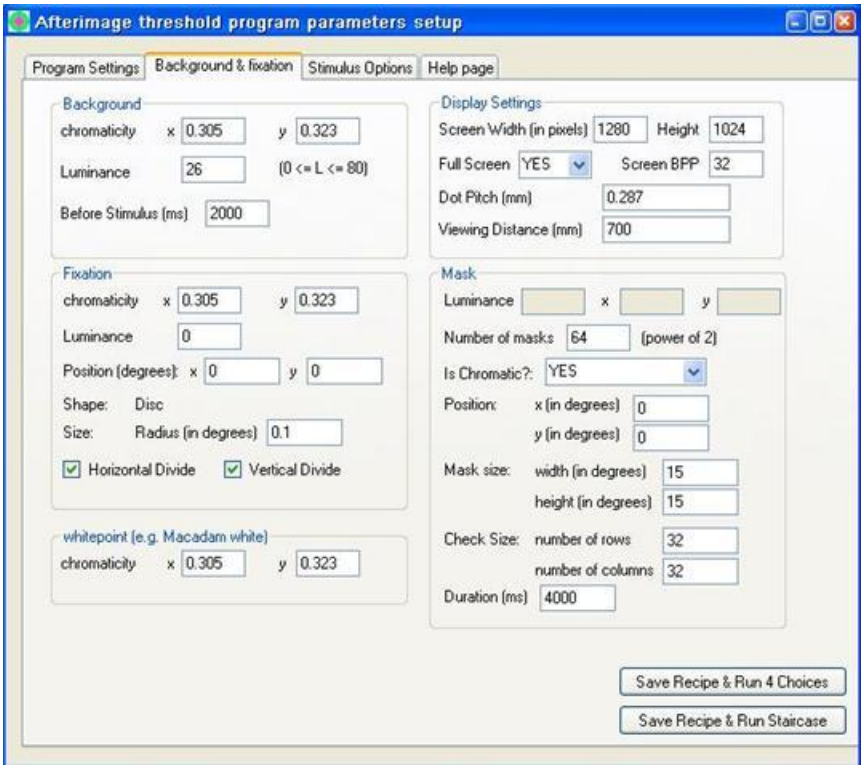
Afterimage threshold program parameters setup
Program Settings
Background & fixation
Stimulus Options
Help page
Background
chromaticity x 0.305 y 0.323
Luminance 26 (0 <= L <= 80)
Before Stimulus (ms) 2000
Fixation
chromaticity x 0.305 y 0.323
Luminance 0
Position (degrees): x 0 y 0
Shape: Disc
Size: Radius (in degrees) 0.1
Horizontal Divide
Vertical Divide
whitepoint (e.g. Macadam white)
chromaticity x 0.305 y 0.323
Display Settings
Screen Width (in pixels) 1280 Height 1024
Full Screen YES Screen BPP 32
Dot Pitch (mm) 0.287
Viewing Distance (mm) 700
Mask
Luminance x y
Number of masks 64 (power of 2)
Is Chromatic?: YES
Position: x (in degrees) 0
y (in degrees) 0
Mask size: width (in degrees) 15
height (in degrees) 15
Check Size: number of rows 32
number of columns 32
Duration (ms) 4000
Save Recipe & Run 4 Choices
Save Recipe & Run Staircase

The afterimage website's home page is shown below. The 4 navigation links in the top menu are always displayed. However, the "Afterimage Results" button only works after users log in.


When the "Log in/out" button is clicked, users can input his username and passwords obtained from the left hand side.

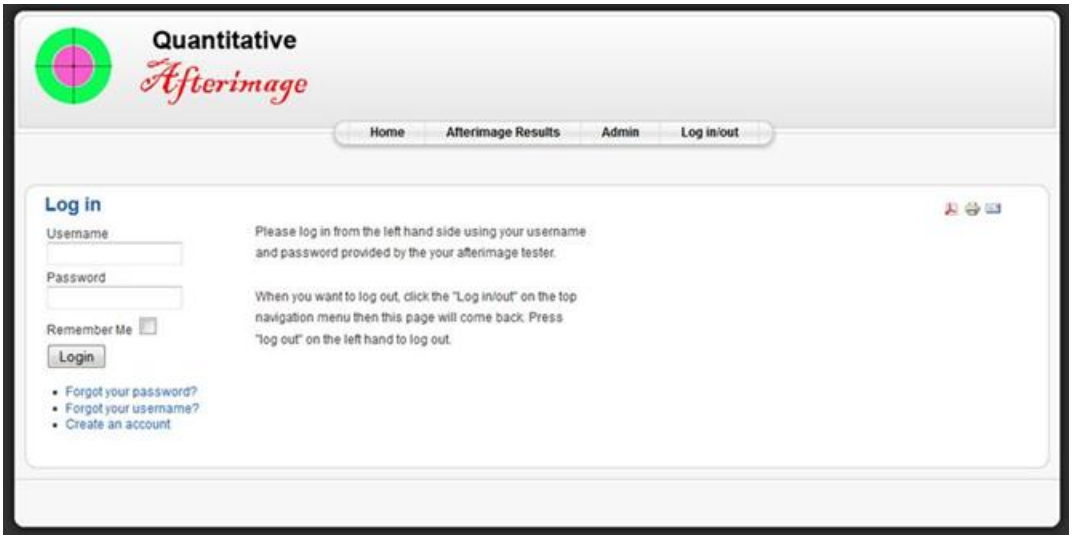


The follow figure shows an example how the log in menu changes after I log in.

Because my account has been assigned a full administrator right, I can browse everybody's detailed results. The following figure shows that after I logged in, I pressed the "Afterimage Results" and searched with a keyword "wei". My first 5 test results are then shown on the page. For a subject, he/she can only browse his/her own result.


| First Name | Second Name | Test Type | Staircase result | Staircase std | 4-choice result | Ref Angle | Ref CD | Ref Dur | Time Between | Modulation Type | Test Dur | BG (x, y) Luminance |
|---|---|---|---|---|---|---|---|---|---|---|---|---|
| Wei | Bi | VaryBgLevel24 | 0.0227599 | 0.00180839 | 0.012 | 125 | 0.09 | 5000 | 1000 | SQUAREWAVE | 1000 | (0.305,0.323), 24 |
| Wei | Bi | VaryBgLevel6 | 0.017956 | 0.00156322 | 0.024 | 125 | 0.09 | 5000 | 1000 | SQUAREWAVE | 1000 | (0.305,0.323), 6 |
| Wei | Bi | VaryBgLevel12 | 0.0210404 | 0.00190359 | 0.024 | 125 | 0.09 | 5000 | 1000 | SQUAREWAVE | 1000 | (0.305,0.323), 12 |
| Wei | Bi | SinSquareModulation | 0.0170316 | 0.00217645 | 0.012 | 125 | 0.09 | 5000 | 0 | SINWAVE | 1000 | (0.305,0.323), 26 |
| Wei | Bi | SinSquareModulation | 0.0266922 | 0.00112057 | 0.012 | 125 | 0.09 | 5000 | 0 | SQUAREWAVE | 1000 | (0.305,0.323), 26 |

# REFERENCES AND BIBLIOGRAPHY


AGUILAR, M. & STILES, W. 1954. Saturation of the rod mechanism of the retina at high levels of stimulation. *Journal of Modern Optics,* 1**,** 59-65.

ALBRIGHT, T. D. 1984. Direction and orientation selectivity of neurons in visual area MT of the macaque. *Journal of Neurophysiology,* 52**,** 1106-1130.

ALEXANDRIDIS, E., LEENDERTZ, J. & BARBUR, J. 1991. Methods for studying the behaviour of the pupil. *Journal of psychophysiology*.

ALEXANDRIDIS, E., TELGER, T. & BLODI, F. 1985. *The pupil*, Springer-Verlag New York.

ALLISON, T., MCCARTHY, G., NOBRE, A., PUCE, A. & BELGER, A. 1994. Human extrastriate visual cortex and the perception of faces, words, numbers, and colors. *Cerebral Cortex,* 4**,** 544.

ALPERN, M. & OHBA, N. 1972. The effect of bleaching and backgrounds on pupil size. *Vision Res,* 12**,** 943-51.

ANDERSON, C. J. & COLOMBO, J. 2009. Larger tonic pupil size in young children with autism spectrum disorder. *Developmental psychobiology,* 51**,** 207-211.

ATCHISON, D. A. & SMITH, G. 2000. *Optics of the human eye*, Butterworth-Heinemann Medical.

BAKER JR, C. L., HESS, R. F. & ZIHL, J. 1991. Residual motion perception in a" motion-blind" patient, assessed with limited-lifetime random dot stimuli. *The Journal of neuroscience,* 11**,** 454-461.

BARBUR, J., CHISHOLM, C. & HARLOW, J. Year. New test for assessing visual performance following corneal refractive surgery. *In*, 2001. Optical Society of America.

BARBUR, J., HARLOW, A. & SAHRAIE, A. 1992. Pupillary responses to stimulus structure, colour and movement. *Ophthalmic and Physiological Optics,* 12**,** 137-141.

BARBUR, J., HARLOW, A. & WEISKRANTZ, L. 1994a. Spatial and temporal response properties of residual vision in a case of hemianopia. *Philosophical Transactions of the Royal Society of London. Series B: Biological Sciences,* 343**,** 157.

BARBUR, J., RUDDOCK, K. & WATERFIELD, V. A. 1980. Human visual responses in the absence of the geniculo-calcarine projection. *Brain: a journal of neurology,* 103**,** 905.

BARBUR, J. & STOCKMAN, A. 2010. Photopic, Mesopic, and Scotopic Vision and Changes in Visual Performance.

BARBUR, J. L. 1996. A study of pupil response components in human vision. *Basic and clinical perspectives in vision research: a celebration of the career of Hisako Ikeda***,** 3.

BARBUR, J. L. 2003. Learning from the pupil-studies of basic mechanisms and clinical applications. MIT Press, Cambridge, MA.

BARBUR, J. L. 2004a. 'Double-blindsight' revealed through the processing of color and luminance contrast defined motion signals. *Prog Brain Res,* 144**,** 243-59.

BARBUR, J. L. 2004b. Learning from the pupil - studies of basic mechanisms and clinical applications. *In:* CHALUPA, L. M. & WERNER, J. S. (eds.) *The Visual Neuroscience.* MIT Press.

BARBUR, J. L., HARLOW, A. J. & PLANT, G. T. 1994b. Insights into the different exploits of colour in the visual cortex. *Proc Biol Sci,* 258**,** 327-34.

BARBUR, J. L., KONSTANTAKOPOULOU, E., RODRIGUEZ-CARMONA, M., HARLOW, J. A., ROBSON, A. G. & MORELAND, J. D. 2010. The Macular Assessment Profile test - a new VDU-based technique for measuring the spatial distribution of the macular pigment, lens density and rapid flicker sensitivity. *Ophthalmic Physiol Opt,* 30**,** 470-83.

BARBUR, J. L., THOMSON, W. D. & FORSYTH, P. M. 1987. A new system for the simultaneous measurement of pupil size and two-dimensional eye movements. *Clin. Vis. Sci.,* 2**,** 11.

BARBUR, J. L., WATSON, J., FRACKOWIAK, R. S. J. & ZEKI, S. 1993. Conscious visual perception without VI. *Brain,* 116**,** 1293.

BARBUR, J. L., WEISKRANTZ, L. & HARLOW, J. A. 1999. The unseen color aftereffect of an unseen stimulus: insight from blindsight into mechanisms of color afterimages. *Proc Natl Acad Sci U S A,* 96**,** 11637-41.

BARLOW, H. & SPARROCK, J. 1964. The role of afterimages in dark adaptation. *Science*.

BECK, R. W. & TROBE, J. D. 1995. What we have learned from the Optic Neuritis Treatment Trial. *Ophthalmology,* 102**,** 1504-8.

BENDER, M. B., FELDMAN, M. & SOBIN, A. J. 1968. Palinopsia. *Brain: a journal of neurology*.

BERSON, D. M. 2007. Phototransduction in ganglion-cell photoreceptors. *Pflügers Archiv European Journal of Physiology,* 454**,** 849-855.

BERSON, D. M., DUNN, F. A. & TAKAO, M. 2002. Phototransduction by retinal ganglion cells that set the circadian clock. *Science,* 295**,** 1070-3.

BIRCH, J. 2001. *Diagnosis of defective colour vision,* Oxfrord, Butterworth-Heinemann.

BIRCH, J., BARBUR, J. L. & HARLOW, A. J. 1992. New method based on random luminance masking for measuring isochromatic zones using high resolution colour displays. *Ophthalmic Physiol Opt,* 12**,** 133-6.

BIRREN, J. E., CASPERSON, R. C. & BOTWINICK, J. 1950. Age changes in pupil size. *Journal of Gerontology,* 5**,** 216.

BOETTNER, E. A. & WOLTER, J. R. 1962. Transmission of the ocular media. *Investigative ophthalmology & visual science,* 1**,** 776.

BOOCH, G., MAKSIMCHUK, R., ENGLE, M., YOUNG, B., CONALLEN, J. & HOUSTON, K. 2007. *Object-oriented analysis and design with applications*, Addison-Wesley Professional.

BOUMAN, M. & TEN DOESSCHATE, J. 1962. The mechanism of dark-adaptation. *Vision research,* 1**,** 386-403.

BOYNTON, R. M. 1979. *Human color vision*, Holt, Rinehart and Winston New York.

BRIDGE, H., THOMAS, O., JBABDI, S. & COWEY, A. 2008. Changes in connectivity after visual cortical brain damage underlie altered visual function. *Brain,* 131**,** 1433-1444.

BRINDLEY, G., GAUTIER-SMITH, P. & LEWIN, W. 1969. Cortical blindness and the functions of the non-geniculate fibres of the optic tracts. *Journal of Neurology, Neurosurgery & Psychiatry,* 32**,** 259.

BROOKS, F. P. 1987. No silver bullet: Essence and accidents of software engineering. *IEEE computer,* 20**,** 10-19.

BROWN, P. K. & WALD, G. 1964. Visual pigments in single rods and cones of the human retina. *Science,* 144**,** 45.

CAMPBELL, F. & GREGORY, A. 1960. Effect of size of pupil on visual acuity.

CARLSON, N. R. 2007. *Physiology of behavior*, Allyn & Bacon.

CASAGRANDE, V. 1994. A third parallel visual pathway to primate area V1. *Trends in Neurosciences,* 17**,** 305-310.

CASAGRANDE, V. A. 1999. The mystery of the visual system K pathway. *The Journal of physiology,* 517**,** 630-630.

CASSIN, B., SOLOMON, S. & RUBIN, M. L. 1990. *Dictionary of eye terminology*, Wiley Online Library.

CIBIS, G. W., CAMPOS, E. C. & AULHORN, E. 1975. Pupillary hemiakinesia in suprageniculate lesions. *Archives of Ophthalmology,* 93**,** 1322.

COMPSTON, A. & COLES, A. 2008. Multiple sclerosis. *Lancet,* 372**,** 1502-17.

COWEY, A. & STOERIG, P. 1991. The neurobiology of blindsight. *Trends in Neurosciences,* 14**,** 140-145.

COWEY, A. & STOERIG, P. 1992. Reflections on blindsight.

CRAMER, G. 1750. *Introduction à l'analyse des lignes courbes algébriques*, chez les frères Cramer et C. Philibert.

CRONER, L. J. & KAPLAN, E. 1995. Receptive fields of P and M ganglion cells across the primate retina. *Vision research,* 35**,** 7-24.

CURCIO, C. A., SLOAN, K. R., KALINA, R. E. & HENDRICKSON, A. E. 1990. Human photoreceptor topography. *The Journal of comparative neurology,* 292**,** 497-523.

DACEY, D. M. & LEE, B. B. 1994. The'blue-on'opponent pathway in primate retina originates from a distinct bistratified ganglion cell type. *Nature,* 367**,** 731-735.

DACEY, D. M., LIAO, H. W., PETERSON, B. B., ROBINSON, F. R., SMITH, V. C., POKORNY, J., YAU, K. W. & GAMLIN, P. D. 2005. Melanopsin-expressing ganglion cells in primate retina signal colour and irradiance and project to the LGN. *Nature,* 433**,** 749-54.

DACEY, D. M. & PETERSEN, M. R. 1992. Dendritic field size and morphology of midget and parasol ganglion cells of the human retina. *Proceedings of the National Academy of sciences,* 89**,** 9666-9670.

DARTNALL, H. 1953. The interpretation of spectral sensitivity curves. *British Medical Bulletin,* 9**,** 24.

DARTNALL, H., BOWMAKER, J. & MOLLON, J. 1983. Human visual pigments: microspectrophotometric results from the eyes of seven persons. *Proceedings of the Royal society of London. Series B. Biological sciences,* 220**,** 115.

DARWIN, R. W. & DARWIN, E. 1786. New Experiments on the Ocular Spectra of Light and Colours. By Robert Waring Darwin, MD; Communicated by Erasmus Darwin, MDFRS. *Philosophical Transactions of the Royal Society of London,* 76**,** 313-348.

DEMB, J. B. & PUGH JR, E. N. 2002. Connexin36 forms synapses essential for night vision. *Neuron,* 36**,** 551-553.

DESIMONE, R. & SCHEIN, S. J. 1987. Visual properties of neurons in area V4 of the macaque: sensitivity to stimulus form. *Journal of Neurophysiology,* 57**,** 835-868.

DUBNER, R. & ZEKI, S. 1971. Response properites and receptive fields of cells in an anatomically defined region of the superior temporal sulcus in the monkey. *Brain Research; Brain Research*.

EHLERS, N., BRAMSEN, T. & SPERLING, S. 1975. Applanation tonometry and central corneal thickness. *Acta Ophthalmologica,* 53**,** 34-43.

ERWIN, E., BAKER, F. H., BUSEN, W. F. & MALPELI, J. G. 1999. Relationship between laminar topology and retinotopy in the rhesus lateral geniculate nucleus: results from a functional atlas. *The Journal of Comparative Neurology,* 407**,** 92-102.

FARRELL, R. J. & BOOTH, J. M. 1975. Design handbook for imagery interpretation equipment. *Unknown,* 1.

FAULK, S. R. 1995. Software requirements: A tutorial. DTIC Document.

FELLEMAN, D. J. & VAN ESSEN, D. C. 1987. Receptive field properties of neurons in area V3 of macaque monkey extrastriate cortex. *Journal of Neurophysiology,* 57**,** 889-920.

FLANAGAN, P. & ZELE, A. J. 2004. Chromatic and luminance losses with multiple sclerosis and optic neuritis measured using dynamic random luminance contrast noise. *Ophthalmic and Physiological Optics,* 24**,** 225-233.

FRANCIS, G. 2010. Modeling filling-in of afterimages. *Attention, Perception, & Psychophysics,* 72**,** 19-22.

GAMLIN, P. D. R., MCDOUGAL, D. H., POKORNY, J., SMITH, V. C., YAU, K. W. & DACEY, D. M. 2007. Human and macaque pupil responses driven by melanopsin-containing retinal ganglion cells. *Vision research,* 47**,** 946-954.

GATTASS, R., SOUSA, A. & GROSS, C. 1988. Visuotopic organization and extent of V3 and V4 of the macaque. *The Journal of neuroscience,* 8**,** 1831-1845.

GOODALE, M. A. & MILNER, A. D. 2005. *Sight unseen: An exploration of conscious and unconscious vision*, Oxford University Press, USA.

GOVARDOVSKII, V. I., FYHRQUIST, N., REUTER, T., KUZMIN, D. G. & DONNER, K. 2000. In search of the visual pigment template. *Visual Neuroscience,* 17**,** 509-528.

GROSS, C. G. 1991. Contribution of striate cortex and the superior colliculus to visual function in area MT, the superior temporal polysensory area and inferior temporal cortex. *Neuropsychologia,* 29**,** 497-515.

GUILD, J. 1932. The colorimetric properties of the spectrum. *Philosophical Transactions of the Royal Society of London. Series A, Containing Papers of a Mathematical or Physical Character,* 230**,** 149.

HARMS, H. 1951. Hemianopische pupillenstarre. *Klin Monatsbl Augenheilkd,* 118**,** 133-147.

HART, R. W. & FARRELL, R. A. 1969. Light scattering in the cornea. *JOSA,* 59**,** 766-773.

HATTAR, S., LIAO, H. W., TAKAO, M., BERSON, D. M. & YAU, K. W. 2002. Melanopsin-containing retinal ganglion cells: architecture, projections, and intrinsic photosensitivity. *Science,* 295**,** 1065-70.

HENDRICKSON, A. E., WAGONER, N. & COWAN, W. M. 1972. An autoradiographic and electron microscopic study of retino-hypothalamic connections. *Cell and Tissue Research,* 135**,** 1-26.

HERING, E. 1964. Outlines of a Theory of the Light Sense.

HESS, R., BAKER JR, C. & ZIHL, J. 1989. The" motion-blind" patient: Low-level spatial and temporal filters. *The Journal of neuroscience,* 9**,** 1628-1640.

HEYWOOD, C. & COWEY, A. 1987. On the role of cortical area V4 in the discrimination of hue and pattern in macaque monkeys. *The Journal of neuroscience,* 7**,** 2601-2617.

HUBEL, D. H. 1995. *Eye, brain, and vision*, Scientific American Library/Scientific American Books.

HUBEL, D. H. & LIVINGSTONE, M. S. 1987. Segregation of form, color, and stereopsis in primate area 18. *The Journal of neuroscience,* 7**,** 3378-3415.

HUBEL, D. H., WENSVEEN, J. & WICK, B. 1995. *Eye, brain, and vision*, Scientific American Library New York.

HURVICH, L. M. & JAMESON, D. 1957. An opponent-process theory of color vision. *Psychological review,* 64**,** 384.

I ARBUS, A. L. 1967. *Eye movements and vision*, Plenum press.

JUDD, D. B., MACADAM, D. L., WYSZECKI, G., BUDDE, H., CONDIT, H., HENDERSON, S. & SIMONDS, J. 1964. Spectral distribution of typical daylight as a function of correlated color temperature. *JOSA,* 54**,** 1031-1036.

KAAS, J. H., HUERTA, M. F., WEBER, J. T. & HARTING, J. K. 1978. Patterns of retinal terminations and laminar organization of the lateral geniculate nucleus of primates. *J Comp Neurol,* 182**,** 517-53.

KANEKO, A. 1970. Physiological and morphological identification of horizontal, bipolar and amacrine cells in goldfish retina. *The Journal of Physiology,* 207**,** 623.

KAPLAN, E., LEE, B. B. & SHAPLEY, R. M. 1990. New views of primate retinal function. *Progress in retinal research,* 9**,** 273-336.

KARDON, R. H. 1992. Pupil perimetry. *Current opinion in ophthalmology,* 3**,** 565.

KAUFMAN, L. 1974. *Sight and mind: An introduction to visual perception*, Oxford U. Press.

KELLY, D. & MARTINEZ-URIEGAS, E. 1993. Measurements of chromatic and achromatic afterimages. *JOSA A,* 10**,** 29-37.

KIMURA, E. & YOUNG, R. S. 1995. Nature of the pupillary responses evoked by chromatic flashes on a white background. *Vision Res,* 35**,** 897-906.

KNIERIM, J. J. & VAN ESSEN, D. C. 1992. Neuronal responses to static texture patterns in area V1 of the alert macaque monkey. *Journal of Neurophysiology,* 67**,** 961-980.

KOHN, M. & CLYNES, M. 1969. Color dynamics of the pupil. *Ann N Y Acad Sci,* 156**,** 931-50.

KOLB, B. 1995. *Brain plasticity and behavior*, Lawrence Erlbaum.

KOLB, H. 1991. *The neural organization of the human retina*, Principles and practices of clinical electrophysiology of vision.

KOMAI, Y. & USHIKI, T. 1991. The three-dimensional organization of collagen fibrils in the human cornea and sclera. *Investigative Ophthalmology & Visual Science,* 32**,** 2244-2258.

KRASNER, G. E. & POPE, S. T. 1988. A description of the model-view-controller user interface paradigm in the smalltalk-80 system. *Journal of object oriented programming,* 1**,** 26-49.

KUPFER, C., CHUMBLEY, L. & DOWNER, J. C. 1967. Quantitative histology of optic nerve, optic tract and lateral geniculate nucleus of man. *Journal of Anatomy,* 101**,** 393.

LA MORGIA, C., ROSS-CISNEROS, F. N., SADUN, A. A., HANNIBAL, J., MUNARINI, A., MANTOVANI, V., BARBONI, P., CANTALUPO, G., TOZER, K. R. & SANCISI, E. 2010. Melanopsin retinal ganglion cells are resistant to neurodegeneration in mitochondrial optic neuropathies. *Brain,* 133**,** 2426.

LAIBSON, P. R. 1971. Cornea and sclera. *Archives of Ophthalmology,* 85**,** 738.

LAPLANTE, P. A. 2007. *What every engineer should know about software engineering*, CRC Press.

LENNIE, P. 1998. Single units and visual cortical organization. *PERCEPTION-LONDON-,* 27**,** 889-936.

LENNIE, P. & MOVSHON, J. A. 2005. Coding of color and form in the geniculostriate visual pathway (invited review). *JOSA A,* 22**,** 2013-2033.

LEOPOLD, D. A. & LOGOTHETIS, N. K. 1996. Activity changes in early visual cortex reflect monkeys' percepts during binocular rivalry. *Nature,* 379**,** 549-553.

LEUBA, G. & KRAFTSIK, R. 1994. Changes in volume, surface estimate, three-dimensional shape and total number of neurons of the human primary visual cortex from midgestation until old age. *Anatomy and embryology,* 190**,** 351-366.

LOEWENFELD, I. E. & LOWENSTEIN, O. 1993. *The pupil: Anatomy, physiology, and clinical applications*, Iowa State University Press.

LOWENSTEIN, O., KAWABATA, H. & LOEWENFELD, I. 1964. THE PUPIL AS INDICATOR OF RETINAL ACTIVITY. *American journal of ophthalmology,* 57**,** 569.

LU, Z. L. & SPERLING, G. 1995. The functional architecture of human visual motion perception. *Vision research,* 35**,** 2697-2722.

LUCAS, R. J., DOUGLAS, R. H. & FOSTER, R. G. 2001. Characterization of an ocular photopigment capable of driving pupillary constriction in mice. *Nat Neurosci,* 4**,** 621-6.

LUCAS, R. J., HATTAR, S., TAKAO, M., BERSON, D. M., FOSTER, R. G. & YAU, K. W. 2003. Diminished pupillary light reflex at high irradiances in melanopsin-knockout mice. *Science,* 299**,** 245-7.

LUECK, C., ZEKI, S., FRISTON, K., DEIBER, M. P., COPE, P., CUNNINGHAM, V. J., LAMMERTSMA, A., KENNARD, C. & FRACKOWIAK, R. 1989. The colour centre in the cerebral cortex of man.

MACADAM, D. L. 1942. Visual sensitivities to color differences in daylight. *JOSA,* 32**,** 247-273.

MARKWELL, E. L., FEIGL, B. & ZELE, A. J. 2010. Intrinsically photosensitive melanopsin retinal ganglion cell contributions to the pupillary light reflex and circadian rhythm. *Clin Exp Optom,* 93**,** 137-49.

MAUNSELL, J. H. R. & NEWSOME, W. T. 1987. Visual processing in monkey extrastriate cortex. *Annual Review of Neuroscience,* 10**,** 363-401.

MCADAMS, C. J. & MAUNSELL, J. H. R. 1999. Effects of attention on orientation-tuning functions of single neurons in macaque cortical area V4. *The Journal of neuroscience,* 19**,** 431-441.

MEADOWS, J. & MUNRO, S. 1977. Palinopsia. *Journal of Neurology, Neurosurgery & Psychiatry,* 40**,** 5-8.

MERIGAN, W. H. & MAUNSELL, J. H. R. 1990. Macaque vision after magnocellular lateral geniculate lesions. *Visual Neuroscience,* 5**,** 347-352.

MILLER, N. D. 1966. Positive afterimage as a background luminance. *JOSA,* 56**,** 1616-1619.

MILLS, S. L. & MASSEY, S. C. 1995. Differential properties of two gap junctional pathways made by AII amacrine cells.

MILNE, E., SWETTENHAM, J., HANSEN, P., CAMPBELL, R., JEFFRIES, H. & PLAISTED, K. 2002. High motion coherence thresholds in children with autism. *Journal of Child Psychology and Psychiatry,* 43**,** 255-263.

MOLLON, J. 1974. After-effects and the brain. *New Scientist,* 61**,** 479-482.

MOLLON, J. & REGAN, B. 1999. The spectral distribution of primate cones and of the macular pigment: Matched to properties of the world? *JOURNAL OF OPTICAL TECHNOLOGY C/C OF OPTICHESKII ZHURNAL,* 66**,** 847-852.

MORO, S., RODRIGUEZ CARMONA, M., FROST, E., PLANT, G. & BARBUR, J. 2007. Recovery of vision and pupil responses in optic neuritis and multiple sclerosis. *Ophthalmic and Physiological Optics,* 27**,** 451-460.

MOTTRON, L., DAWSON, M., SOULIERES, I., HUBERT, B. & BURACK, J. 2006. Enhanced perceptual functioning in autism: an update, and eight principles of autistic perception. *Journal of autism and developmental disorders,* 36**,** 27-43.

MROSOVSKY, N. & HATTAR, S. 2003. Impaired masking responses to light in melanopsin-knockout mice. *Chronobiol Int,* 20**,** 989-99.

MULLEN, K. T. & PLANT, G. T. 1986. Colour and luminance vision in human optic neuritis. *Brain,* 109**,** 1.

OSTERBERG, G. 1935. *Topography of the layer of rods and cones in the human retina*, Nyt Nordisk Forlag.

OYSTER, C. W. 1999. *The human eye: structure and function*, Sinauer Associates.

PACKER, O. & WILLIAMS, D. R. 2003. Light, the retinal image, and photoreceptors. *The science of color,* 2**,** 41-102.

PANDA, S., SATO, T. K., CASTRUCCI, A. M., ROLLAG, M. D., DEGRIP, W. J., HOGENESCH, J. B., PROVENCIO, I. & KAY, S. A. 2002. Melanopsin (Opn4) requirement for normal light-induced circadian phase shifting. *Science,* 298**,** 2213-6.

PICKARD, G. E. 1985. Bifurcating axons of retinal ganglion cells terminate in the hypothalamic suppachiasmatic nucleus and the intergeniculate leaflet of the thalamus. *Neuroscience letters,* 55**,** 211-217.

PLAISTED GRANT, K. & DAVIS, G. 2009. Perception and apperception in autism: rejecting the inverse assumption. *Philosophical Transactions of the Royal Society B: Biological Sciences,* 364**,** 1393-1398.

POKORNY, J., SMITH, V. C. & LUTZE, M. 1987. Aging of the human lens. *Applied Optics,* 26**,** 1437-1440.

POKORNY, J., SMITHSON, H. & QUINLAN, J. 2004. Photostimulator allowing independent control of rods and the three cone types. *Vis Neurosci,* 21**,** 263-7.

POLYAK, S. L. 1941. *The retina*, University of Chicago Press.

PROVENCIO, I., JIANG, G., DE GRIP, W. J., HAYES, W. P. & ROLLAG, M. D. 1998. Melanopsin: An opsin in melanophores, brain, and eye. *Proc Natl Acad Sci U S A,* 95**,** 340-5.

PROVENCIO, I., RODRIGUEZ, I. R., JIANG, G., HAYES, W. P., MOREIRA, E. F. & ROLLAG, M. D. 2000. A novel human opsin in the inner retina. *J Neurosci,* 20**,** 600-5.

ROBERTSON, G. G., MACKINLAY, J. D. & CARD, S. K. Year. Cone trees: animated 3D visualizations of hierarchical information. *In*, 1991. 194.

RODIECK, R. W. 1998. *The first steps in seeing*, Sinauer Associates Sunderland, MA.

RODRIGUEZ-CARMONA, M. L., HARLOW, J. A., WALKER, G. & BARBUR, J. L. Year. The variability of normal trichromatic vision and the establishment of the "normal" range. *In:* Proceedings of 10th Congress of the International Colour Association. , 2005 Granada. 979-982.

RUBY, N. F., BRENNAN, T. J., XIE, X., CAO, V., FRANKEN, P., HELLER, H. C. & O'HARA, B. F. 2002. Role of melanopsin in circadian responses to light. *Science,* 298**,** 2211-3.

RUMBAUGH, J., BLAHA, M., PREMERLANI, W., EDDY, F. & LORENSON, W. 1991. Object-oriented modeling and design.

SADUN, A. A., WIN, P. H., ROSS-CISNEROS, F., WALKER, S. & CARELLI, V. 2000. Leber's hereditary optic neuropathy differentially affects smaller axons in the optic nerve. *Transactions of the American Ophthalmological Society,* 98**,** 223.

SAHRAIE, A. & BARBUR, J. L. 1997. Pupil response triggered by the onset of coherent motion. *Graefe's archive for clinical and experimental ophthalmology,* 235**,** 494-500.

SCHAEFFEL, F., GLASSER, A. & HOWLAND, H. C. 1988. Accommodation, refractive error and eye growth in chickens. *Vision research,* 28**,** 639-657.

SCHWARTZ, S. H. 2004. *Visual perception: A clinical orientation*, McGraw-Hill Medical.

SHAPIRO, A. G., POKORNY, J. & SMITH, V. C. 1996. Cone-rod receptor spaces with illustrations that use CRT phosphor and light-emitting-diode spectra. *J Opt Soc Am A Opt Image Sci Vis,* 13**,** 2319-28.

SHARPE, L. T., STOCKMAN, A., JAGLE, H. & NATHANS, J. 1999. Opsin genes, cone photopigments, color vision, and color blindness. *In:* GEGENFURTNER, K. R. & SHARPE, L. T. (eds.) *Color Vision: From Genes to Perception.* Cambridge: Cambridge University Press.

SHAW, M. & GARLAN, D. 1996. Software architecture: perspectives on an emerging discipline.

SHIMOJO, S., KAMITANI, Y. & NISHIDA, S. 2001. Afterimage of perceptually filled-in surface. *Science,* 293**,** 1677.

SHIPP, S. & ZEKI, S. 1985. Segregation of pathways leading from area V2 to areas V4 and V5 of macaque monkey visual cortex. *Nature,* 315**,** 322-324.

SHIPP, S. & ZEKI, S. 1995. Segregation and convergence of specialised pathways in macaque monkey visual cortex. *Journal of Anatomy,* 187**,** 547.

SILBERSTEIN, L. & MACADAM, D. L. 1945. The distribution of color matchings around a color center. *JOSA,* 35**,** 32-38.

SMITH, V. C., POKORNY, J., DAVIS, M. & YEH, T. 1995. Mechanisms subserving temporal modulation sensitivity in silent-cone substitution. *J Opt Soc Am A Opt Image Sci Vis,* 12**,** 241-9.

SNODDERLY, D., BROWN, P., DELORI, F. & AURAN, J. 1984. The macular pigment. I. Absorbance spectra, localization, and discrimination from other yellow pigments in primate retinas. *Investigative ophthalmology & visual science,* 25**,** 660.

SQUIRE, T. J., RODRIGUEZ-CARMONA, M., EVANS, A. D. & BARBUR, J. L. 2005. Color vision tests for aviation: comparison of the anomaloscope and three lantern types. *Aviat Space Environ Med,* 76**,** 421-9.

STILES, W. 1939. The directional sensitivity of the retina and the spectral sensitivities of the rods and cones. *Proceedings of the Royal Society of London. Series B, Biological Sciences,* 127**,** 64-105.

STOCKMAN, A. & SHARPE, L. T. 2000. The spectral sensitivities of the middle-and long-wavelength-sensitive cones derived from measurements in observers of known genotype. *Vision research,* 40**,** 1711-1737.

STOCKMAN, A., SHARPE, L. T. & FACH, C. 1999. The spectral sensitivity of the human short-wavelength sensitive cones derived from thresholds and color matches. *VISION RESEARCH-OXFORD-,* 39**,** 2901-2927.

STOERIG, P. & COWEY, A. 1997. Blindsight in man and monkey. *Brain,* 120**,** 535-559.

SUZUKI, S. & GRABOWECKY, M. 2003. Attention during adaptation weakens negative afterimages. *Journal of Experimental Psychology: Human Perception and Performance,* 29**,** 793.

TAYLOR, S. & CLEMENTE, R. 2005. Confirmation of nasogastric tube position by pH testing. *Journal of human nutrition and dietetics,* 18**,** 371-375.

THOMPSON, H. S. 1992. The pupil. *Adler's physiology of the eye. 9th ed. St Louis: Mosby-Year Book***,** 416-17.

THOMPSON, P. & BURR, D. 2009. Visual aftereffects. *Current Biology,* 19**,** R11-R14.

TS'O, D. Y., GILBERT, C. D. & WIESEL, T. N. 1986. Relationships between horizontal interactions and functional architecture in cat striate cortex as revealed by cross-correlation analysis. *The Journal of neuroscience,* 6**,** 1160-1170.

TSUCHIYA, N. 2005. *Attention and awareness: visual psychophysics and aversive conditioning in humans.* California Institute of Technology.

TSUJIMURA, S., UKAI, K., OHAMA, D., NURUKI, A. & YUNOKUCHI, K. 2010. Contribution of human melanopsin retinal ganglion cells to steady-state pupil responses. *Proc Biol Sci,* 277**,** 2485-92.

TSUJIMURA, S., WOLFFSOHN, J. & GILMARTIN, B. 2001. A linear chromatic mechanism drives the pupillary response. *Proc. R. Soc. Lond. B,* 268**,** 7.

VAN BUREN, J. 1963. Trans-synaptic retrograde degeneration in the visual system of primates. *Journal of Neurology, Neurosurgery & Psychiatry,* 26**,** 402-409.

VAN ENGELAND, H., ROELOFS, J. W., VERBATEN, M. N. & SLANGEN, J. L. 1991. Abnormal electrodermal reactivity to novel visual stimuli in autistic children. *Psychiatry research,* 38**,** 27-38.

VAN ORDEN, K. F., LIMBERT, W., MAKEIG, S. & JUNG, T. P. 2001. Eye activity correlates of workload during a visuospatial memory task. *Human Factors: The Journal of the Human Factors and Ergonomics Society,* 43**,** 111-121.

VIMAL, R., POKORNY, J., SMITH, V. & SHEVELL, S. K. 1989. Foveal cone thresholds. *Vision Research,* 29**,** 61.

WALD, G. & GRIFFIN, D. R. 1947. The change in refractive power of the human eye in dim and bright light. *JOSA,* 37**,** 321-334.

WALL, M. 1990. Loss of P retinal ganglion cell function in resolved optic neuritis. *Neurology,* 40**,** 649.

WATANABE, M. & RODIECK, R. 1989. Parasol and midget ganglion cells of the primate retina. *The Journal of comparative neurology,* 289**,** 434-454.

WEDE, J. & FRANCIS, G. 2007. Attentional effects on afterimages: theory and data. *Vision research,* 47**,** 2249-2258.

WEISKRANTZ, L., COWEY, A. & BARBUR, J. 1999. Differential pupillary constriction and awareness in the absence of striate cortex. *Brain,* 122**,** 1533.

WEISKRANTZ, L., COWEY, A. & LE MARE, C. 1998. Learning from the pupil: a spatial visual channel in the absence of V1 in monkey and human. *Brain,* 121**,** 1065.

WENT, L. N. & PRONK, N. 1985. The genetics of tritan disturbances. *Hum Genet,* 69**,** 255-62.

WILHELM, B., WILHELM, H., LÜDTKE, H., ADLER, M. & STREICHER, P. 1996. Pupillography for objective vigilance assessment. Methodological problems and possible solutions]. *Der Ophthalmologe: Zeitschrift der Deutschen Ophthalmologischen Gesellschaft,* 93**,** 446.

WILHELM, B. J., WILHELM, H., MORO, S. & BARBUR, J. L. 2002. Pupil response components: studies in patients with Parinaud's syndrome. *Brain,* 125**,** 2296-307.

WILLIAMS, D. R. & COLETTA, N. J. 1987. Cone spacing and the visual resolution limit. *JOSA A,* 4**,** 1514-1523.

WINN, B., WHITAKER, D., ELLIOTT, D. B. & PHILLIPS, N. J. 1994. Factors affecting light-adapted pupil size in normal human subjects. *Investigative Ophthalmology & Visual Science,* 35**,** 1132-1137.

WOLFFSOHN, J. S., SHEPPARD, A. L., VAKANI, S. & DAVIES, L. N. 2011. Accommodative amplitude required for sustained near work. *Ophthalmic and Physiological Optics,* 31**,** 480-486.

WRIGHT, W. D. 1929. A re-determination of the trichromatic coefficients of the spectral colours. *Transactions of the Optical Society,* 30**,** 141.

WRIGHT, W. D. 1952. The characteristics of tritanopia. *J Opt Soc Am,* 42**,** 509-21.

YOSS, R. E., MOYER, N. J. & HOLLENHORST, R. W. 1970. Pupil size and spontaneous pupillary waves associated with alertness, drowsiness, and sleep. *Neurology,* 20**,** 545.

ZAIDI, F. H., HULL, J. T., PEIRSON, S. N., WULFF, K., AESCHBACH, D., GOOLEY, J. J., BRAINARD, G. C., GREGORY-EVANS, K., RIZZO, J. F., 3RD, CZEISLER, C. A., FOSTER, R. G., MOSELEY, M. J. & LOCKLEY, S. W. 2007. Short-wavelength light sensitivity of circadian, pupillary, and visual awareness in humans lacking an outer retina. *Curr Biol,* 17**,** 2122-8.

ZEKI, S. 1978. The third visual complex of rhesus monkey prestriate cortex. *The Journal of physiology,* 277**,** 245.

ZHANG, X., KEDAR, S., LYNN, M., NEWMAN, N. & BIOUSSE, V. 2006. Homonymous hemianopias. *Neurology,* 66**,** 906.